

# The 23<sup>rd</sup> Annual Fall Field Frolic

---

Department of Geological Sciences Field Trip  
California State University, Northridge  
Weds. Aug. 24 to Sat. Aug. 27  
(fall classes start Aug. 29)

## The San Bernardino Mountains

*Trip Leaders: Dr. Doug Yule, Dr. Jorge Vazquez, and Dave Liggett*

Some of the things that we will see:

- The San Andreas fault and active tectonics related to the Big Bend!
- The highest mountain in Southern California ... San Geronio
- 1.8 Ga Baldwin Gneiss... among the oldest rocks in California
- Precambrian metasedimentary rocks of the Big Bear Group
- Yucaipa Ridge ... a rapidly uplifted part of the range
- Barton Flats...landslide or fan?
- Headwaters of the Santa Ana and Mojave Rivers

To reserve your place: Sign up on the trip roster in the Geology Department Office by Aug. 5<sup>th</sup>.

Transportation will be provided by state vehicles.

## FFF '05 STOPS

### Day One

1. Zanja
2. Mouth of Mill Creek
3. Pelona Schist in Mill Creek Formation
4. Mill Creek fm
5. Upper Mill Creek Canyon
6. Manzanita Springs Triassic Megaporphyry

Barton Flats Campground

### Day Two

Geology overview

1. Barton Creek debris flow
2. Jenks Lake - Pelona Schist
3. Santa Ana Formation
4. Basalt roadcut
5. Lower contact of Big Bear Group on Lightning Gulch road
6. Hike to Late Proterozoic-Paleozoic metasediments
7. Baldwin Gneiss.
8. Holcomb Valley (Belleville)

Tanglewood Campground

### Day Three

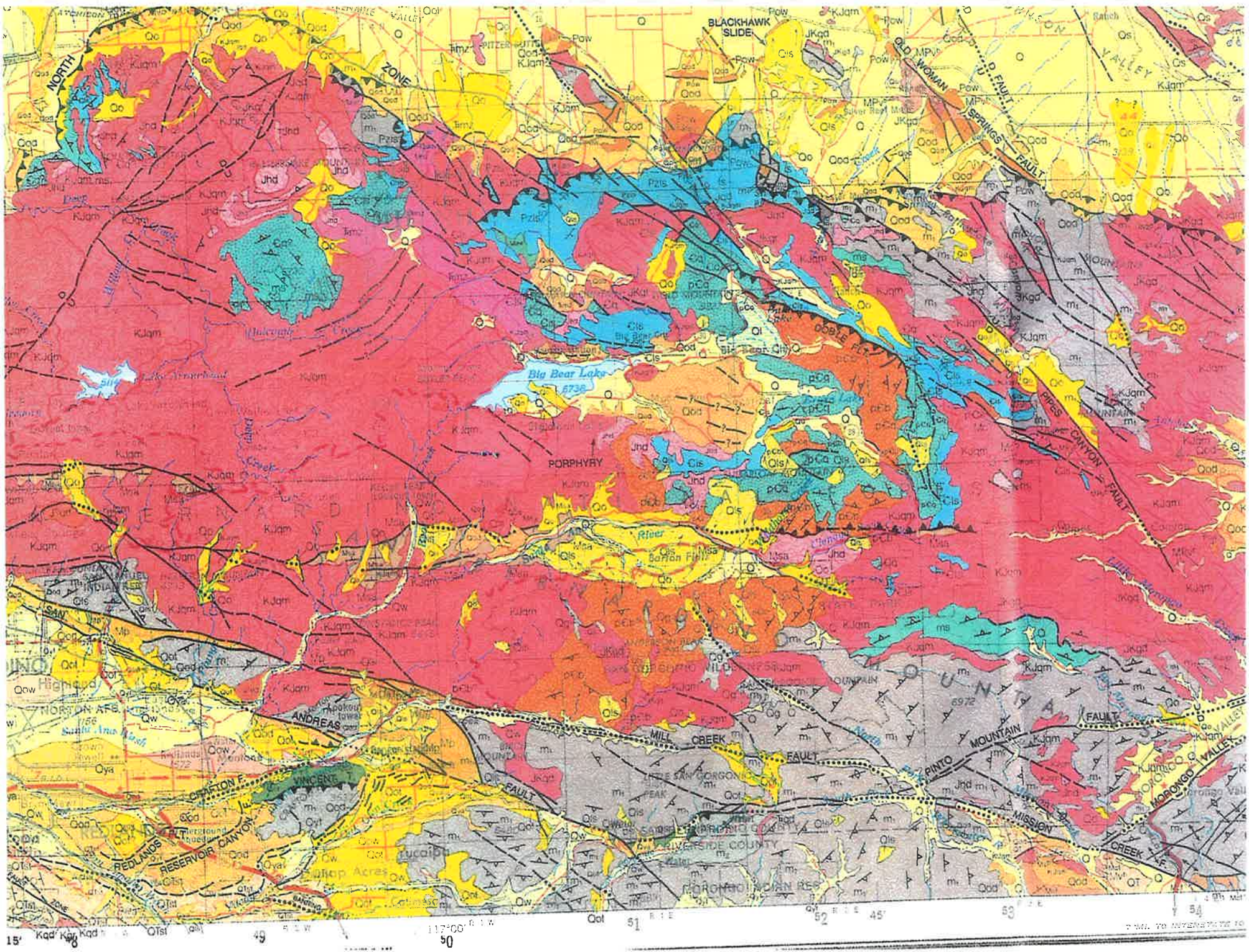
1. Howard Brown tour of Paleozoic metasediments and frontal fault system
2. Rattlesnake Mountain Pluton
3. Fawnskin monzonite pluton

Tanglewood Campground

### Day Four

1. Cactus Flat granite
2. Blackhawk Landslide
3. Landers fault scarp (if time permits)











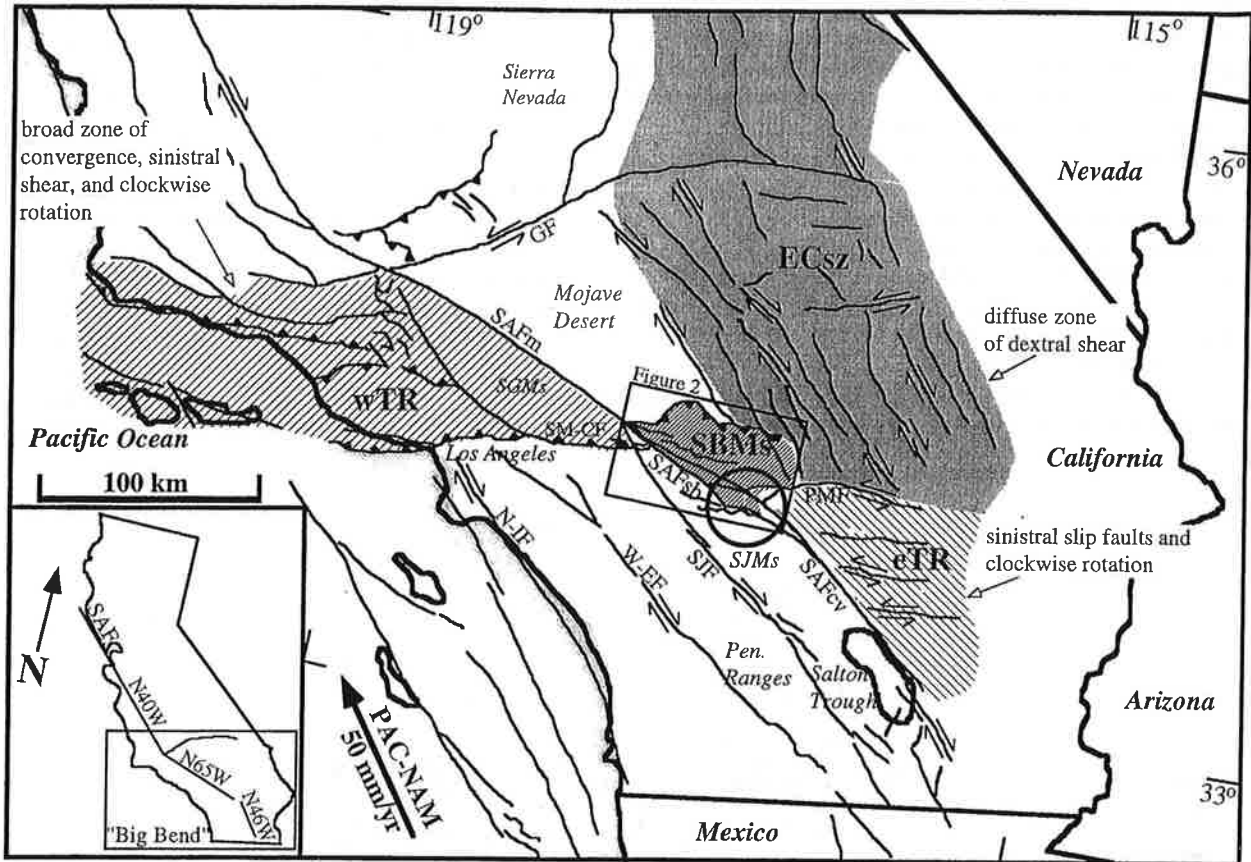








**Figure 4.** Aerial overview of the northeastern San Bernardino Mountains. Mill Creek and Yucaipa Ridge in lower right; Morton Peak with complex of nested landslides at lower center; Santa Ana River Canyon with extensive terraces and landslides in mid-ground; Big Bear and Baldwin Valleys on the plateau in the upper ground; eroded slopes of Slide Peak in center left; Gold Mountain and Bertha Ridge on skyline. John H. Shelton photo 3118.



**Figure 1.** Active tectonic context of the San Bernardino Mountains (SBMs). The "Big Bend" of the San Andreas fault occurs south of the Garlock fault (GF) and north of the small restraining bend at San Gorgonio Pass (circle). Relative plate motion vector is from *DeMets* [1995]. ECsz, eastern California shear zone (gray); eTR, eastern Transverse Ranges (ruled); N-IF, Newport-Inglewood fault; Pen. Ranges, Peninsular Ranges; PMF, Pinto Mountain fault; SAF, San Andreas fault (m, Mojave; sb, San Bernardino; cv, Coachella Valley segments); SGMs, San Gabriel Mountains; SJF, San Jacinto fault; SJMs, San Jacinto Mountains; SM-CF, Sierra Madre-Cucamonga fault; W-EF, Whittier-Elsinore fault; wTR, western Transverse Ranges.

To better understand how horizontal plate motion is manifest as crustal deformation along transpressive strike-slip fault systems, the architecture and kinematic history of structural arrays at intermediate distances to strike-slip fault zones must be quantified. The San Bernardino Mountains (SBMs) extend from near-field to intermediate distance from the San Andreas fault zone (Figure 1) and have been elevated over the past few million years in association with transpressive deformation [Dibblee, 1975; Meisling and Weldon, 1989; Spotila et al., 1998]. This young mountain system thus represents an ideal opportunity to study long-term transpressive orogenesis associated with the San Andreas fault system. The bulk of the range consist of the broad Big Bear plateau, which has been raised along two east-west trending thrust faults with opposing dips (North Frontal thrust system (NFTS) and Santa Ana thrust (SAT)) (Figure 2). Critical to understanding the structural kinematics of the SBMs is knowing whether the subsurface geometry of these thrusts mimics the high-angle deformation observed within the

San Andreas fault zone or the low-angle deformation that occurs at greater distance from its trace. Although both have been proposed as models for the SBMs [Sadler, 1982; Li et al., 1992], the subsurface structural geometry and displacements of the faults have not been well constrained. Previous efforts have been stymied because the SBMs consist mainly of crystalline bedrock that cannot be palinspastically restored in balanced cross sections.

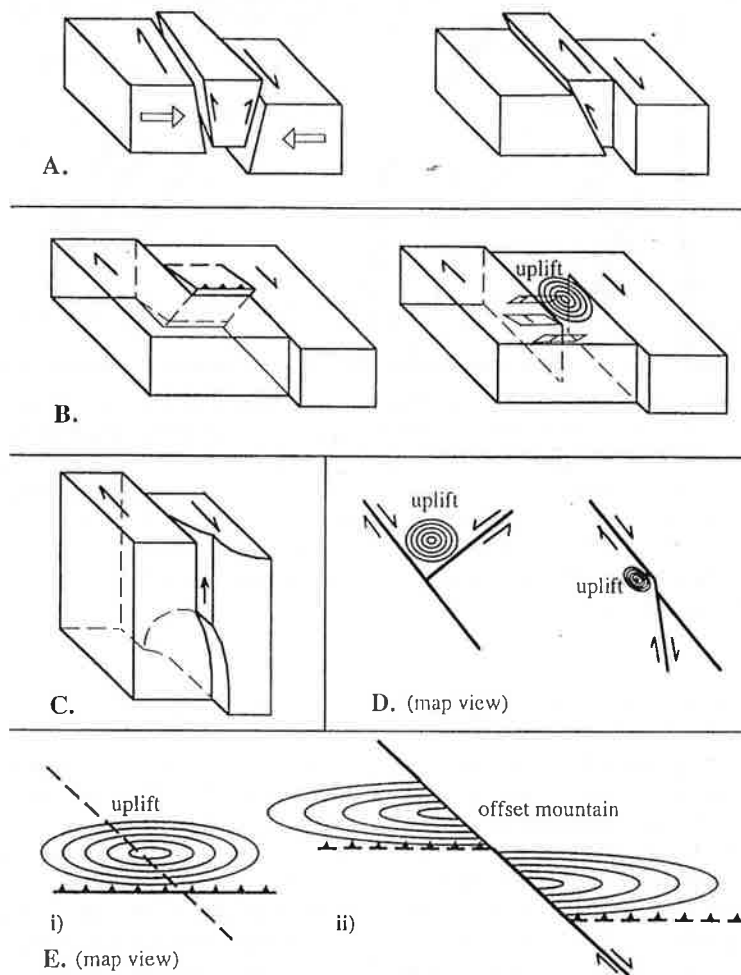
We have used a geomorphic feature as a structural datum to quantify the pattern of rock uplift in the SBMs and thereby place constraints on the displacement and geometry of the major structures. Atop the SBMs and across the surrounding lowlands is a low-relief, deeply weathered, granitic erosion surface (Figure 3). Geologic and geomorphic relationships argue that this surface is relict, in that it formed prior to recent mountain building and was subsequently separated by the major thrust faults of the range [Oberlander, 1972; Meisling, 1984; Spotila, 1999]. We have used the distribution of this easily identified geologic marker to reconstruct the vertical



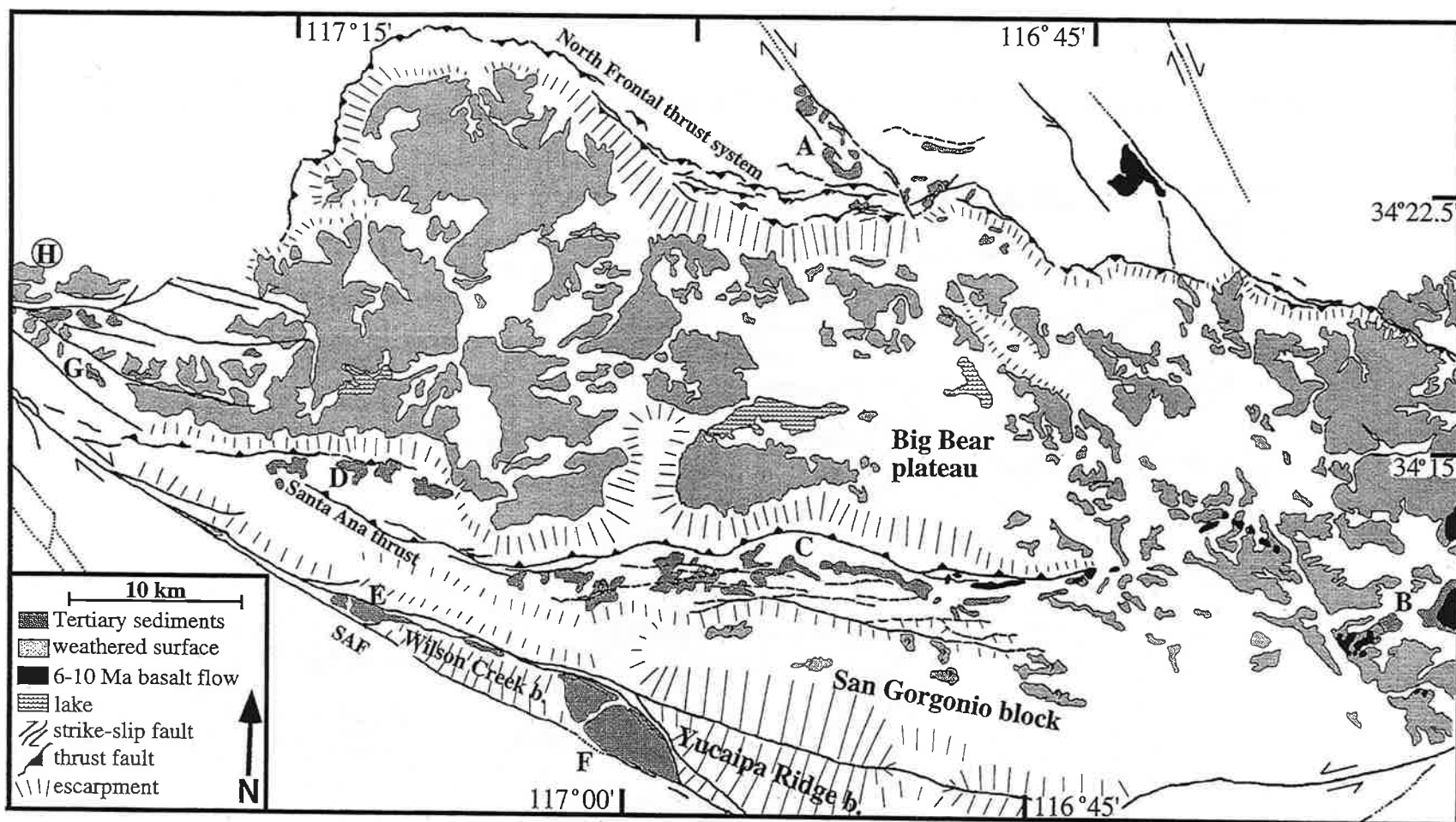
lack of helium ages from the Morongo block prevents us from knowing whether it has experienced a similar magnitude of rock uplift. The greater relief of the YR block relative to the Morongo block suggests uplift may have been localized to north of the Mission Creek fault. If the YR block did rise relative to the Morongo block, the sense and magnitude of motion would mimic the north-side-up separation of the base in seismicity (~15-20 km depth) below the surface trace of the Mission Creek fault [Corbett, 1984; Webb and Kanamori, 1985; Magistrale and Sanders, 1996]. The exhumation suggested by the helium ages thus appears consistent with the surrounding geologic relations.

Vertical motion along a strike-slip system can result from a number of different configurations of active

faulting. For example, reverse slip can accommodate horizontal displacement if a strike-slip fault is nonvertical and there is convergence across the fault zone (Figure 6a). Such slip partitioning can occur on oblique-slip faults that are parallel to and decoupled from the main strand of a strike-slip system when the maximum horizontal stress is nearly perpendicular to the fault zone [Mount and Suppe, 1987]. Ruptures during the 1989 Loma Prieta and 1986 Palm Springs earthquakes are recent examples of this, in which substantial components of horizontal plate motion were accommodated by vertical slip [Jones and Wesnousky, 1992]. Depending on the dip of the fault, slip partitioning can result in large vertical displacements. For example, the ratio of horizontal to vertical slip on the 45° dipping rupture that produced the Palm Springs earthquake was

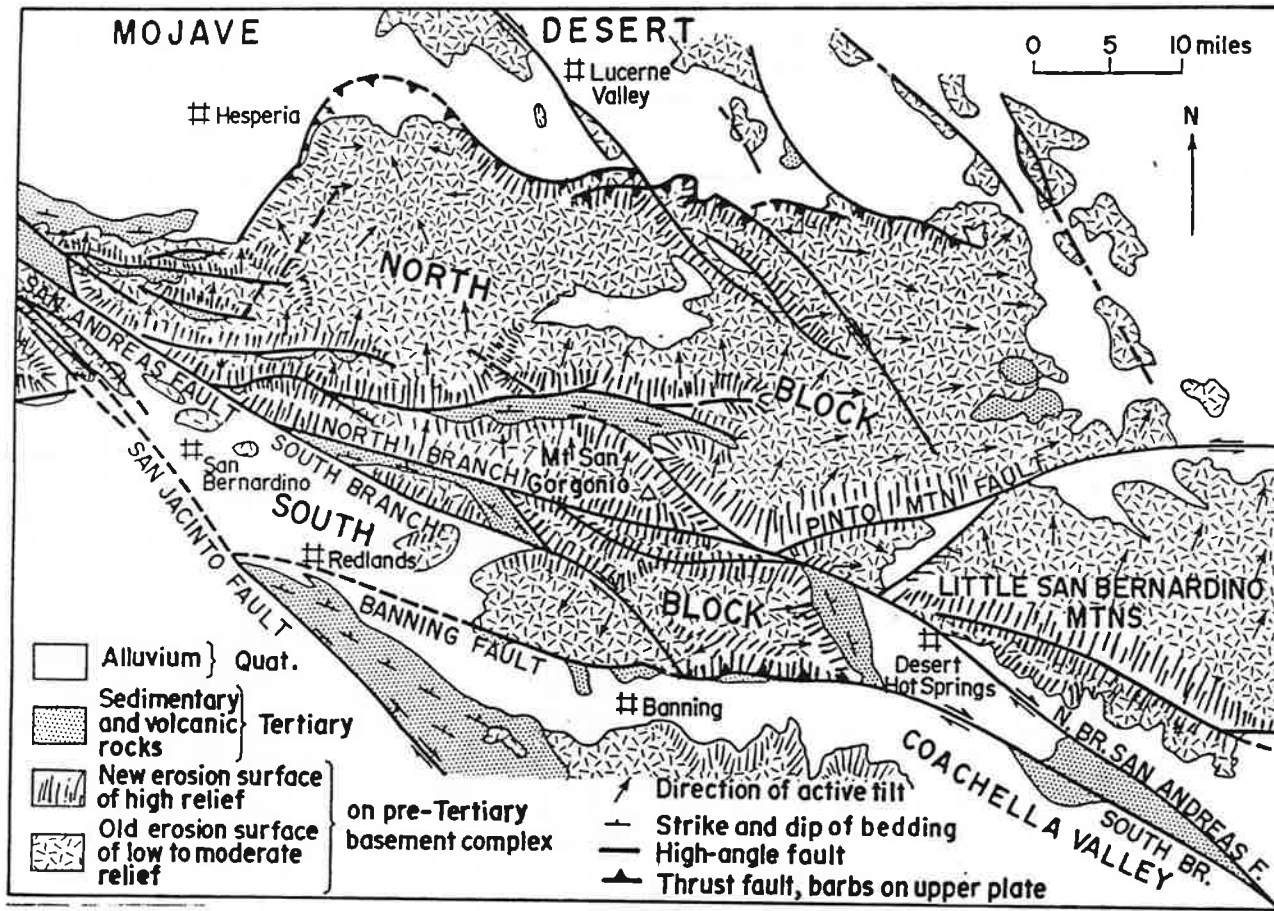


**Figure 6.** Generalized block diagrams that show examples of how vertical motion may occur in association with strike-slip faulting. (a) Uplift of block due to vertical motion associated with slip partitioning on a dipping fault strand in a strike-slip zone. (b) Uplift of block due to convergence within a fault stepover or restraining bend, either as a single thrust ramp or as diffuse internal shortening (concentric circles are elevation contours symbolizing uplift and small planes represent minor reverse faults at depth). (c) Uplift due to a subsurface bend or other geometric perturbation propagating along a strike-slip fault (the western San Bernardino arch [Meisling and Weldon, 1989]). (d) Uplift due to convergence associated with intersecting subparallel or conjugate strike-slip faults. (e) Apparent uplift along a strike-slip fault due to pure strike-slip offset of a topographic high.



**Figure 3.** Simplified geomorphic-geologic map of the SBMs showing the distribution of the weathered surface, Tertiary sediments, and basalt within the range. These are critical elements in constraining the recent deformation of the range. The approximate distribution of steep bedrock escarpments appear as a lined pattern, which represents the direction and size of the escarpment. Only major faults of the range that define the major structural blocks are drawn. Letters refer to locations of Tertiary sediments: A, Old Woman Sandstone; B, Santa Ana Sandstone overlying weathered surface; C, central Santa Ana Sandstone; D, eastern Crowder Formation; E, Potato Sandstone; F, Mill Creek formation; G, Crowder Formation overlying weathered surface; H, general location of Cajon, Crowder, and Phelan Peak formations.





**Figure 7a:** Reproduction of Dibblee's (1975) interpretation of the geomorphology of the San Bernardino Mountains, including the distribution of the "old erosion surface".

Matti and Morbin, ASA Memoir 178, 1993

11

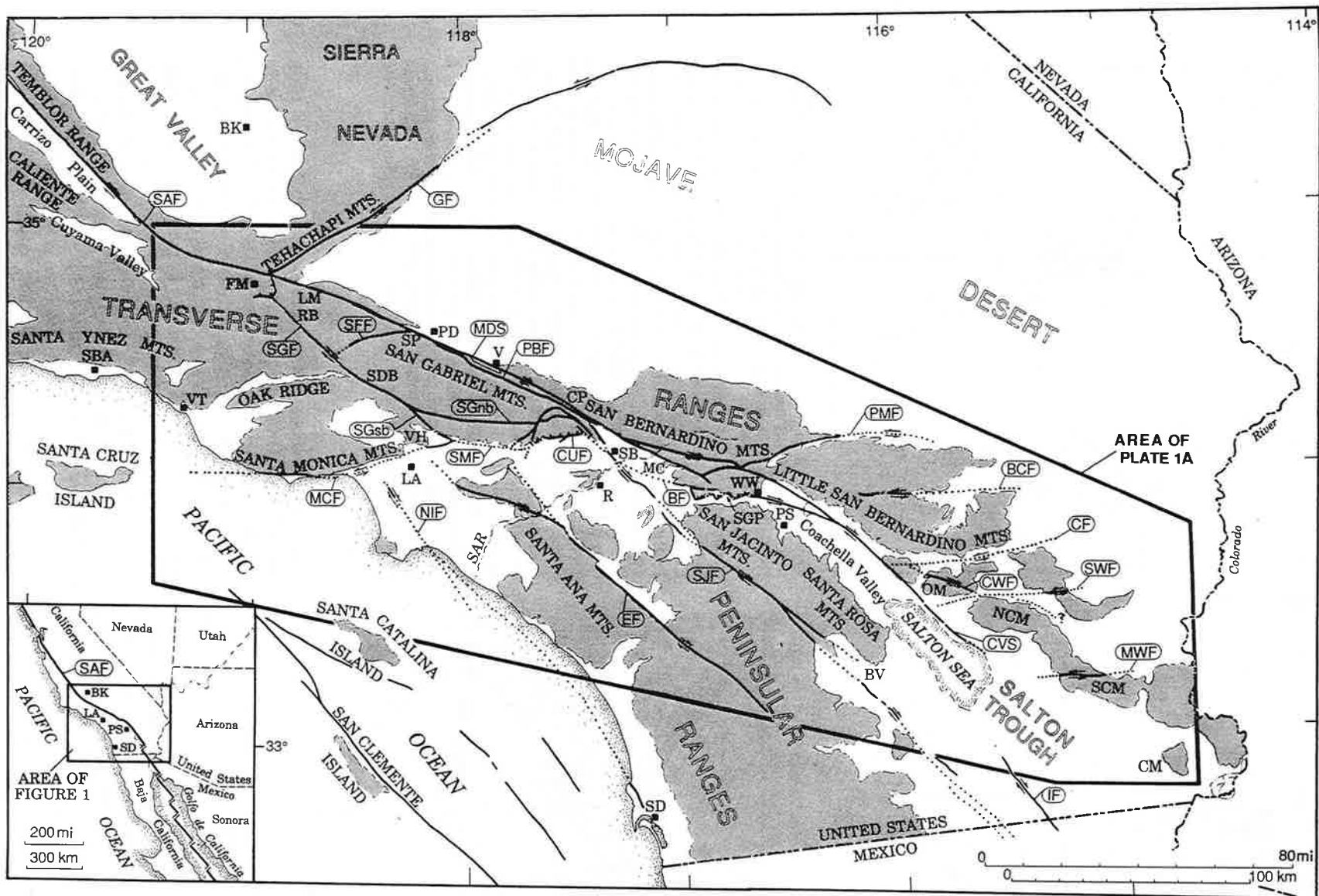


Figure 1. Index map showing geographic features and faults discussed in this report. BCF = Blue Cut fault; BF = Banning fault; BK = Bakersfield; BV = Borrego Valley region; CF = Chiriaco fault; CM = Cargo Muchacho Mountains; CP = Cajon Pass region; CUF = Cucamonga fault; CVS = Coachella Valley segment, San Andreas fault; CWF = Clemens Well fault; EF = Elsinore fault; FM = Frazier Mountain region; GF = Garlock fault; IF = Imperial fault; LA = Los Angeles; LM = Liebre Mountain; MCF = Malibu Coast-Santa Monica-Raymond fault; MC = Mill Creek; MDS = Mojave Desert segment, San Andreas fault; MWF = Mammoth Wash fault; NCM = northern Chocolate Mountains; NIF = Newport-Inglewood fault; OM = Orocochia Mountains; PBF = Punchbowl fault; PD = Palmdale; PMF = Pinto Mountain fault; R = Riverside; RB = Ridge Basin; SAF = San Andreas fault; SAR = Santa Ana River; SB = San Bernardino; SBA = Santa Barbara; SBM = San Bernardino Mountains; SCM = southern Chocolate Mountains; SD = San Diego; Soledad basin; SFF = San Francisquito fault; SGF = San Gabriel fault; SGnb = north branch, San Gabriel fault; SGsb = south branch, San Gabriel fault; SGP = San Gorgonio Pass; SJF = San Jacinto fault; SMF = Sierra Madre fault; SP = Sierra Pelona; SWF = Salton Wash fault; V = Valyermo; VT = Ventura; WW = Whitewater.



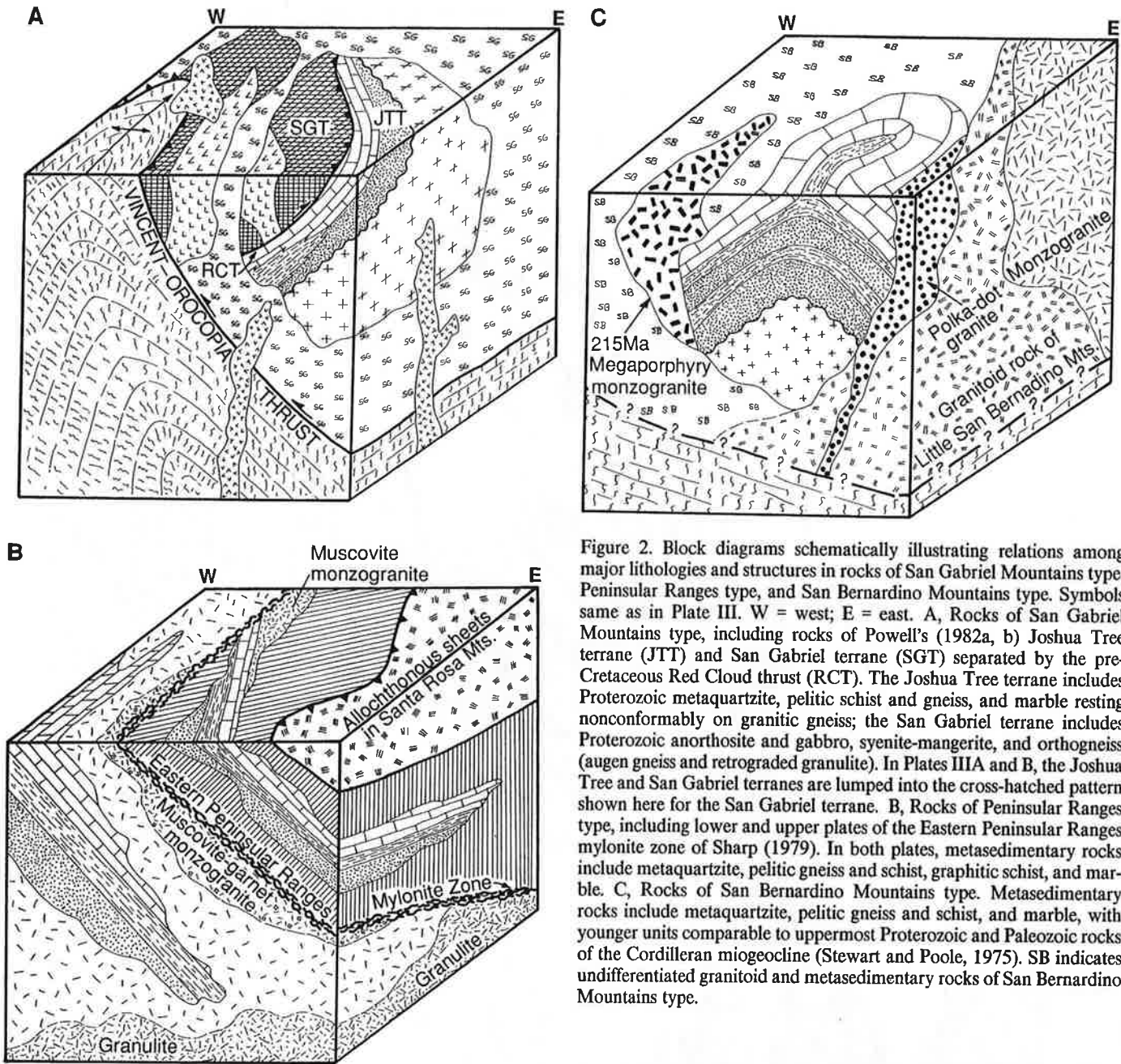


Figure 2. Block diagrams schematically illustrating relations among major lithologies and structures in rocks of San Gabriel Mountains type, Peninsular Ranges type, and San Bernardino Mountains type. Symbols same as in Plate III. W = west; E = east. A, Rocks of San Gabriel Mountains type, including rocks of Powell's (1982a, b) Joshua Tree terrane (JTT) and San Gabriel terrane (SGT) separated by the pre-Cretaceous Red Cloud thrust (RCT). The Joshua Tree terrane includes Proterozoic metaquartzite, pelitic schist and gneiss, and marble resting nonconformably on granitic gneiss; the San Gabriel terrane includes Proterozoic anorthosite and gabbro, syenite-mangerite, and orthogneiss (augen gneiss and retrograded granulite). In Plates IIIA and B, the Joshua Tree and San Gabriel terranes are lumped into the cross-hatched pattern shown here for the San Gabriel terrane. B, Rocks of Peninsular Ranges type, including lower and upper plates of the Eastern Peninsular Ranges mylonite zone of Sharp (1979). In both plates, metasedimentary rocks include metaquartzite, pelitic gneiss and schist, graphitic schist, and marble. C, Rocks of San Bernardino Mountains type. Metasedimentary rocks include metaquartzite, pelitic gneiss and schist, and marble, with younger units comparable to uppermost Proterozoic and Paleozoic rocks of the Cordilleran miogeocline (Stewart and Poole, 1975). SB indicates undifferentiated granitoid and metasedimentary rocks of San Bernardino Mountains type.

**STRIKE-SLIP FAULTS OF THE SAN ANDREAS FAULT SYSTEM**

**Introduction**

Rocks of Peninsular Ranges type, San Gabriel Mountains type, and San Bernardino Mountains type are traversed by a series of northwest-trending strike-slip faults (Fig. 1, Plate IIIA) that most workers assign to the San Andreas transform-fault system—a family of right-lateral faults that has evolved along the continental margin of western North America since middle Miocene time in response to interactions between the North Ameri-

can plate and various oceanic plates to the west (Atwater, 1970; Crowell, 1979; Dickinson and Snyder, 1979a, b). Youthful faults commonly viewed as modern components of the San Andreas system include the San Andreas fault proper; the San Jacinto, Whittier-Elsinor, and Newport-Inglewood faults; and various northwest-trending faults occurring in the offshore continental borderland (see Allen, 1957, p. 346; Crowell, 1975a, p. 10–11, 1981, p. 593). Older faults commonly viewed as abandoned components of the San Andreas system include the Punchbowl, San Gabriel, and Banning faults (Allen, 1957; Crowell, 1962, 1975a, 1981; Ehlig, 1976, 1981). Even older right-lateral faults that may belong to the San Andreas system include the San Juan–St. Francis and San Francisquito–Fenner–Clemens Well

*Matti and Morley, GSA Memoir 178, 1993*

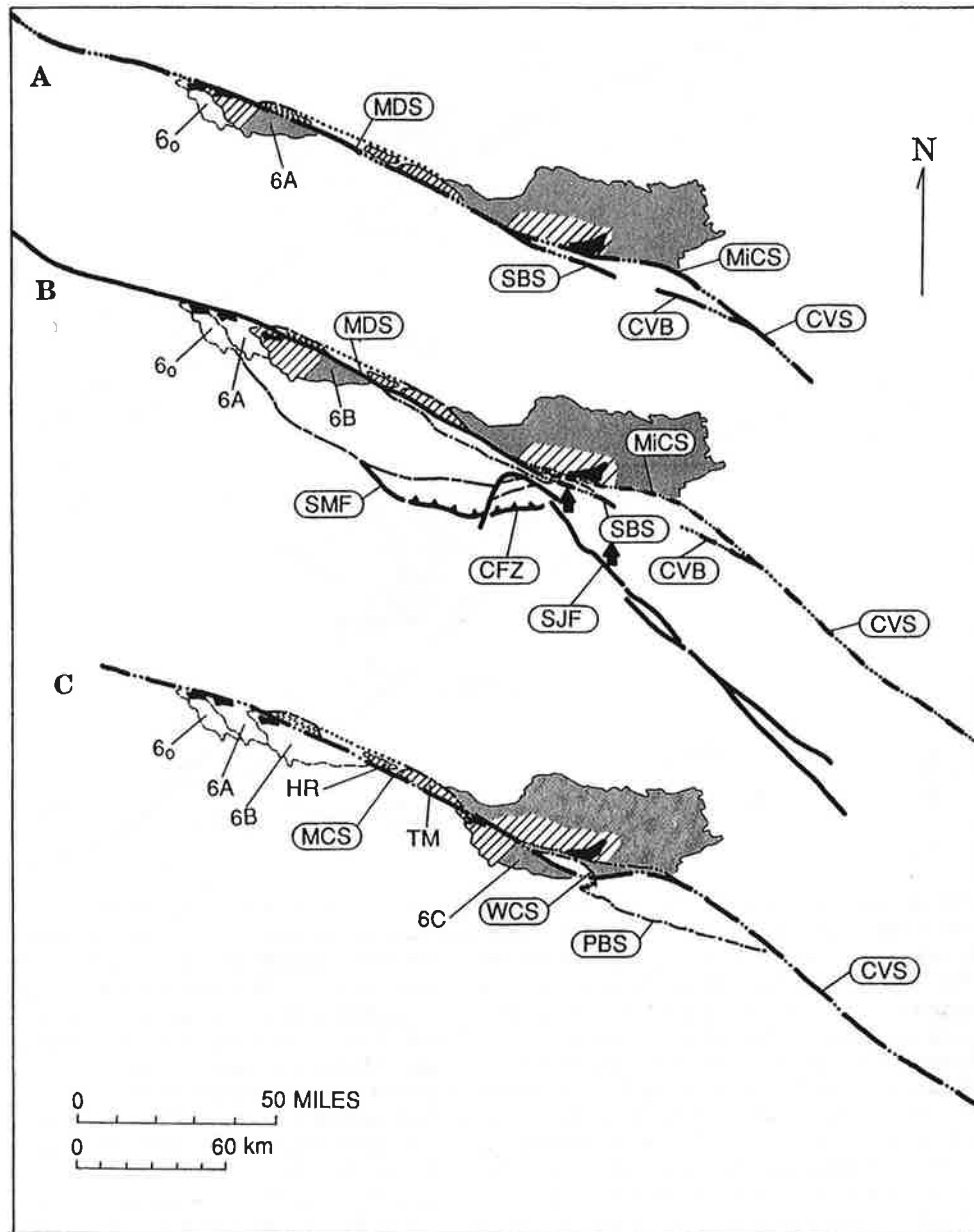
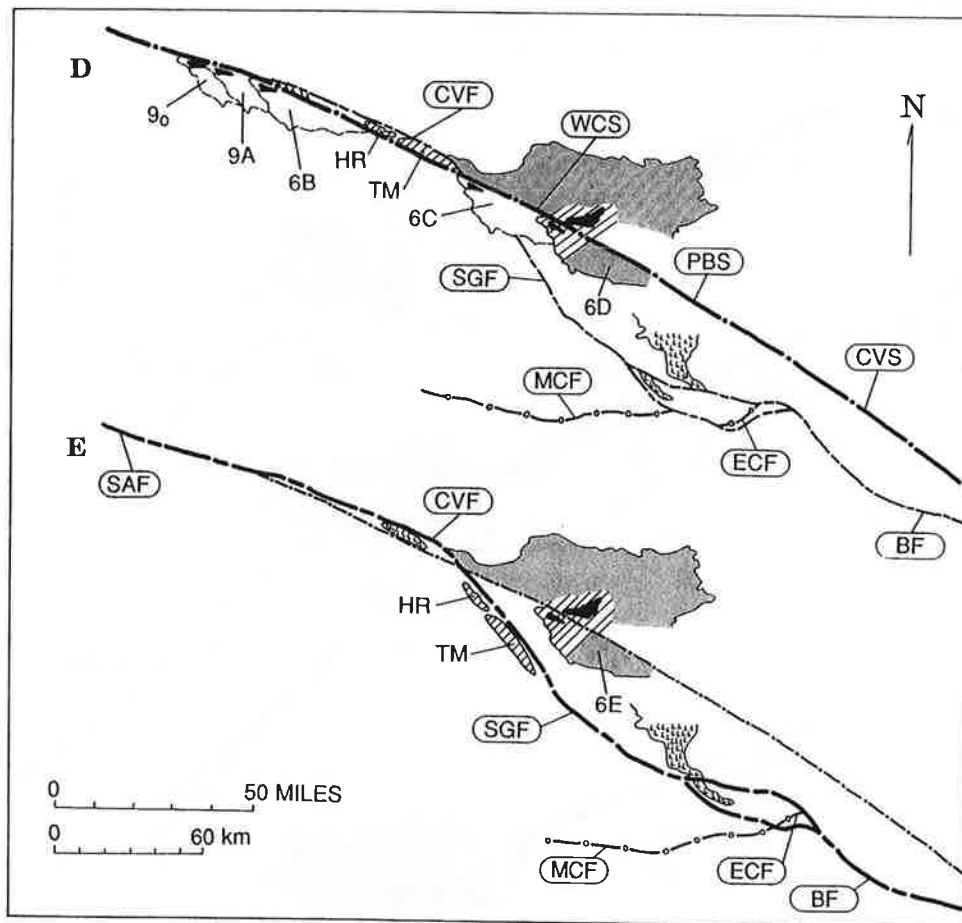


Figure 6. Schematic diagram illustrating sequential restoration of right slip on strands of the San Andreas fault system required to generate the palinspastic reconstruction of Plate IIIB. In each part of the figure (A-E), the Liebre Mountain Triassic megaporphyry body is restored to a palinspastic position closer to the Mill Creek megaporphyry body as a result of restored right slip on fault strands designated for each figure; preceding positions for the Liebre Mountain body are indicated by dashed outlies of the Liebre Mountain block. Rock and fault symbols same as Plates IIIA and B. A, The Liebre Mountain megaporphyry body is removed 11 km from its present position ( $6_o$ ) by restoring displacements on the San Bernardino strand (SBS, 3 km) and Mill Creek strand (MiCS, 8 km), which merge with the Mojave Desert strand. B, The Liebre Mountain megaporphyry body is removed 20 km from its former position (6A) by restoring displacements on the San Jacinto fault (SJF); slip on the San Jacinto steps right onto the San Andreas fault and contributes to displacements on the Mojave Desert strand (MDS). CFZ = Cucamonga fault zone; CVB = Coachella Valley segment, Banning fault; CVS = Coachella Valley segment, San Andreas fault; MiCS = Mill Creek strand, San Andreas fault; SBS = San Bernardino strand, San Andreas fault; SMF = Sierra Madre fault. C, The Liebre Mountain megaporphyry body is removed 89 km from its former position (6B) by restoring displacements on the Mission Creek strand of the San Andreas fault (MCS), which merges with the Mojave Desert strand (MDS). This restoration approximately aligns the northwest end of the Punchbowl strand (PBS) with the southeast end of the

GSA Memoir 178, 1993





Wilson Creek strand (WCS). CVS = Coachella Valley segment, San Andreas fault; HR = Holcomb Ridge; TM = Table Mountain. D, The Liebre Mountain megaporphyry body is removed 40 km from its former position (6C) by restoring displacements on the continuous Punchbowl-Wilson Creek strand (PBS and WCS, respectively). This restoration reassembles the Liebre Mountain and Mill Creek occurrences of the Triassic megaporphyry body and completes the sequence of restorations required to reconstruct about 160 km of right slip on the San Andreas fault (*sensu stricto*) in southern California. Restoration of the Liebre Mountain and Mill Creek megaporphyry bodies approximately aligns the northwest end of the San Gabriel fault (SGF) with the southeast end of the Cajon Valley fault (CVF). BF = Banning fault; CVS = Coachella Valley segment, San Andreas fault; ECF = Evey Canyon fault; HR = Holcomb Ridge; MCF = Malibu Coast-Santa Monica-Raymond fault; TM = Table Mountain. E, About 22 km of right slip is removed on the north branch of the San Gabriel fault (SGF) by reuniting exposures of the Lowe igneous pluton as proposed by Ehlig (1973, 1975, 1981); approximately 22 km of right slip is removed on the south branch of the San Gabriel fault by matching the east end of the Malibu Coast-Santa Monica-Raymond fault (MCF) with the southwest end of the Evey Canyon fault (ECF). Reconstruction of 44 km of right slip on the San Gabriel fault completes the sequence of restorations required to generate the palinspastic reconstruction of Plate IIIB. BF = Banning fault; CVF = Cajon Valley fault; HR = Holcomb Ridge; SAF = San Andreas fault; TM = Table Mountain.

were completed on the Clemens Well-Fenner-San Francisquito fault of Powell (1981; this volume) but before displacements on the San Gabriel-Banning fault.

### Implications

The reconstruction in Plate IIIB leads to a new way of viewing the restored positions of some well-known crystalline and sedimentary terranes in southern California.

**Reunited crystalline rocks. Liebre Mountain-San Bernardino Mountains.** The Liebre Mountain block is positioned adjacent to the San Bernardino and northern Little San Bernardino Mountains, rather than adjacent to the southern Little San Bernardino Mountains as in most reconstructions (Fig. 5). This juxtaposition yields an attractive comparison between batholithic and prebatholithic rocks: (1) It places the Liebre Mountain megaporphyry body within a Mojave Desert province of alkali-rich monzonitic rocks (Miller, 1978) that includes early Mesozoic

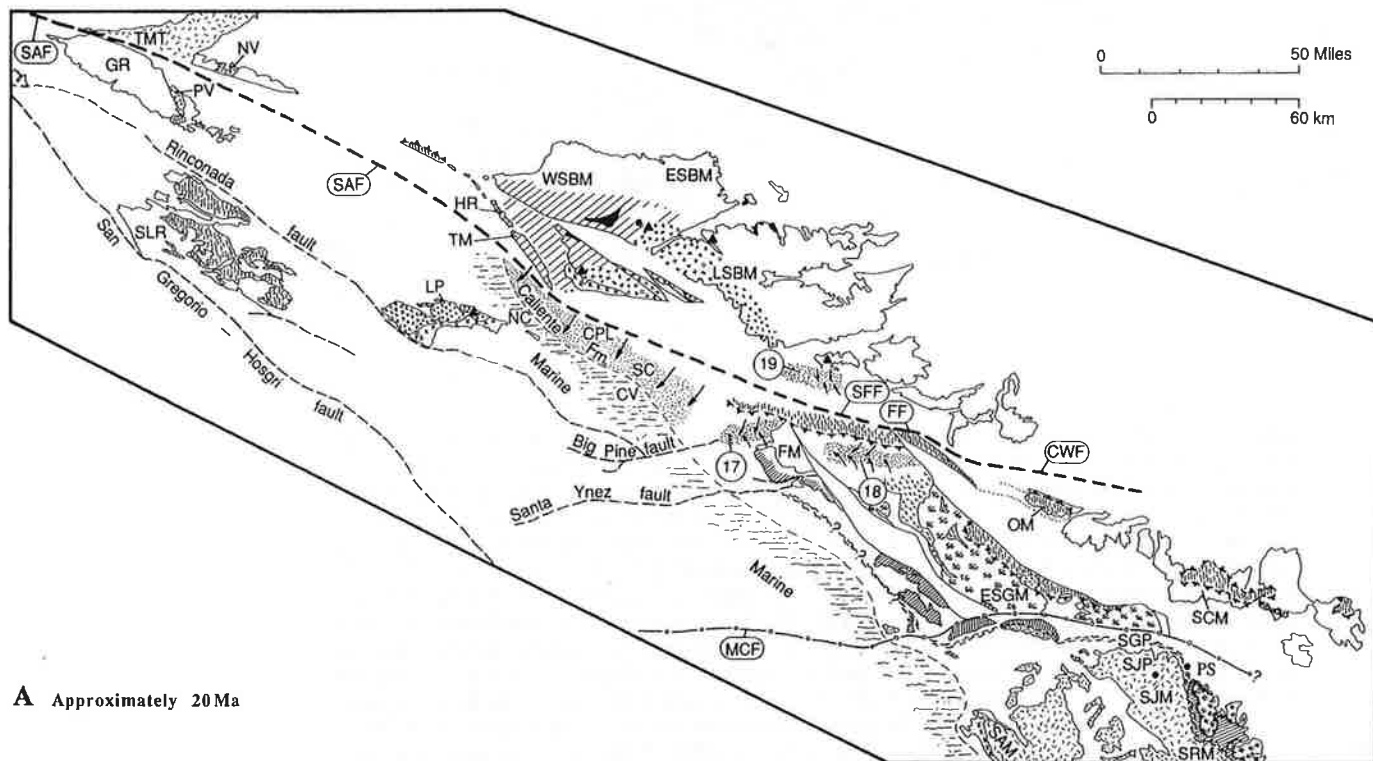
**DISASSEMBLY OF SOUTHERN CALIFORNIA:  
STEP-BY-STEP INSTRUCTIONS FOR  
REARRANGING A CONTINENTAL MARGIN**

In this section we develop one possible interpretation of how the paleogeography of southern California evolved since the early Miocene (20 Ma to present). The reconstructions make no attempt to accommodate block rotations proposed for southern

California on the basis of paleomagnetic data (Luyendyk and others, 1980, 1985; Luyendyk and Hornafius, 1987).

**Paleogeography prior to disassembly  
(early Miocene [20 Ma], Fig. 7A)**

**Fault activity.** The reconstruction in Figure 7A depicts the paleogeographic setting for southern California prior to major right slip within the San Andreas fault system. The reconstruction



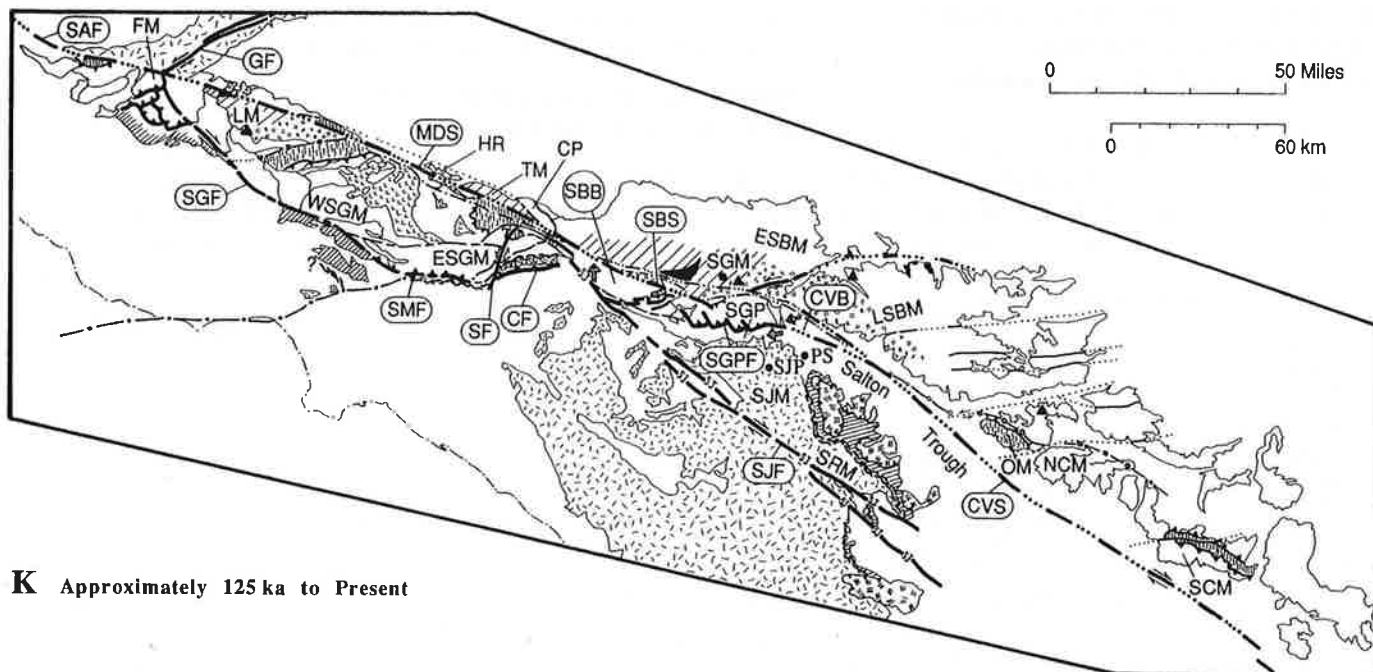
**A** Approximately 20 Ma

Figure 7A through K. Diagrams illustrating paleogeographic evolution of the San Andreas fault system in southern California from early Miocene to present. See text for discussion. Fault and rock symbols and sedimentary unit numbers same as in Plates IIIA and B. Heavy bold faults indicate structures that are active (dashed where soon to be initiated); thinner faults indicate structures whose displacement history is completed. Stippled pattern indicates active nonmarine sedimentation; short-dash pattern indicates active marine sedimentation; arrows indicate streamflow direction.

Figure 7A. Palinspastic reconstruction at about 20 Ma, prior to right-lateral displacements within the San Andreas fault system. About 50 km of right slip is restored on the Rincónada fault following Ross (1984), but we do not know how (or if) the Rincónada fault extended into southern California and affected the paleogeographic setting there. CPL = Carrizo Plain region; CWF = Clemens Well fault; CV = Cuyama Valley region; ESBM = eastern San Bernardino Mountains; ESGM = eastern San Gabriel Mountains; FF = Fenner fault; FM = Frazier Mountain region; GR = Gabilan Range; HR = Holcomb Ridge; LP = La Panza Range; LSBM = Little San Bernardino Mountains; MCF = Malibu Coast fault zone; NC = northern Caliente Range; NV = Neenach Volcanic field; OM = Orocopia Mountains; PS = Palm Springs; PV = Pinnacles Volcanic field; SAF = San Andreas fault; SAM = Santa Ana Mountains; SCM = southern Chocolate Mountains; SCR = southern Caliente Range; SFF = San Francisquito fault; SGM = San Gorgonio Mountain; SGP = San Gorgonio Pass; SJM = San Jacinto Mountains; SJP = San Jacinto Peak; SLM = Santa Lucia Mountains; SRM = Santa Rosa Mountains; TM = Table Mountain; TMT = Tehachapi Mountains; WSBM = western San Bernardino Mountains; WSGM = western San Gabriel Mountains.

Mutti and Morton, GSA Memoir 178, 1993





**K** Approximately 125 ka to Present

Figure 7K. The modern neotectonic and geomorphic setting of southern California reflects continued complexities within the San Andreas fault system. In a continuing attempt to breach the San Gorgonio Pass slip barrier, right slip on the San Andreas fault has reactivated the Banning fault in the Salton Trough to produce the neotectonic Coachella Valley segment of the Banning (CVB). Slip steps left from the Coachella Valley segment of the San Andreas (CVS) to the Banning fault (ruled arrows) and thence into San Gorgonio Pass, where convergence within the San Gorgonio Pass fault zone (SGPF) prevents a throughgoing connection between the Coachella Valley segment of the Banning fault and the newly evolved San Bernardino strand of the San Andreas (SBS). The San Bernardino basin (SBB) continues to subside as the right step (ruled arrow) between the San Jacinto fault and the San Bernardino strand creates extension within the San Bernardino Valley region. Complications created by integration of slip on the San Jacinto and San Andreas faults leads to convergence and uplift in the southeastern San Gabriel Mountains. CF = Cucamonga fault; CP = Cajon Pass region; CVS = Coachella Valley segment, San Andreas fault; ESBM = eastern San Bernardino Mountains; ESGM = eastern San Gabriel Mountains; FM = Frazier Mountain region; GF = Garlock fault; LSBM = Little San Bernardino Mountains; MDS = Mojave Desert segment, San Andreas fault; PMF = Pinto Mountain fault; PS = Palm Springs; SAF = San Andreas fault; SF = San Antonio fault; SGF = San Gabriel fault in Ridge Basin region; SGM = San Gorgonio Mountain; SGP = San Gorgonio Pass; SJF = San Jacinto fault; SJM = San Jacinto Mountains; SJP = San Jacinto Peak; SMF = Sierra Madre fault; SRM = Santa Rosa Mountains; TM = Table Mountain; WSBM = western San Bernardino Mountains; WSGM = western San Gabriel Mountains.

relations among the Coachella Valley segments of the San Andreas and Banning faults, the San Jacinto fault, and the San Bernardino strand of the San Andreas fault have produced a complex left- and right-stepping geometry by which right-lateral strain in the Salton Trough is passed around, not through, the structural knot in San Gorgonio Pass (Matti and others, 1985, Fig. 4). This geometry has created convergence in the San Gorgonio Pass fault zone and extension in the San Bernardino Valley region.

## DISCUSSION

Our paleogeographic model for the late Miocene through recent evolution of southern California (Fig. 7A-K) is based on our palinspastic model for how crystalline and sedimentary ter-

ranes now dispersed throughout the San Andreas fault system (Plate IIIA) can be restored to their original positions (Plate IIIB). The reconstruction in Plate IIIB is based on two premises: (1) Bodies of Triassic megaporphyritic monzogranite that crop out on opposite sides of the San Andreas fault in the Liebre Mountain and Mill Creek regions are displaced counterparts that constrain right slip on the San Andreas fault (*sensu stricto*) to no more than 160 km; and (2) the two megaporphyry bodies must be reassembled using sequential fault restorations that conform to the timing and amount of displacement documented for individual strands of the San Andreas and San Gabriel faults. The first premise was evaluated by Frizzell and others (1986), who concluded that isotopic, petrologic, and geochronologic evidence directly support cross-fault correlation of the two megaporphyry

San Gorgonio Mountain. From 200 to 1,500 m of sandstone, conglomerate, and clay can be found in tilted and folded (Fig. 2) sequences exposed beneath the surficial deposits. The surficial sediments are typically darker and contain more clay.

The older sediments were recognized by Vaughan (1922), who coined the term Santa Ana Sandstone for the conglomerate, sandstone, and shale exposed beneath the surficial gravels near the center of the basin. Dibblee (1964) mapped more of the unit to the east and west, and included sediments of different composition, some of them interbedded with basalt. Subsequent, more detailed, mapping (Sadler, 1981, 1982; Jacobs, 1982; Strathouse, 1982, 1983; Powell and others, 1983) has followed Dibblee's extended usage. Since the name has been applied to all the deposits that predate tilting and uplift in the basin, the Santa Ana Sandstone is essentially a tectono-stratigraphic unit. Not surprisingly, the practice creates difficulties at the east and west ends of the basin where the tectonic setting changes. The westernmost outcrops that Dibblee attributed to the Santa Ana Sandstone lie unconformably beneath Mud Flat. Thin-bedded silty sandstone is exposed there, together with conglomerate in which R. J. Weldon (written communication, 1988) has recognized clast suites that are diagnostic for the Crowder Formation. The easternmost outcrops that might deserve to be included are sandstones interbedded with basalt flows at Pioneertown (Fig. 1); these were originally assigned to the Old Woman Sandstone (Dibblee, 1967).

The outcrop of the Santa Ana Sandstone is a narrow, nearly continuous, east-west strip more than 30 km long and at most about 2 km wide (Fig. 2). Weakly indurated, pale colored boulder conglomerates and coarse pebbly sands, with limited lateral continuity of bedding, dominate the exposures. Immature paleosols, cut-and-fill lenses, and very poorly sorted debris-flow

beds are common. The overall character is indicative of alluvial deposition. Well-bedded sandstone, silt, and clay with a lacustrine character are subordinate except at the center of the basin. The conglomerates of the Santa Ana Sandstone include four significantly different clast suites, which define four areally discrete (Fig. 4) compositional facies.

The key to the Tertiary history of the Santa Ana basin is the age and provenance of the four compositional facies. The rest of this section describes the facies from west to east, presents the evidence for their ages, and finally suggests possible sources.

### Granitoid-dominated facies

The conglomerates in the western third of the main outcrop are characterized by clasts of granitoids and granitoid-gneiss. There is a paucity of distinctive clasts in this suite. The granitoids include biotite monzonite and a hornblende-rich diorite. A distinctive pre-Cretaceous, megaporphyritic hornblende granodiorite to monzonite (Morton and others, 1980, Matti and others, 1985) locally forms the basement to this part of the Santa Ana Sandstone and crops out through Angelus Oaks to the south (Fig. 1). It is rarely seen as clasts except at the very base of the formation. The granitoid gneisses bear superficial resemblance to the Baldwin Gneiss of San Gorgonio Mountain. But they may be distinguished from this local source by the paucity of coarsely foliated, biotite-rich varieties, and by the presence of a high percentage of gneiss with a mylonitic fabric. Weakly imbricated cobble fabrics in the conglomerates indicate transport from the south and south-southwest.

The base of the Santa Ana Sandstone in this western area is marked by a thick, red paleosol succeeded by fossiliferous red siltstones and sandstones that thicken eastward and become intercalated with pale pink, pebbly sandstone and green clay (Fig. 5).

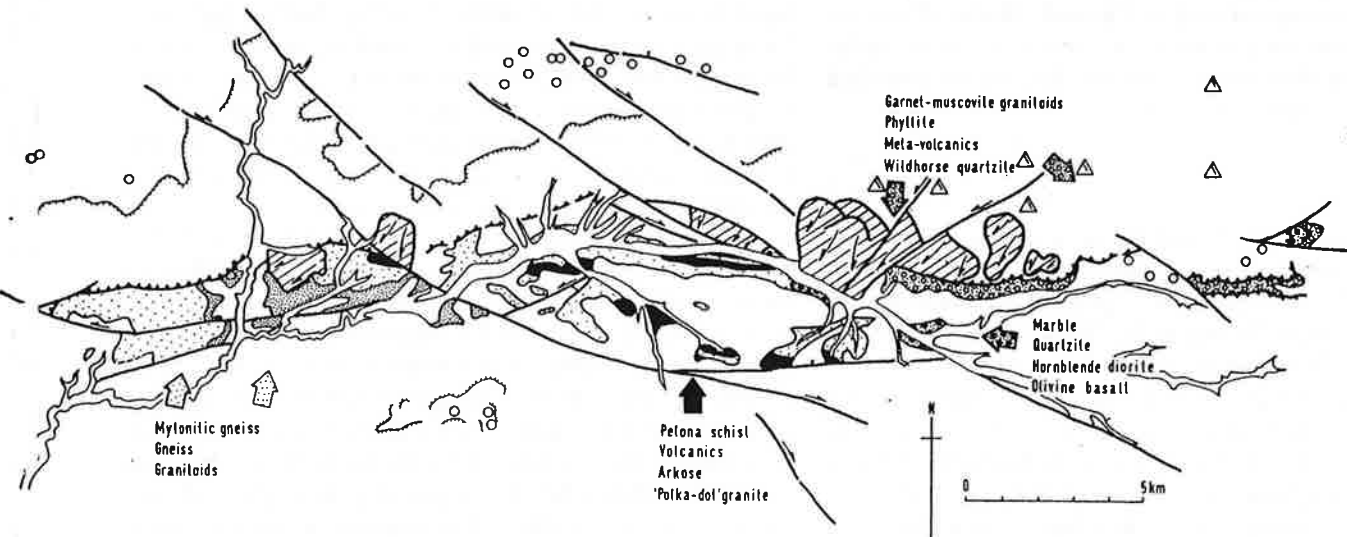


Figure 4. Facies and provenance of the Santa Ana basin. Arrows indicate transport directions and key clast types. Solid black indicates Pelona schist-bearing facies; dense stipple, basal red facies; sparse stipple, mylonitic gneiss-bearing facies; solid circles with stipple, marble-bearing facies; open circles with stipple, quartzite-bearing facies; large open circles, remnant of the upland veneer of quartzite gravels; triangles, main quartzite sources for the veneer.



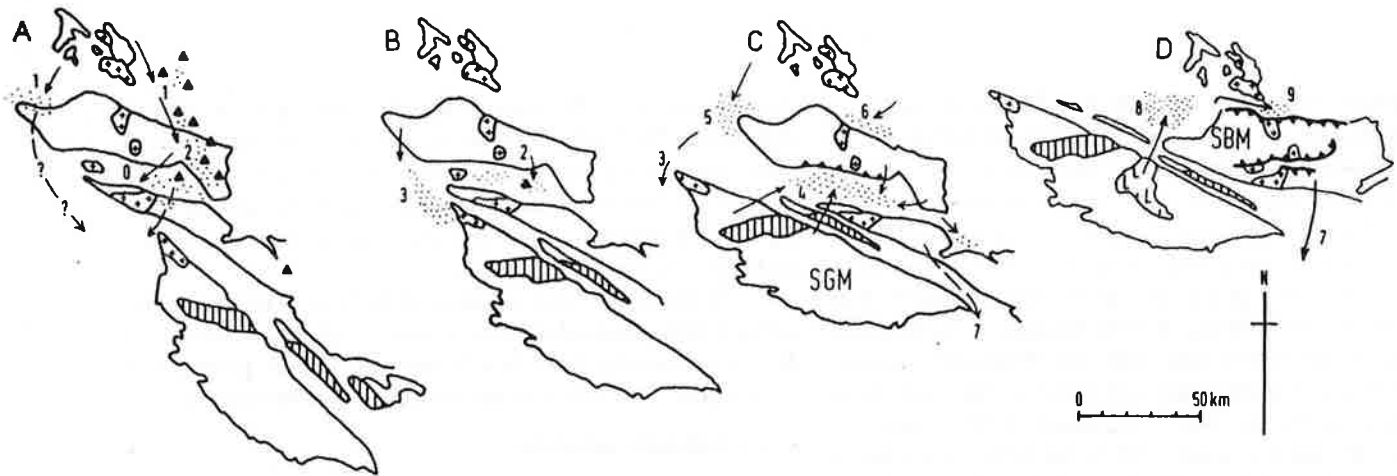


Figure 11. Possible regional restorations of deposits and their sources. The modern margins of San Gabriel Mountains, San Gorgonio massif, and northern plateau of the San Bernardino Mountains are included for reference. The four frames A-D represent different time spans. They follow in necessary sequence, but the total ranges of possible age for each include overlap: A, 15 to 6 m.y.; B: 9 to 4 m.y.; C; 9 to 3 m.y.; D: 2 to 1 m.y. L: Lowe Granodiorite. Crosses indicate megaporphyry of Matti and others (1985); triangles, 6- to 9-m.y. olivine basalt flows; vertical ruling, Pelona Schist; stipple, active deposition. Sequence key to numbers: 0, Paleosoils form in western Santa Ana basin. 1, Sidewinder Volcanics clasts transported from Mojave Desert; two routes into the Ridge basin are tentatively suggested. 2, Quartzite clasts, derived principally from Sugarloaf Mountain, enter eastern Santa Ana basin; some reach west end of future San Gorgonio Mountain block, others mix with 1 and travel at least to Pioneertown. 3, Ridge basin in position to deposit Hungry Valley Formation by reworking from Crowder Formation of Cajon Pass. 4, Clast assemblage with Pelona Schist can now enter Santa Ana basin around west end of future San Gorgonio Mountain. 5, Phelan Formation. 6, Earliest deposition in Old Woman Sandstone basin. 7, Clasts from San Gorgonio Mountain available to San Timoteo Badlands. 8, Victorville Fan. 9, Youngest, synorogenic deposition in Old Woman Sandstone basin.

and Weldon, 1990), the history may be allowed to expand up to about 9 Ma. The Pelona Schist clasts may have entered the Santa Ana basin before 6 Ma, but only if the San Andreas fault was initiated earlier than is popularly supposed. Perhaps it is time to question this conventional wisdom. Certainly, Weber (1986) has written that there are grounds to reexamine the relationships between the San Andreas fault and the older San Gabriel fault that are said to constrain their ages.

## SUMMARY

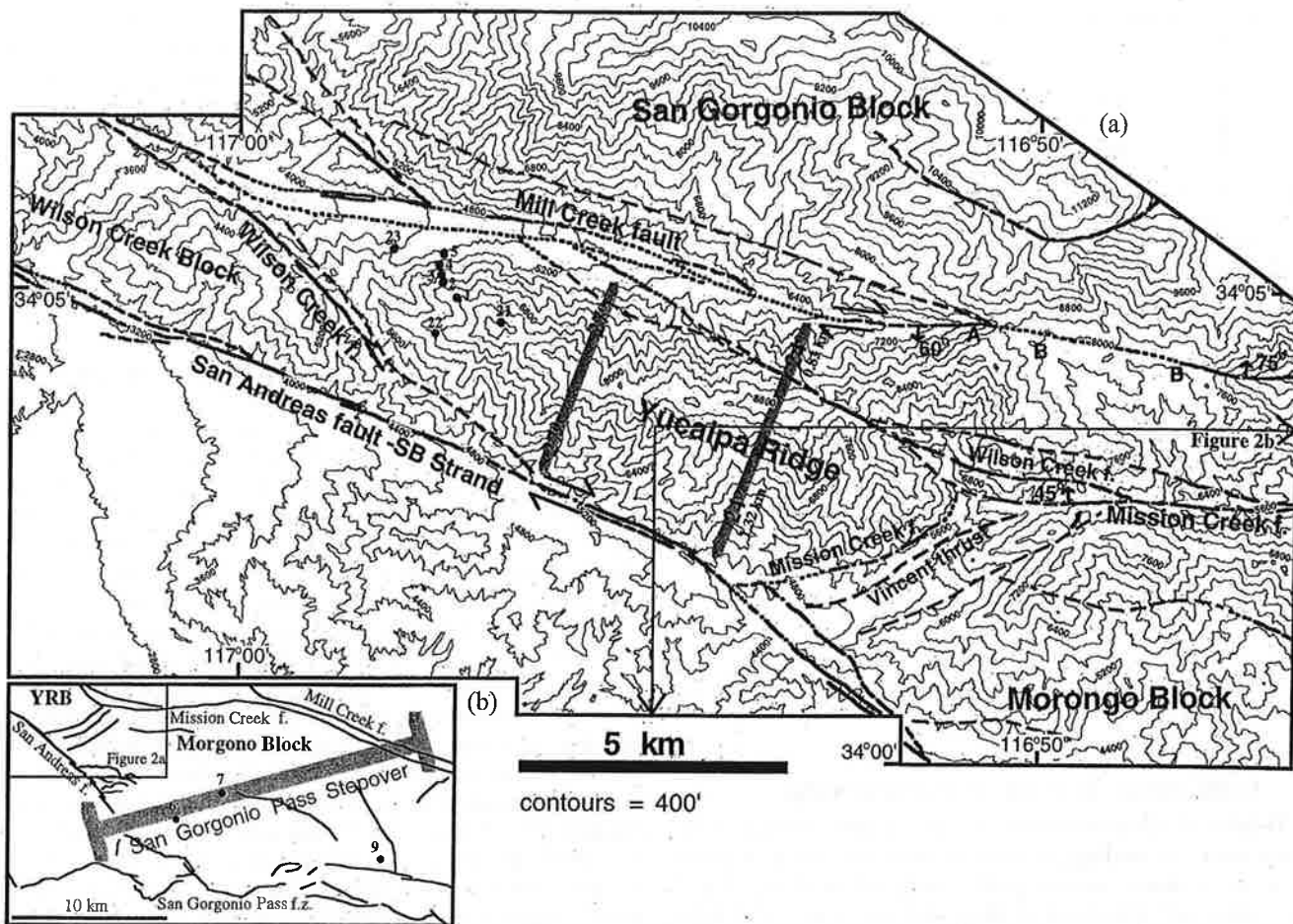
The Santa Ana basin has a three-phase history. There was a Tertiary Santa Ana basin that is quite distinct from the Quaternary basin; the two are separated by a phase of considerable uplift in the San Bernardino Mountains. The Santa Ana Sandstone was deposited in the Tertiary basin.

The Tertiary Santa Ana basin received sediment from high ground to the south as already uplifted rocks, now seen in the Sierra Pelona and Blue Ridge portions of the San Gabriel Mountains slipped along the southern margin of the basin. At the time of this sediment transfer, the crystalline basement rocks now exposed on San Gorgonio Mountain were probably buried. They were certainly located farther from the basement rocks of the

northern plateau of the San Bernardino Mountains than today, probably to the southwest.

The source of the Pelona Schist clasts in the Santa Ana basin now lies about 120 km to the northwest, separated from the basin by all the strands of the Punchbowl and San Andreas fault zones. From the discussion above and the strand sequence proposed by Matti and others (1985), it seems most likely that one strand of the Punchbowl fault and all strands of the San Andreas fault have been active since deposition of the Pelona Schist clasts. The Tertiary history of Santa Ana basin offers no evidence for the apportionment of the 120 km between these strands.

Presumably as a result of the restraining bend in the San Andreas fault system, San Gorgonio Mountain was uplifted and forced northwest into the Santa Ana basin. The basin folded immediately north of the San Gorgonio block; to the east and west the basinal deposits were simply tilted northward. The deformation extended to basement rocks north of the basin, which rose as a thrust-bound plateau, and partially overrode the Tertiary basin fill. The elongate form of the Quaternary Santa Ana basin thus developed as a welt in a region of general uplift and compression. Streams that drained the slopes of the basin were integrated into the modern Santa Ana River by capture.



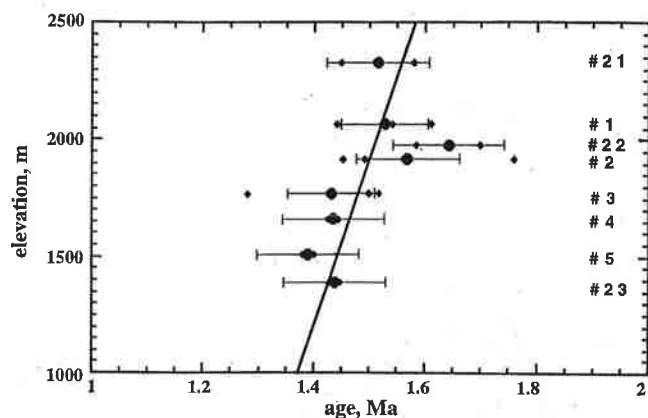
**Figure 2.** (a) Map of Yucaipa Ridge and associated faults of the San Andreas system, based on *Spotila and Sieh* [2000] and topography from 1:62,500-scale maps. The main faults are the San Bernardino (SB) strand, which is the active strand of the San Andreas system, and the Mill Creek fault, which is thought to have been the main strand in the mid to late Pleistocene [*Matti et al.*, 1992]. Dips on the Mill Creek and Mission Creek fault are from *Allen* [1957]. Sample locations for (U-Th)/He analysis are indicated. Hillslope gradients from the north to south sides of the ridge for two profiles (gray lines) are labeled 27° and 24°. For the eastern profile the gradient is the same on both the north and south hillslopes, despite different reliefs (labeled). Location of the Mill Creek jumpoff is labeled (A), as is the location of gravels (B) that have been offset a minimum of 8–10 km along the Mill Creek fault from their source [*Matti et al.*, 1992]. (b) Smaller scale map, showing the three sample locations in the Morongo block of San Gorgonio Pass. Location of this map is referenced on Figure 2a.

#### 4. Results

Apatite helium ages from the vertical transect along Yucaipa Ridge are young relative to ages measured on other crystalline mountain blocks in the region [*Spotila et al.*, 1998; *House et al.*, 1997; *Wolf et al.*, 1997; *Reiners et al.*, 2000] and vary only slightly with elevation (Table 1). Ages are between  $1.4 \pm 0.09$  and  $1.6 \pm 0.10$  Ma and increase erratically with elevation (Figure 3). These ages are consistent with but are more precise than those presented in our earlier work on the Yucaipa block [*Spotila et al.*, 1998] and are similar to fission track ages on two of the same samples (SBHe21 and SBHe23 [*Blythe et al.*, 2000b]). The steep gradient of average apatite age with elevation indicates an apparent exhumation rate of  $\sim 7$  mm/yr (Figure 3). The large uncertainty in this slope stems from the fact that error bars on individual ages are nearly as great as the total range in age for the entire sample set. This suggests that the Yucaipa block experienced extremely rapid denudation and cooling for a several hundred thousand year period

roughly 1.5 Myr ago. Apatite ages from the Morongo block are slightly older than from Yucaipa Ridge ( $\sim 5$ –13 Ma), suggesting that this block has experienced less exhumation in the past few million years.

Titanite was recovered in only three of our eight samples from the Yucaipa block. Titanite helium ages are much older than apatite ages (Table 2), ranging from  $\sim 82$  Ma at the ridgetop (2323 m) to  $\sim 57$  Ma midslope (1658 m). These ages show that the rapid exhumation of the last few million years did not exhume rocks from temperatures greater than the base of the titanite helium partial retention zone ( $\sim 210^\circ\text{C}$  [*Reiners and Farley*, 1999]). The rocks had to have been cooler than this temperature, or above  $\sim 6$  km depth (assuming a  $30^\circ\text{C}/\text{km}$  geothermal gradient, see section 5), throughout most of the Cenozoic, given the amount of helium that they contain. This restricts the total exhumation experienced by the block during the most recent stages of transpressive deformation. The gentle slope of titanite age versus elevation further indicates either



**Figure 3.** (U-Th)/He apatite ages plotted against elevation for the eight samples from Yucaipa Ridge. Individual ages are shown as small diamonds, and average ages are shown as large diamonds. Error bars are  $2\sigma = 8.6\%/n^{1/2}$ , where  $n$  is the number of replicates. A regression line is shown based on a regression analysis treating helium age as the dependent variable ( $\beta = 0.00015 \text{ Myr m}^{-1}$ ,  $1/\beta = 7 \text{ mm yr}^{-1}$ ,  $R^2 = 0.30$ ).

very slow cooling or crustal stasis for a prolonged period during the Cenozoic.

### 5. Exhumation History of Yucaipa Ridge

To infer an exhumation history from our data, we must make assumptions regarding geothermal gradient. As a starting point, we assume a constant geothermal gradient of  $30^\circ\text{C km}^{-1}$  and ignore additional complexities such as the effect of fluid flow on cooling. This is the median gradient typically reported for present-day southern California and the vicinity of the San Andreas fault zone [Wright, 1987; Lachenbruch et al., 1985; Sass et al., 1992]. At shallow depths this gradient is likely perturbed by the overlying topography of the ridge. We approximate this effect by treating the 5-km-wide ridge as a part of periodic topography [Turcotte and Schubert, 1982; House et al., 1998]. The gradient is slightly reduced directly beneath the ridge and increased beneath the adjacent valleys, but isotherms in the range of expected closure temperatures for rapidly cooling apatite ( $70\text{--}100^\circ\text{C}$  [Wolf et al., 1996]) are not significantly perturbed (Figure 4a). This was likely valid for the duration of the block's exhumation, given the likelihood that the ridge maintained steady state relief. However, there may have been a significant perturbation of geothermal gradient due to exhumation-induced advection. We further assume that the present-day elevation differences between samples represent their depth differences during cooling. This assumption is supported by a lack of evidence for significant tilting and by the minimal horizontal separation between samples (Figure 2a).

Simple inferences of the block's exhumation history can be made directly from our data. Apatite helium ages indicate that the block experienced a period of rapid exhumation within the last several million years. The rate of this exhumation is illustrated by the lack of significant age increase with elevation (Figure 3). During this period the block had to have experienced a minimum amount of exhumation to expose the base of the helium partial retention zone above the highest elevation sample. A geothermal gradient of  $30^\circ\text{C/km}$  would put the base of the partial retention zone at  $\sim 3\text{-km}$  depth, thus requiring a minimum exhumation of  $\sim 3\text{ km}$ . An additional 1 km of surface uplift is also required to generate the 1-km relief of the ridge. Titanite helium ages provide an upper limit to the amount of recent exhumation. None of our samples could have been exhumed from below the titanite partial retention zone in the last few million years because their helium contents require  $>57 \text{ Myr}$  of radiogenic production. The base of this zone lies at  $\sim 6.7\text{ km}$  depth for a gradient of  $30^\circ\text{C km}^{-1}$ , such that the top of the block must have been at  $\leq 5.7\text{ km}$  depth prior to rapid exhumation. This limits the amount of recent exhumation along the ridge top to a maximum of  $\sim 5.7\text{ km}$ .

Model thermal histories more tightly define the exhumation the block experienced over the past several million years. We tested candidate thermal histories by comparing ages predicted by numerical solutions of the helium production-diffusion equation to measured ages [Wolf et al., 1998]. A representative thermal history for the Yucaipa block is shown in Figure 4b. The time-temperature paths shown for the bottom and top samples predict respective helium ages of 1.45 Ma and 1.58 Ma, which match our observations (Figure 3). They further predict  $\sim 210^\circ\text{C Myr}^{-1}$  cooling between  $\sim 1.25$  and  $\sim 1.65$  Ma, which translates to  $\sim 7 \text{ mm/yr}$  exhumation and matches the observed elevation-age gradient. The position and slope of this rapid-cooling segment of the thermal history cannot be significantly changed without resulting in helium ages that do not match our results.

The cooling proceeding and prior to this segment are more poorly constrained. The final 1–2 km of exhumation occurred after 1.25 Ma and is not included in the well-constrained, steep portion of the cooling path (Figure 4b). This exhumation could have continued at  $7 \text{ mm yr}^{-1}$  and terminated at  $\sim 1 \text{ Ma}$ , or it could have decelerated to as low as  $\sim 1 \text{ mm yr}^{-1}$  and continued to the present. Geologic data do not demonstrate whether exhumation or surface uplift continue today. Youthful topography and south-side-up scarps along the Mill Creek fault in late Pleistocene alluvium [Farley, 1979; Matti et al., 1992] suggest that rock uplift continues, but the incised character of the Mill Creek jump-off (Figure 2a) implies that recent erosion also relates to base level lowering of the trunk stream. The exhumation rate prior to 1.65 Ma is also poorly constrained. The  $\geq 2\text{ km}$  of exhumation that brought samples from the titanite partial retention zone to the bottom of the apatite

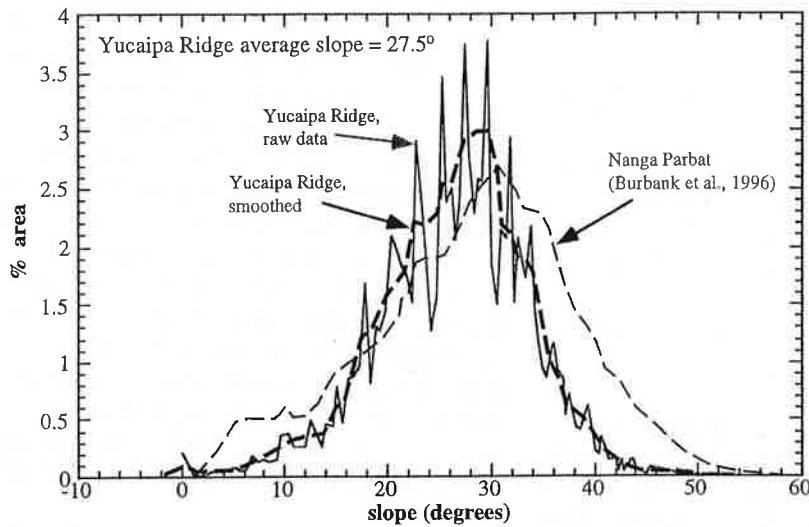
**Table 2.** Titanite Data

Sample	Elevation, m	Latitude $\times$ Longitude	Rock Type	He, nec	U, ng	Th, ng	Measured Age, Ma	Average Age, <sup>a</sup> Ma
SBHe21-1	2323 $\pm$ 6	116.9453 $^\circ$ $\times$ 34.0778 $^\circ$	qg	223	11.9	44.6	81.8	81.8 $\pm$ 8
DYJS3-1	1768 $\pm$ 24	116.9587 $^\circ$ $\times$ 34.0860 $^\circ$	qd	17.2	1.33	3.00	69.7	69.4 $\pm$ 7
DYJS3-3				24.7	1.94	4.28	69.0	
DYJS4-2	1658 $\pm$ 24	116.9590 $^\circ$ $\times$ 34.0873 $^\circ$	qd	9.81	0.69	3.09	57.1	57.1 $\pm$ 6

<sup>a</sup>With  $2\sigma$  error bars of 10%.



JGR, 2001

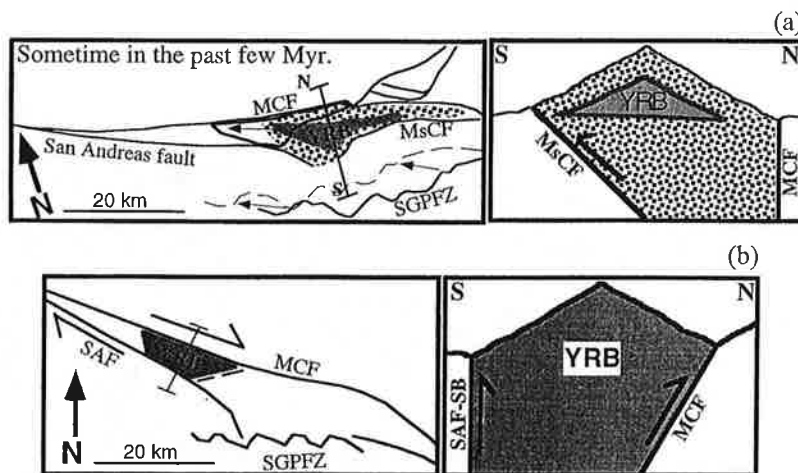


**Figure 5.** Slope distribution along Yucaipa Ridge (solid gray line (raw data) and dashed line (smoothed)), based on 90-m-resolution digital elevation models. The slope distribution of the Nanga Parbat-Haramosh massif in the northwest Himalaya is also shown at the same scale (thin dashed line), based on work by Burbank *et al.* [1996].

## 8. Mechanism of Yucaipa Block Exhumation

Before conclusions can be drawn from the rapid exhumation of Yucaipa Ridge the mechanism of its denudation must be examined. Spotila *et al.* [1998] proposed several mechanisms for localized exhumation adjacent to the San Andreas fault, but several of these were ruled out as being inconsistent with the timing of exhumation. Our new data still argue that exhumation of the Yucaipa block occurred too recently to be associated with a subsurface bend in the San Andreas fault that may presently sit below Valyermo [Meisling and Weldon, 1989],

the oblique termination of the San Jacinto fault against the San Andreas [Morton and Matti, 1993], or with motion along the Cucamonga thrust prior to horizontal translation along the San Andreas fault [Spotila *et al.*, 1998] (Figure 1). One mechanism that may be consistent with new data is convergence due to the restraining bend in the San Andreas fault at San Gorgonio Pass (Figures 1 and 6a). Spotila and Sieh [2000] explore this as a possible cause for uplift of the entire San Bernardino Mountains on the basis of mainly the spatial association of horizontal shortening in the range and the location of the fault bend. If



**Figure 6.** (a) Uplift of the Yucaipa Ridge block (YRB) via convergence associated with the small restraining bend in San Gorgonio Pass. The position of the Yucaipa block prior to  $\sim 10$  km right slip on the Mill Creek fault (MCF) in the mid to late Pleistocene [Matti *et al.*, 1992] is shown schematically as the shaded polygon, whereas the present position is shown as the open polygon to the northwest. The block could have uplifted due to slip along the Mission Creek fault (MsCF) while in this position, as shown schematically in cross section. The block is shown wider (stippled area) than its present geometry because of the greater width of the fault zone in the step over. Uplift is unlikely to have occurred due to slip on the San Gorgonio Pass fault zone (SGPFZ) because it too would have been  $\sim 10$  km farther southeast at the time. (b) Schematic map and cross section illustrating rock uplift of Yucaipa Ridge in its present position due to slip partitioning and reverse motion along the Mill Creek fault and/or San Andreas fault (SAF).

aces of these landslides.

Continue on Highway 38 to the Mill Creek ranger station. Parking, rest rooms, water, and information on road and fire conditions are usually available. Note mileage. 1.3 miles beyond the ranger station, after crossing Mill Creek bridge, the road skirts a toe of landslide debris. At 1.7 miles park in a large turnout to the right that is opposite a near vertical, fresh road cut.

A complex landslide (Fig. 6) developed in the Mill Creek Formation can be seen back down the road. The recent scar is vegetation free and includes steep active scarps. The vegetated slopes above show numerous nested scarps. The scar and scarps that are visible from this stop are a small part of a much larger ancient slide that occupies nearly all of this flank of Morton Peak (Fig. 5). Locally high moisture content in the slide material supports more vigorous brush, so the whole slide complex appears relatively pink in color-infrared (CIR) images, as contrasted with adjacent areas.

Several factors contribute to the instability of this slope. This part of the Mill Creek Formation consists of competent sandstones and conglomerates interbedded with shale. The proportion of shale is greatest

near the base of the slope. Thus the material of the slope includes zones of weak lithology. Surrounding outcrops suggest that bedding initially dipped at 20-25 degrees out of the slope near the crest and less steeply at the foot, providing potential slip planes. Erosion by Mill Creek at the toe of the slope leaves the beds unsupported down dip. Finally, the slopes are close to the active strand of the San Andreas fault, and consequently subject to intense seismic shaking. The moderate north Palm Springs earthquake (magnitude 5.9; July 8, 1986) was over 45 km to the southeast, but dislodged boulders onto the dirt roads of Yucaipa Ridge.

Furthermore, natural and artificial factors promote continued movement of the slide. Any stabilizing buttress of failed material that might naturally accumulate at the toe of the slope is subject to episodic removal by stream erosion. Clearance of slide debris from the highway has the same effect. This portion of Highway 38 is difficult to maintain. There was extensive damage in the floods of 1969, and road closures in the hard winters of the late 1970's to remove landslide material.

Figure 6 indicates the location of a facies change from gray-green conglomerates to buff sandstone at a slope break, high on

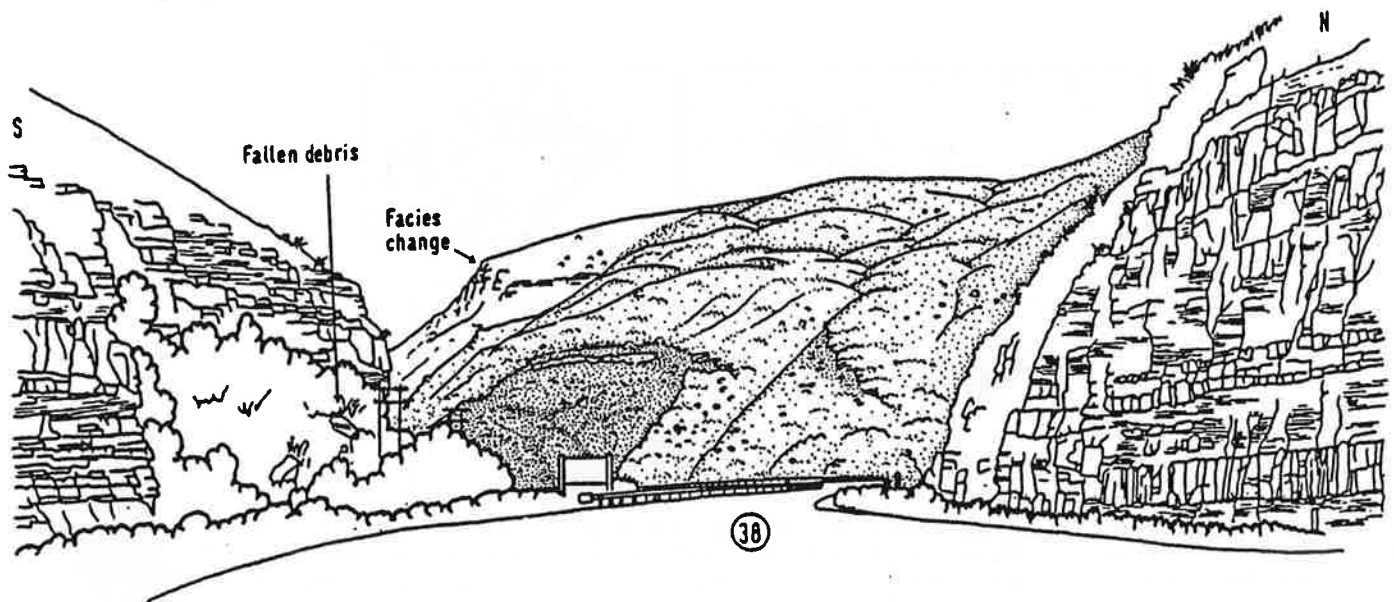


Figure 6. Landslide scar (stippled) at Highway 38 below Morton Peak.

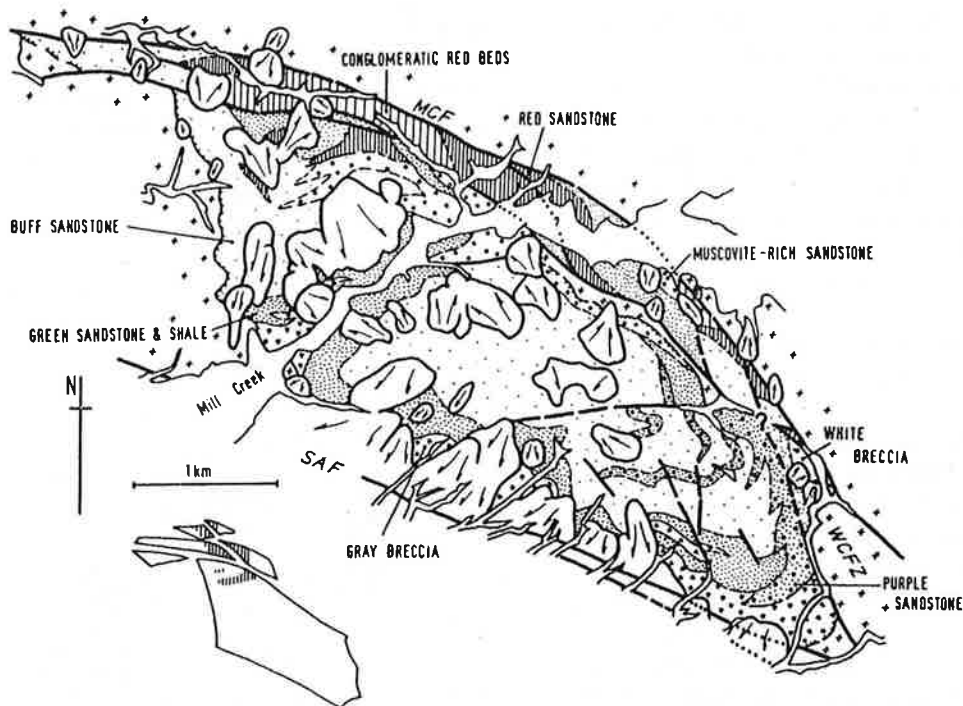


Figure 4. Simplified geologic map of sedimentary facies of the Mill Creek Formation and Potato Sandstone in the Mill Creek area. Arrows indicate landslides; crosses, crystalline basement rocks. Inset shows the most conservative strike-slip restoration of the Yucaipa Ridge and Wilson Creek fault zones; it collects together outcrops of silty redbeds (ruling).

### Axial Facies

The sedimentary sequence in the basin axis is described in terms of two facies, beginning with the older.

**Green Sandstone Facies.** Thin-bedded gray-green sandstone and shale form the base of the fill, or the oldest exposed facies, in the center of the basin. This basal facies is characterized by several tens of meters of interbedded shale and dark gray-green, micaceous wacke with subordinate calcareous shale, and algal limestone. The sandstone beds are typically bounded by well-defined, parallel, bedding surfaces, but packets of several beds are locally deformed into isoclinal slump folds. Some of the thinner sandstones (less than 15 cm) show complete or partial sets of the internal structure sequence described by Bouma (1962) from turbidites. These beds are rarely conglomeratic. The thicker sandstone beds have sharp bases and a pervasive parallel lamination, that is often contorted by soft-sediment deformation. Bed thickness generally increases up-section, where thick, cross-bedded packets of conglomeratic sandstone interfinger with the sandstone and shale. The proportion of interbedded shale decreases up-section. Where conglomeratic sandstone dominates in the upper part of the section, parallel bedding surfaces are replaced by less regular, scoured contacts. Plant remains are abundant in the sandstone; ostracods occur in the shale and limestone.

The granule- and pebble-sized clasts in the conglomerates are not readily compared with the coarser clasts in the conglomerates of other facies. As a result of the fine grain size, quartz and

feldspar clasts are abundant. Some conglomeratic layers contain Pelona Schist fragments.

The basal, green sandstone facies is interpreted to be of lacustrine origin, representing the bottomset and lower foreset deposits of a southeastward prograding, "Gilbert-type" delta (Stanley and Surdam, 1978). The bottomset beds, which have incomplete Bouma sequences of internal structure, resemble lacustrine turbidites described elsewhere (Ludlam, 1974; Sturm and Matter, 1978). Ripple lamination, grain orientation, and sole marks indicate transport from the north and northwest (Gibson, 1964; Demirel, 1985). The uppermost part of the sequence exhibits the fluvial character of topset deltaic deposits, and passes conformably upward into a buff sandstone facies that fills much of the basin.

**Buff Sandstone Facies.** The younger and more extensive axial facies is dominated by light buff-colored, massive, and thick-bedded conglomeratic sandstone, interbedded with greenish brown shaly siltstone. Thick sets of tabular cross-beds occur near the transition to the basal green sandstones. The sandstone in this younger axial facies is still micaceous, but biotite is much more abundant and chlorite is less abundant than in the underlying green sandstones. The facies may exceed 1,000 m in thickness, but probably consists of thinner imbricated packets. The most abundant conglomeratic beds have clasts of biotite quartz monzonite, leucocratic granitoids, biotite gneiss, and schist. The proportion of gneissic clasts is rather variable. Hornblende-bearing granodiorite and diorite clasts are present in some beds. These



characteristic conglomerate beds are intercalated with subordinate conglomerates of different composition. Near the base of the unit there are conglomeratic beds with Pelona Schist clasts, and others with andesite clasts. Near the top of the unit in the northwest, conglomeratic beds appear that are dominated by muscovite- and garnet-bearing granitoid clasts. To the southeast, andesite clasts appear in an increasing proportion of conglomerate beds. All these minor, but compositionally distinct, conglomerate beds are distal intercalations of facies from the margins of the outcrop.

The buff sandstone facies is interpreted as braided stream deposits atop a shallow delta that prograded into the basin from the north-northwest.

**Age and Provenance.** The axial facies provide the only evidence for the age of the Mill Creek Formation. Fossil plants from the green sandstone and buff sandstone members of the formation, collected by Owens (1959), Smith (1959), and Gibson (1964), were identified by D. I. Axelrod, who inferred an "early Pliocene" age to be most likely. He reported to Gibson (1964, p. 9) that the flora might be "as old as Late Miocene or as young as mid-Pliocene," but the boundary of these time-stratigraphic units had not then been re-calibrated to the currently accepted age of 5 Ma. Using more recent equations of floras with land mammal faunas, Woodburne (1975, p. 69) translated the age determination to Clarendonian; this implies that age of the Mill Creek Formation is more likely 10 to 13 Ma. Even for this age the sandstones might be considered unusually well indurated. But induration would have been accelerated by the high content of detrital phyllosilicates and perhaps a high heat flow in the fault zone.

Abundant sedimentary structures indicate that most of the axial deposits entered the basin from the northwest (Gibson, 1964, 1971; Demirer, 1985). The clasts in the conglomerate beds are rounded, so the sources were not necessarily close. Also, since paleoflow directions in the center of a basin probably reflect redirection by the axial topography, the position of sources is not accurately indicated. The rather nondistinctive granitoid and gneissic clasts in the buff sandstones might be derived from the Little San Bernardino Mountains. We show below that the conglomerates of the Potato Sandstone are similar.

Smith (1959, p. 30) reported a limestone clast with well-preserved Permian fusulinids from the buff sandstone facies. The source of this clast is not known, but we suggest that it was not the Furnace Limestone of the San Bernardino Mountains, north of Big Bear Lake. We have found fusulinids in marbles at localities where Richmond (1960) reported corals and brachiopods from the Furnace Limestone. Unlike Smith's find, nearly all of these fusulinids were too recrystallized to preserve diagnostic wall structures. Furthermore, Furnace Limestone crops out in close association with very resistant Cambrian and Pre-Cambrian quartzites; the limestone is unlikely to become part of a detrital assemblage such as the Mill Creek Formation that lacks quartzite clasts.

### Marginal Facies

Three marginal facies can be distinguished from the sediments of the basin axis by major differences in composition that impart distinctly different colors (Figs. 5, 6). Where exposed, the northern and southern flanks of the basin are each occupied by a single alluvial facies. A fluvial facies occupies the southeast corner. These facies and possible sources for them are described below in anticlockwise sequence, beginning on the south flank.

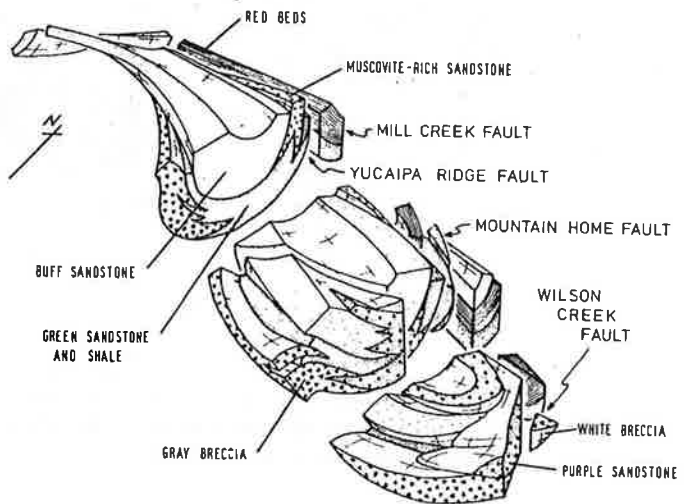


Figure 5. Block diagram of structure and lateral facies relationships in the Yucaipa Ridge syncline and adjoining fault zones. Simplified from Figures 3 and 4.

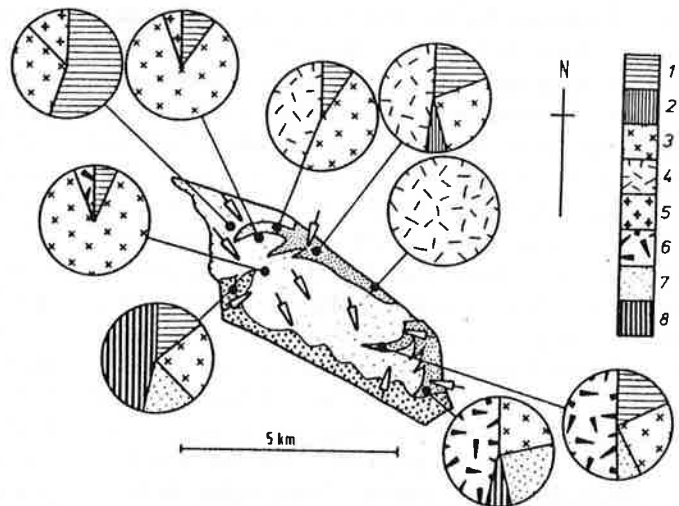


Figure 6. Provenance of the Mill Creek Formation. Arrows summarize paleocurrents determined from sedimentary structure. Proportionally divided circles show composition of clast suites in conglomerates. Key to numbers: 1, biotite-gneiss; 2, foliated biotite-bearing granitoid; 3, biotite quartz-monzonite; 4, muscovite-garnet-bearing granitoid; 5, hornblende diorite and granodiorite; 6, volcanic rocks, mostly andesite; 7, sandstones; 8, Pelona grayschist.

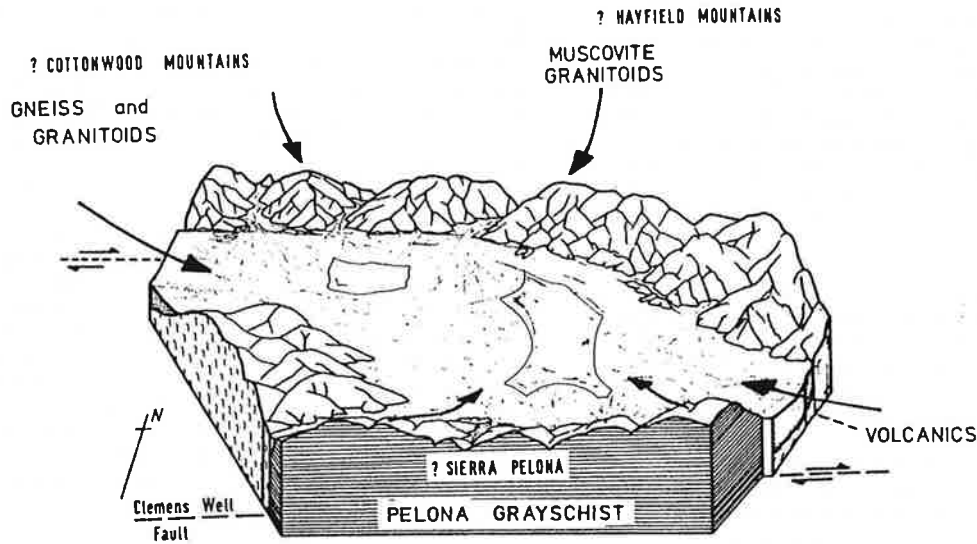


Figure 9. Speculative reconstruction of the morphology of the Mill Creek basin.

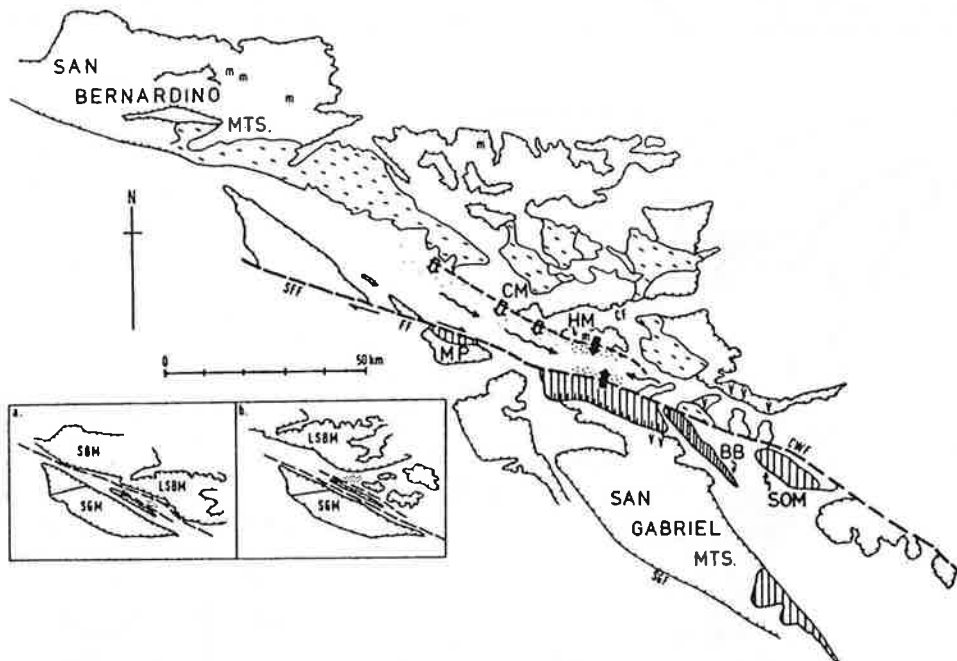


Figure 10. Suggested original location of the Mill Creek basin in the San Francisquito-Fenner-Clemens Well fault zone (SFF-FF-CWF). Outlines of modern bedrock ranges have been repositioned by restoring slip on the San Andreas fault, the San Gabriel fault (SGF), and the Chiriaco fault (CF) after Powell (1981). Vertical ruling indicates Pelona and Orocopia schist; wavy dashes, major gneiss outcrops close to basin; m's, large outcrops of muscovite- and garnet-bearing granitoids; v's, volcanic rocks; dense stipple and black arrows, deposition of Mill Creek Formation; sparse stipple and open arrows, possible deposition of Potato Sandstone. BB = Blue Ridge; CM = Cottonwood Mountains; HM = Hayfield Mountains; MP = Mount Pinos; SOM = southern Orocopia Mountains. Inset shows two stages of restoration of Mill Creek Formation (stippled) to original location. a, Slip relative to San Bernardino Mountains (SBM) and Little San Bernardino Mountains (LSBM), accomplished on Mission Creek strand of San Andreas fault. b, Slip relative to San Gabriel Mountains (sgm) accomplished by Punchbowl-Nadeau fault and Wilson Creek strand of San Andreas fault.

to be of lacustrine origin, representing the bottomset and lower foreset deposits of a southeastward prograding "Gilbert-type" delta (Stanley and Surdam, 1978). The bottom set beds include lacustrine turbidites, which typically show incomplete Bouma sequences (Ludlam, 1974; Sturm and Matter, 1978). The coarsest and uppermost part of the sequence exhibits the fluvial character of topset deltaic deposits as the basal facies pass conformably into a buff sandstone facies that fills much of the basin and oversteps the Pelona Schist-bearing gray breccias.

The buff sandstone facies is the youngest and most extensive. It is dominated by light buff-coloured, massive and thickly bedded conglomeratic sandstones, interbedded with greenish-brown shaly siltstone. The facies may exceed 1000 meters in thickness, but probably consists of thinner imbricated packets. Most of the conglomerate clasts are gneisses and schistose metamorphic rocks. The facies is interpreted as braided stream deposits resulting from paleoflow to the south-southeast.

To the southeast the buff sandstone facies interfingers with a different braided stream deposit, differentiated by paleoflow to the east or northeast, and a clast suite with volcanic rocks and reworked sandstones. It is about 400 meters thick and often of purple colour. Maximum clast size is about 15cm and the clasts are rounded. The volcanic clasts include basaltic andesite, a porphyritic hornblende andesite, a trachyandesite, vesicular basalt and a

porphyritic rhyolite. Clearly, the clast suite of this purple sandstone facies is shared with the southeastern part of the Pelona Schist-bearing, gray breccia facies. Two more facies that are best exposed in the Wilson Creek fault zone appear to interfinger with the purple sandstone facies. It is difficult to locate the western limit of the fault zone, so their assignment to the Mill Creek basin is tentative.

One of these facies is a white breccia of limited extent near the eastern edge of the basin. It is a coarse basal unit, with a maximum thickness of 150 meters, previously mapped as plutonic basement and/or fault breccia. This white breccia facies interfingers with the fluvial purple sandstone facies and probably also with the lacustrine green sandstone facies. Dominant clast types are a more abundant porphyritic biotite quartz monzonite, and a less abundant hornblende-biotite quartz diorite. Most clasts are 3-8 cm in diameter, but a few are 25 cm in diameter. The white breccia is interpreted to be a very proximal alluvial facies.

The purple sandstone facies of the Mill Creek Basin appears to change composition northward, so that close to the Wilson Creek fault zone it includes lenses of conglomerate dominated by granitoid and granitoid-gneiss clasts, and lacking the volcanic rock clasts. Very similar rocks occur in the fault zone, and figure 1 shows how they may be represented as shingled slices of the north margin, displaced by right slip. Inclusion in the Mill Creek basin of

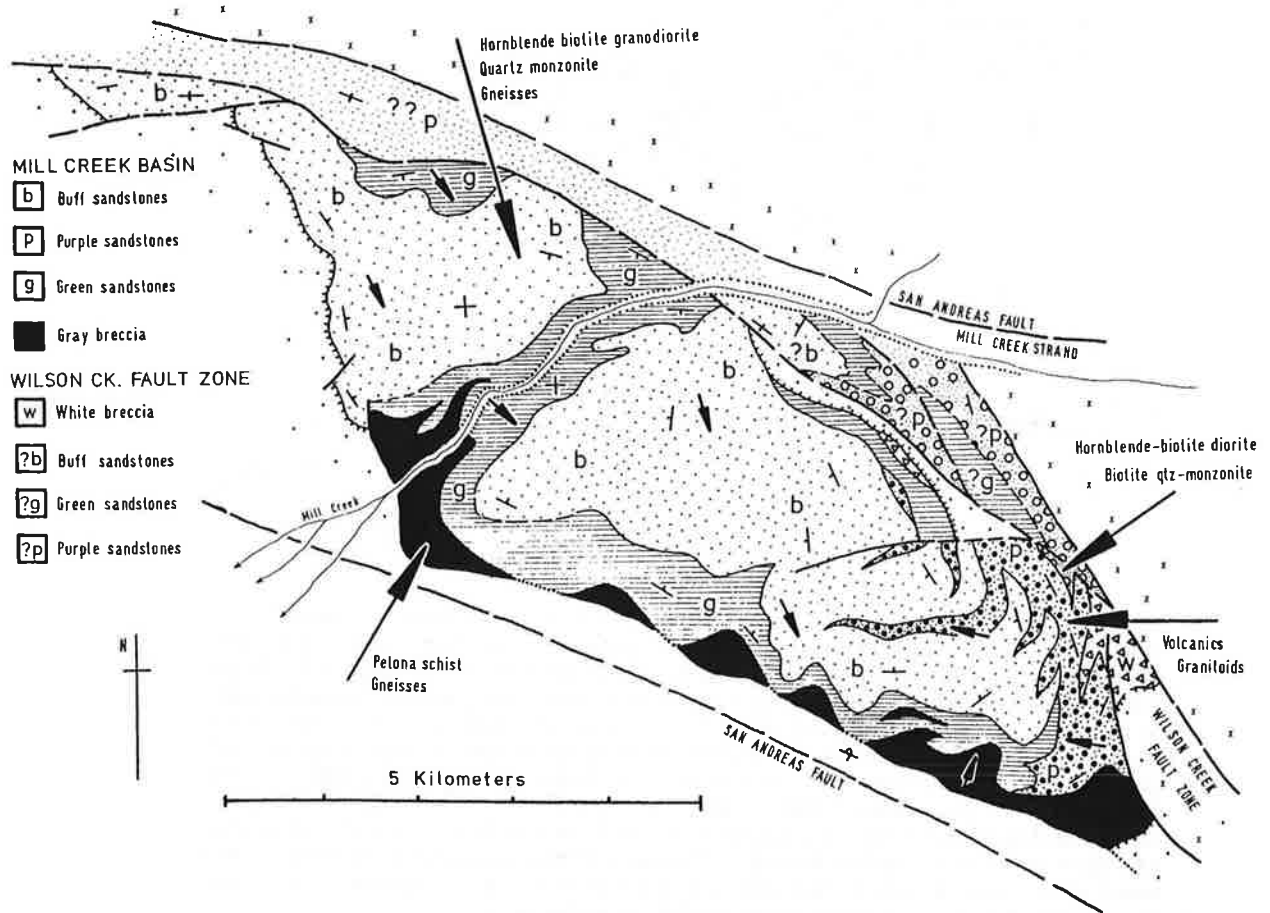


Figure 2. Facies and provenance of the Mill Creek basin. Arrows show representative paleocurrent directions. Larger arrows have lists of key clast types.



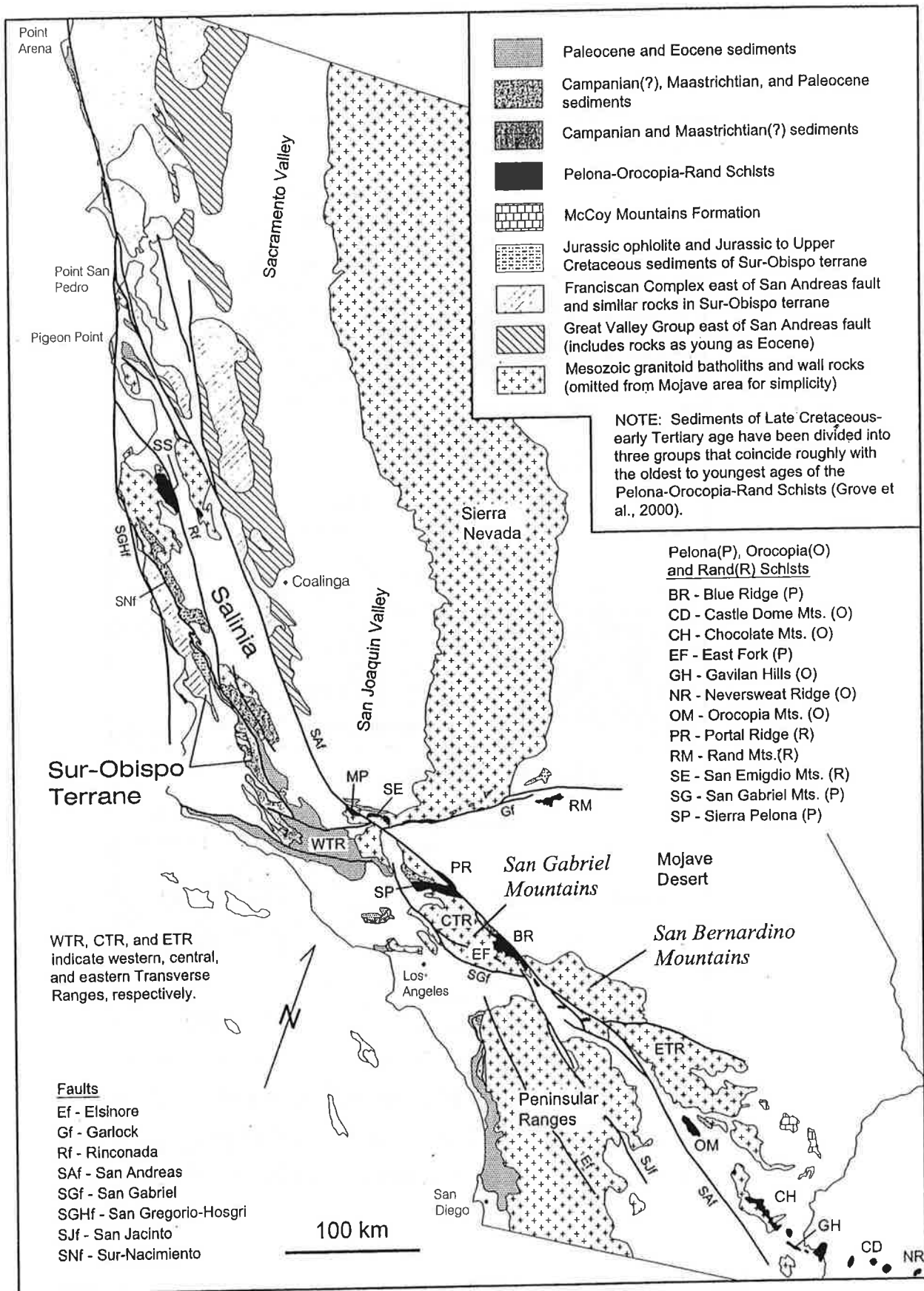


Figure 1. Simplified geologic map of southern and central California (after Jennings, 1997).

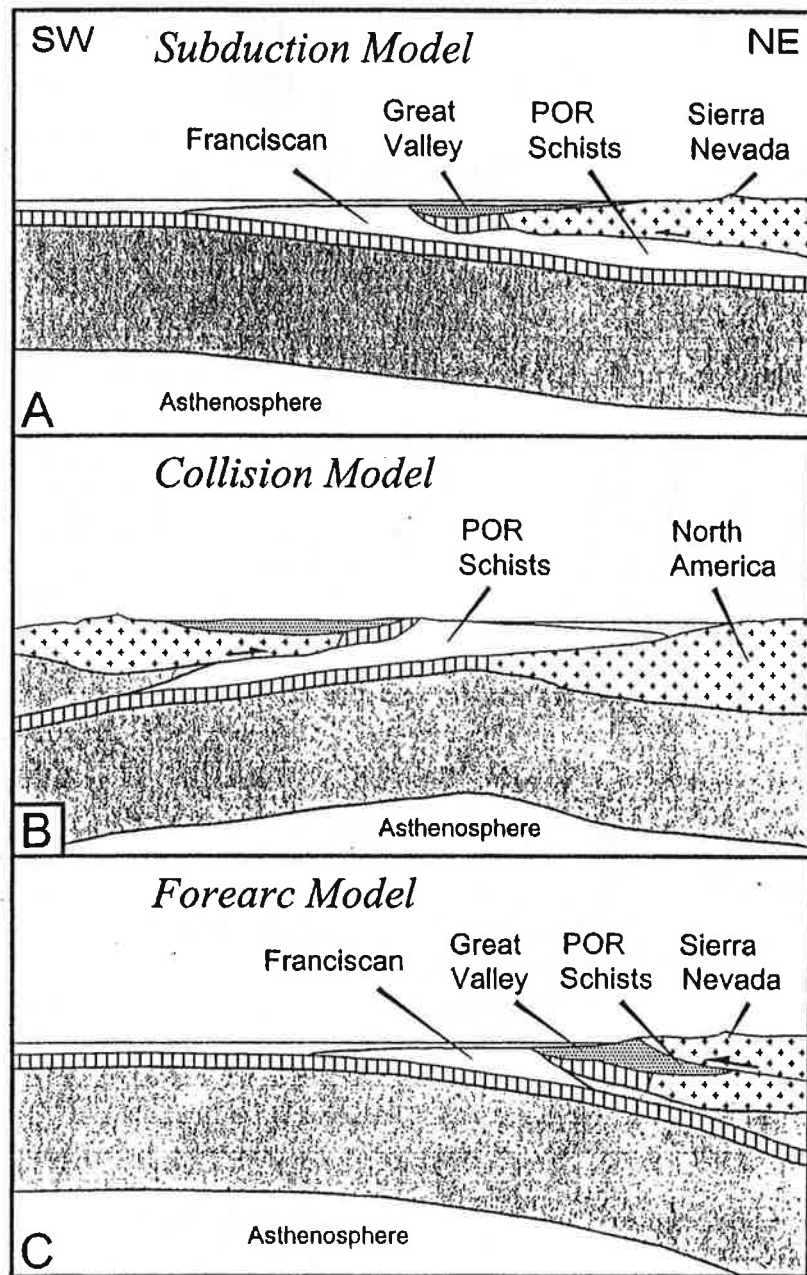


Figure 9. Models for the origin of the Pelona-Orocopia-Rand (POR) Schists. Solid gray pattern indicates oceanic and continental lithosphere.

3.. Final count was 1 fatality with reports of any missing persons being unfounded.

High-intensity short-duration rainfall produced debris flows in the late afternoon of July 11 in the community of Forest Falls. Forest Falls is located along the south side of a major canyon, Mill Creek Canyon, in the southeastern part of the San Bernardino Mountains. Mill Creek Canyon is a very steep-walled canyon developed along the Mission Creek strand ("North Branch") of the San Andreas Fault zone. Erosion of the highly fractured rock along the fault zone in this rapidly uplifting part of the San Bernardino Mountains has produced an unstable, steep-sided, deep canyon. The canyon wall on the south side of Forest Falls rises abruptly about 3,000 feet to elevations of nearly 9,000 feet at the crest of Yucaipa ridge that is underlain by a variety of gneissic rocks. Numerous avalanche chutes scar the canyon wall. Most of Forest Falls is located on bouldery debris flow deposits that form a relatively narrow shelf sloping from the base of Yucaipa ridge northward to Mill Creek. Mill Creek (Figure 1) is frequently subject to flood conditions, and has eroded the distal parts of the debris flow deposits on which Forest Falls is located. Pervasive physiographic features that typify debris flows cover the surface on which Forest Falls is located. The most evident features are widespread active debris flow channels and levees, short stretches of abandoned debris flow channels, snouts of debris flows, and remnants of debris flow levees.

Forest Falls has frequently been the site of debris flows produced primarily during periods of high-intensity short-duration rainfall during the summer monsoon season. Based on the past 45 year period of time, the recurrence interval for significant debris flows in the Forest Falls area is about 4 years. The most recent damaging debris flows prior to the July 11, 1999 debris flows was on September 4, 1997. Other relatively recent significant debris flows have occurred in 1955, 1958, 1961, 1963, 1965 (two debris flow events on two consecutive days), 1984 (two debris flow events on two consecutive days), and 1989. In the late afternoon of July 11, 1999, about 1.5" of rain fell on Yucaipa ridge south of the eastern part of Forest Falls. This intense rainfall produced boulder debris flows particularly in the small drainages of Spring Creek, Rock Creek, and Slide Creek. In these drainages the debris flows over-topped their natural channels spreading boulder debris over extensive areas. Debris flows deposited wide stretches of boulder-laden debris to depths up to about 6 feet on the only access road to Forest Falls, isolating the community until the afternoon of the 12th (Figure 2). Over 30 homes and numerous automobiles were damaged or destroyed. One confirmed fatality occurred at Spring Creek and on July 12 there were still several persons reported missing.





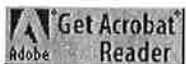
*Damage to structures produced down fan on the east side of the 3rd(?) wave of the debris avalanche (from figure 52 of this report).*

## Contents

This CD-ROM contains a Portable Document Format (PDF) file that contains 67 pages with 57 illustrations. For those who would like to use the illustrations in this report for other purposes, we have provided all 57 of them in the "illustrations" folder. The 55 photographs are in .tif format and are generally six inches in the longest dimension and 300 dots per inch (dpi). The two maps (figures 1 and 3) are in .ai8 (Adobe Illustrator(2) 8.0) format. The figure captions are also provided separately as an ASCII file (figure-captions.txt).

This report was produced under the Southern California Areal Mapping Project (SCAMP) which is part of the Western Earth Surface Processes Team at the U.S. Geological Survey

---



## View the report as a PDF

The report is provided as a PDF file for which you will need Adobe Acrobat Reader to view. You can download a copy of the latest version (5.0 at the time of this publication) by clicking the button above.

To view the PDF file (of01-146.pdf), [CLICK HERE](#) (18.1 MB).

## Download data

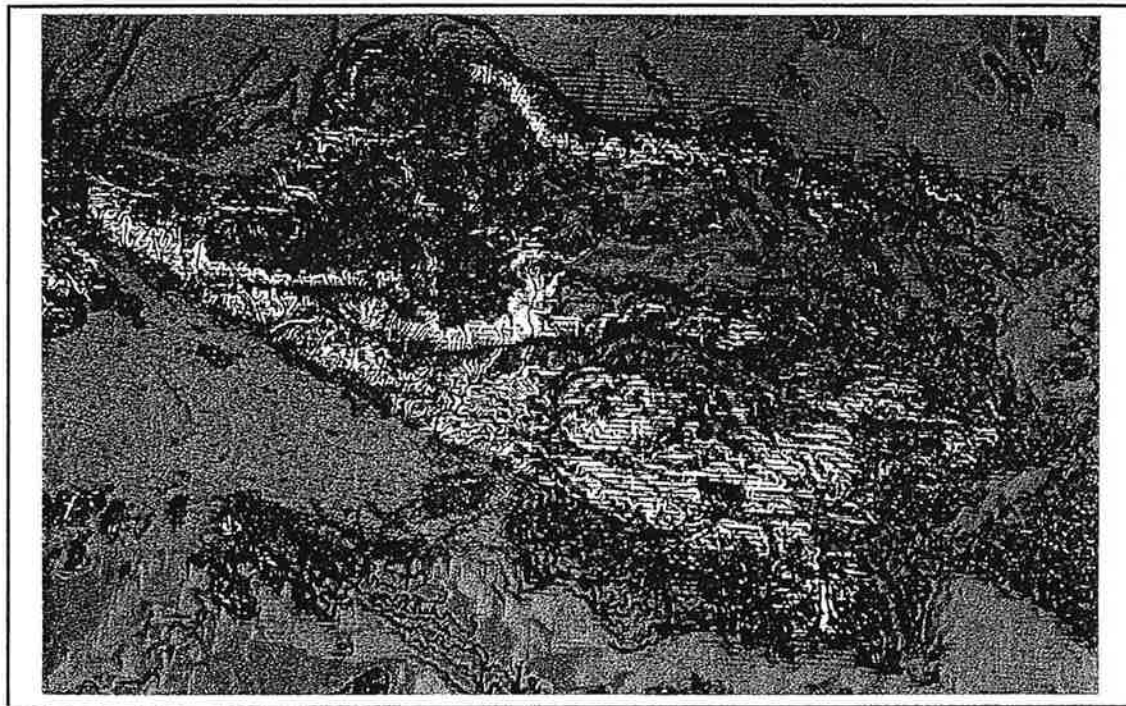
To browse the illustrations folder and download any of the image files via FTP, [CLICK HERE](ftp://geopubs.wr.usgs.gov/pub/open-file/of01-146/illustrations/).

## View the Readme file

[CLICK HERE](#) view the Readme file for CD-ROM version of this report.

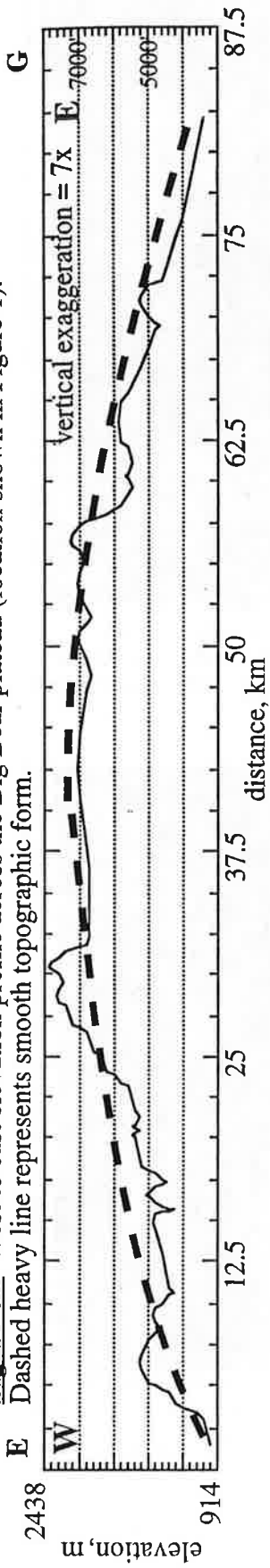


**Figure 2a:** Elevation distribution in the San Bernardino Mountains, based on the USGS 90-m-resolution digital elevation model. Elevations are color-coded in 100 m bins, with light blue as the lowest elevation (<1000 m), dark blue to purple intermediate (1000-2000 m), and red to yellow high elevation (2000-3500 m).

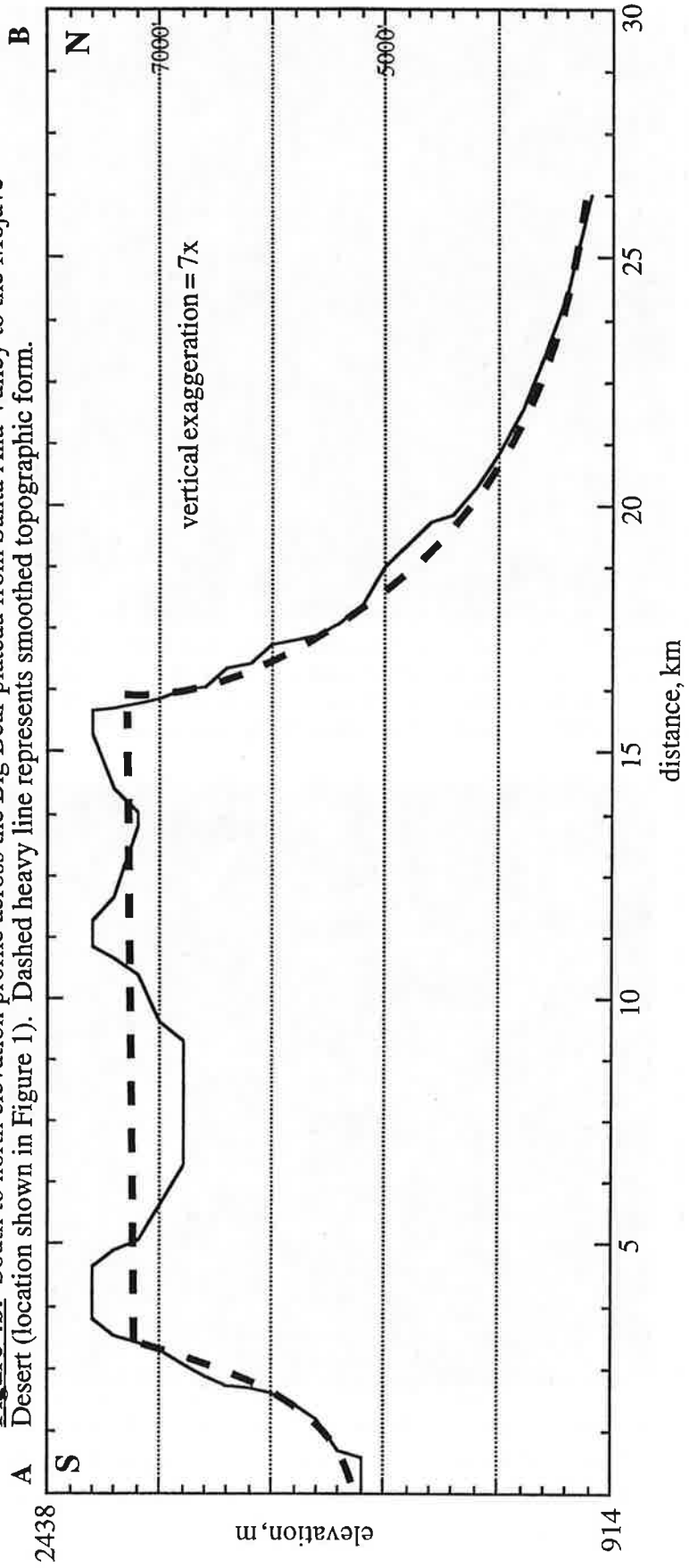


**Figure 2b:** Slope distribution in the San Bernardino Mountains, based on the elevation data shown in Figure 2a. Slopes increase from green to light blue (0-6°), to purples (7-12°), to reds (13-24°), to yellows (25-30°), to white (>30°).

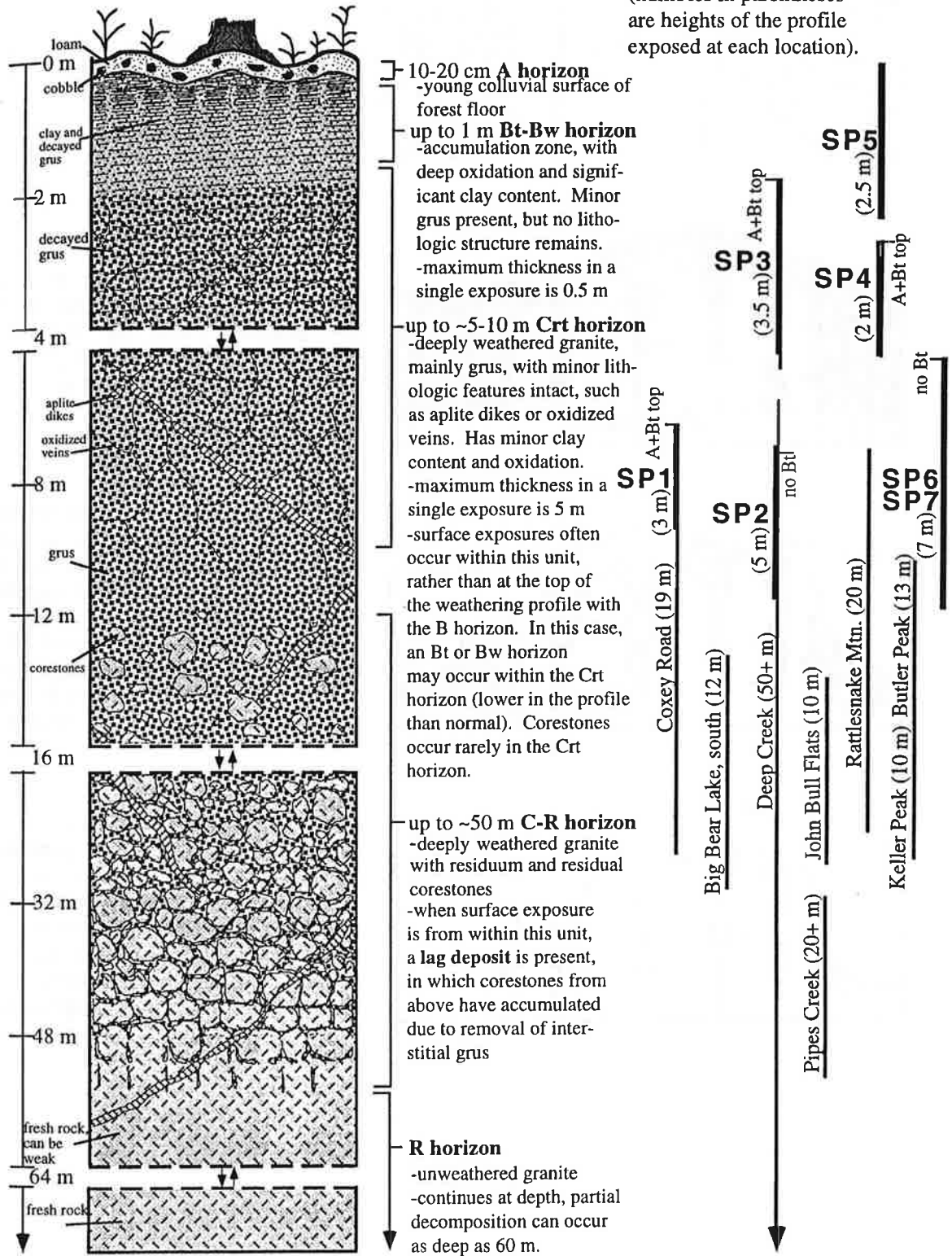
**Figure 4a:** West to east elevation profile across the Big Bear plateau (location shown in Figure 1).



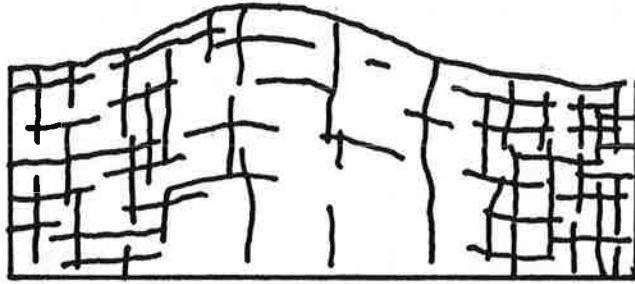
**Figure 4b:** South to north elevation profile across the Big Bear plateau from Santa Ana Valley to the Mojave Desert (location shown in Figure 1). Dashed heavy line represents smoothed topographic form.



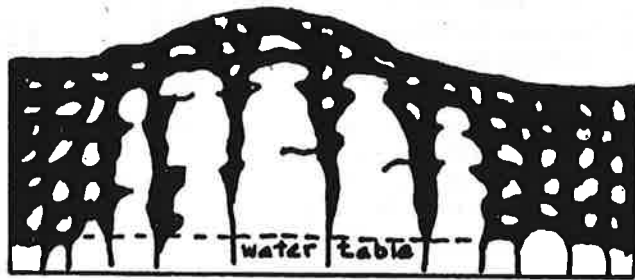
**Figure 23:** Schematic diagram of the characteristic profile of the weathered surface atop the San Bernardino Mountains. This representation is based on compilation of observations at specific locations atop the range, which expose different levels of the profile as shown on the right (refer to Figure 1 for locations). SP = soil profile.



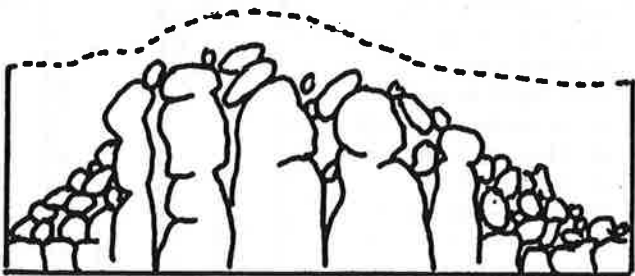




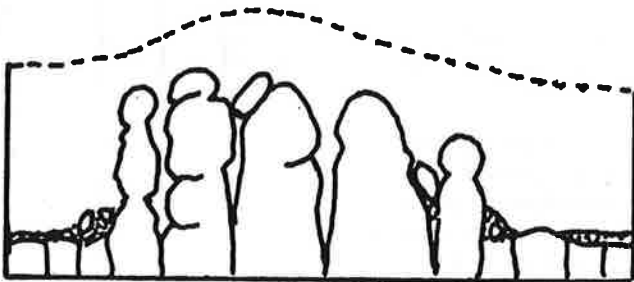
A. Vertical section through granitic rocks with a varied spacing of joints in the Miocene or Pliocene prior to the uplift of the San Bernardino Mountains.



B. During the Pliocene at a time of sub-humid climate and chemical decomposition of the granitic rocks by ground water that percolated downward along joints to the water table. The decomposed rock (grus) is shown in black.



C. Boulder-mantled slopes developed during the last few thousands of years of the Pleistocene Epoch by the removal of grus probably under more arid conditions as the San Bernardino Mountains began rising and the stream drainage network began cutting downward toward a new base level of erosion. Some of the granitic slopes in the Cactus Flat area are at this stage of development.



D. Bold, craggy inselberg-like outcrops at higher elevations on the plateau-like Cactus Flat area. These exposures have suffered longer exposure to sub-aerial weathering and erosion resulting in decomposition and removal of most of their boulder mantles, leaving abrupt steep-sided bold outcrops elevated in areas of widely-spaced joints. A thin veneer of grus may cover the surface at the bases of these crags.

Figure 5. Development of boulder-mantled slopes and rocky crags at Cactus Flat. (After Oberlander, 1972; Trent 1984).

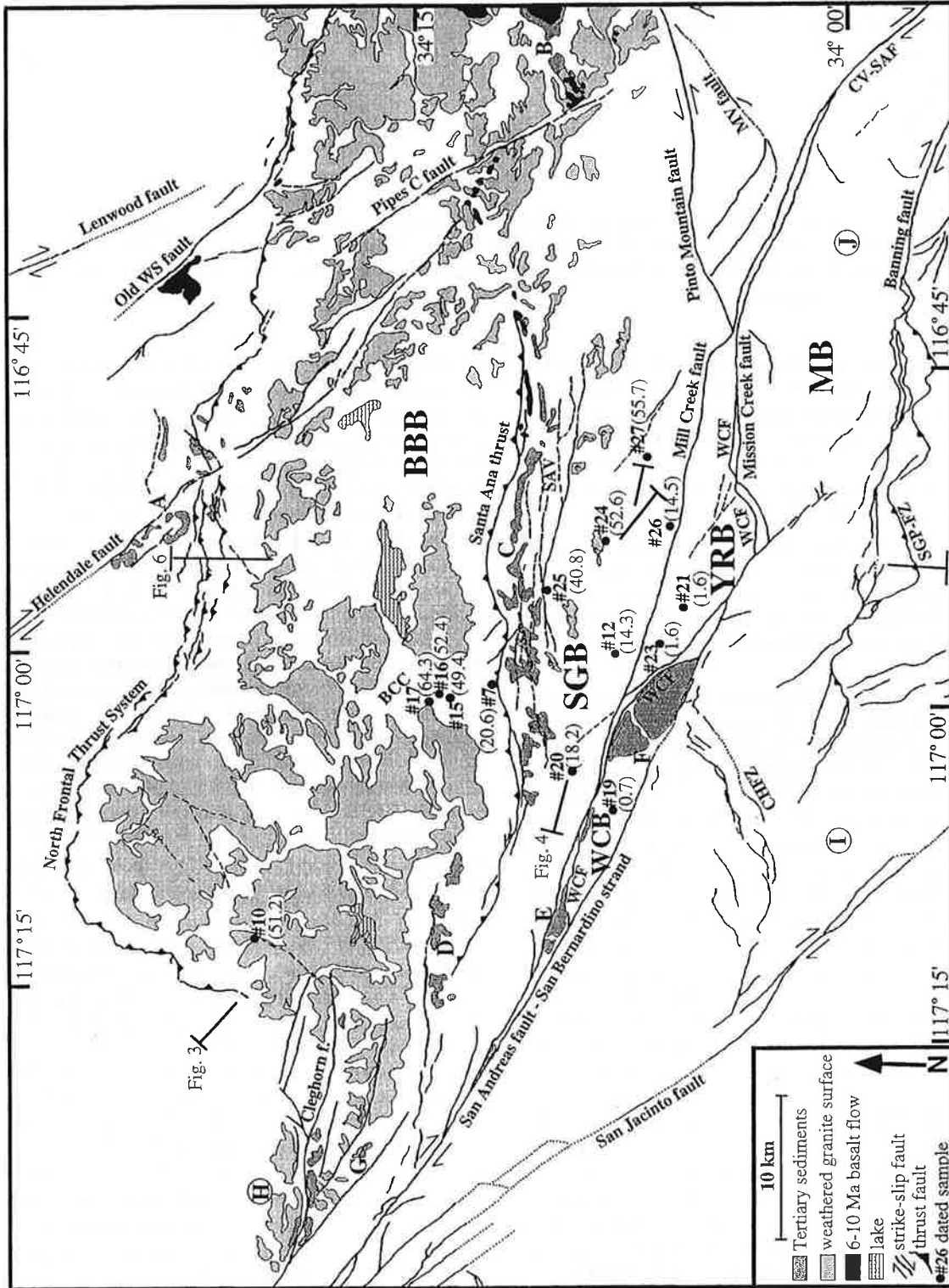
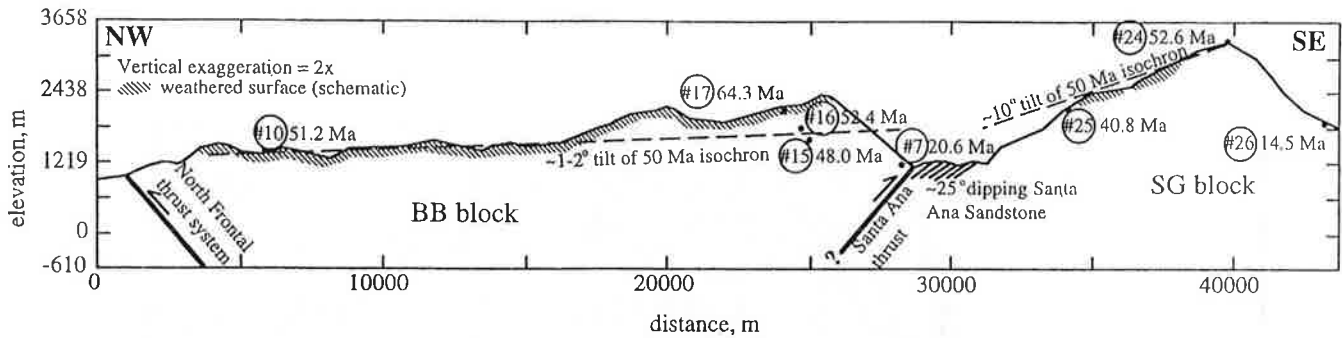


Figure 1.



**Figure 3.** Elevation profile from northwest to southeast along the Big Bear and San Gorgonio blocks. The weathered surface, shown schematically by hachures, tilts more steeply northwestward than the 50-Ma helium isochron. Helium ages from Bear Creek Canyon are projected onto this section. Line of section shown in Figure 1.

Cretaceous exhumation event associated with the Laramide orogeny [cf. *George and Dokka, 1994; Foster et al., 1991*] or cooling of a shallowly emplaced granitic pluton [cf. *House et al., 1997; Wolf et al., 1997*]. Following this rapid cooling, sample 17 had to have been cooler than the temperature range of helium partial retention ( $<40^{\circ}\text{C}$  or  $<2$  km depth for a typical geothermal gradient) to have achieved such an old age. This suggests that there has been very little erosion from the top of the BB block since the Late Cretaceous. It is also consistent with the idea that granitic weathering atop the plateau has been preserved because of very limited erosion since the Miocene [*Oberlander, 1972*].

The suite of younger helium ages beneath sample 17 along the side of Bear Creek Canyon (samples 16, 15, and 7) (Figures 1 and 2) further constrains the thermal history of the BB block. The steep age-elevation profile of these samples ( $\sim 50$  Myr/km) is indicative of very slow cooling but is not easy to interpret. Because the profile consists of only one uniform segment without a break in slope, there is no segue into the more recent thermal history of the block. The difficulty in interpreting such age profiles has been discussed in fission track studies [cf. *Gleadow and Fitzgerald, 1987*]. However, there are two end-member thermal histories involving slow cooling that are consistent with geologic constraints, which we explore below. First, the steep age-elevation gradient could have been produced by very slow, uniform uplift through the helium partial retention zone, in which case different ages would correspond to the same closure temperature, and the age gradient could be inverted for the approximate uplift rate ( $\sim 0.02$  mm/yr). The second possibility is that the ages represent temporary stagnation (zero uplift) in the zone, in which case the age gradient would have steepened with time (deeper samples retaining less helium than higher, cooler ones) and represent an exhumed helium partial retention zone when subsequently uplifted to the surface [*Wolf et al., 1997; Wolf, 1997*].

Numerical solutions to the helium production/diffusion equation determine the helium age that would be produced for a hypothetical thermal history of a given rock (based on calibration of Durango apatite [*Wolf, 1997; Wolf et al.,*

1996b]). Such numerical modeling can thus be used to test the viability of these end-member thermal histories for the BB block. To be viable, a thermal history must produce the observed set of helium ages at different elevations and meet the thermal constraints of other data, which in this case include the K/Ar ages from atop the plateau and the likelihood that the plateau was exposed to deep weathering and deposition of basalt flows in the late Miocene [*Oberlander, 1972*]. Implicit assumptions to this test are that exhumation and cooling were uniform over the horizontal distance between samples and that the present-day elevation difference between samples approximates the difference in paleodepth during exhumation and cooling.

In each case, the numerical model is run with the above constraints for different geothermal gradients on hypothetical samples separated by depths corresponding to present elevation differences. In the first thermal history, slow, constant cooling/uplift follows rapid unroofing in the Late Cretaceous. For example, the helium age from the uppermost sample ( $64.3 \pm 5.1$  Ma, sample 17) could have been produced if it cooled from  $300^{\circ}\text{C}$  to  $60^{\circ}\text{C}$  between 70 and 67 Ma, then cooled slowly ( $<1^{\circ}\text{C}/\text{Myr}$ ) to  $15^{\circ}\text{C}$  by 10 Ma, and remained at ambient surface temperature until the present. This thermal history could have produced the observed helium ages beneath sample 17 only if the geothermal gradient was  $\sim 50^{\circ}\text{C}/\text{km}$  throughout the Tertiary, which is geologically unlikely [*Lachenbruch et al., 1985*]. In the second example, a prolonged period of crustal stasis follows the rapid unroofing of the Late Cretaceous, which, in turn, is followed by a short period of exhumation. For example, the helium age from the upper sample could have been produced if it cooled from  $300^{\circ}\text{C}$  to  $40^{\circ}\text{C}$  between 70 and 67 Ma, remained at  $40^{\circ}\text{C}$  until 20 Ma, and cooled to ambient surface temperature ( $15^{\circ}\text{C}$ ) by 10 Ma. This thermal history could have produced the helium ages of the lower samples with a more reasonable geothermal gradient of  $\sim 25^{\circ}\text{C}/\text{km}$ . This suggests that the case of temporary crustal stasis gives a thermal history that is more consistent with helium ages for the BB block.

Although these numerical models are nonunique, the thermal history that best reproduces the available data

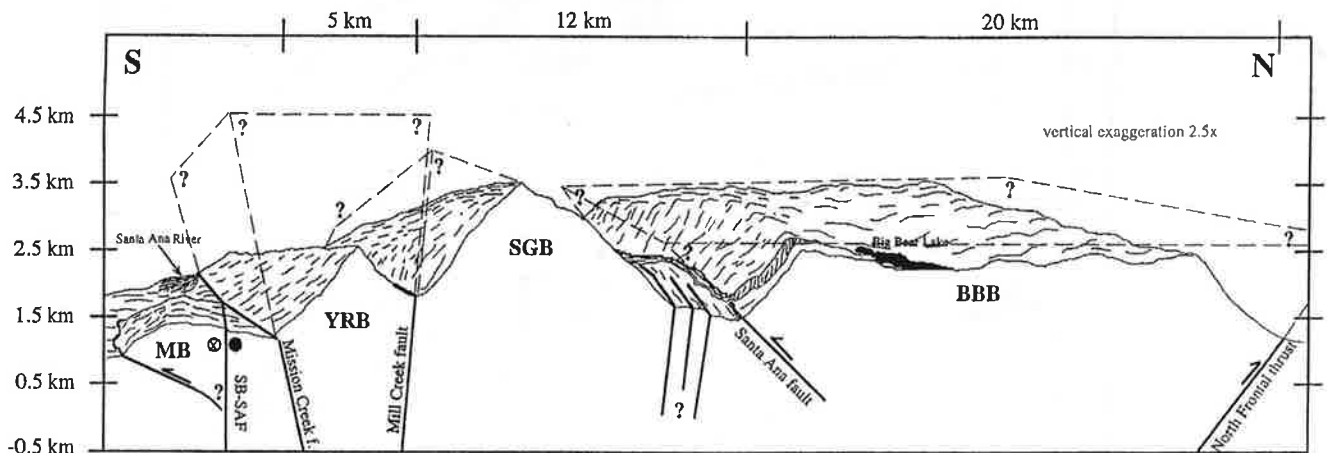
WC block, the cooling history of this block is more difficult to interpret. Suites of helium ages more tightly constrain a thermal history than does a single sample age, and the exhumation histories of the YR and WC blocks cannot be interpreted jointly because of the poor constraint on the slip history of the intervening Wilson Creek fault (Figure 1). In addition, the presence of the Mill Creek Formation (10-13 Ma) in the WC block (Figure 1) requires that both subsidence (i.e., transtension) and uplift (i.e., transpression) have occurred since the mid-Miocene [Sadler *et al.*, 1993]. For these reasons, we focus our interpretation on the magnitude and rate of exhumation of the YR block.

Given that the ages from the YR block are so young (1.6 Ma), their large errors ( $\pm 0.5$  Ma) significantly affect interpretations of cooling/uplift history. If the average ages are accepted at face value, their similarity suggests that the two samples shared cooling histories and exhumed from the helium partial retention zone at roughly the same time. Because these samples were separated by  $\sim 1$ -km elevation (Table 1), this scenario implies extremely rapid exhumation over a short period. For example, 4 km of exhumation at 10 mm/yr between 1.7 and 1.3 Ma would have resulted in nearly identical upper and lower ages (1.6 and 1.5 Ma), based on numerical solutions to the helium production/diffusion equation and the above geothermal gradient. Although even more rapid exhumation rates are permitted by these data, much slower YR block cooling is also possible given the large error bars. For example, exhumation of the block at a constant rate of 1.5 mm/yr over the past few Myr would have produced upper and

lower ages of 2.1 Ma (within error limits of sample 21) and 1.6 Ma (sample 23). In another possible case, exhumation at 2.25 mm/yr could have produced an upper age of 1.6 Ma (sample 21) and a lower age of 1.1 Ma (within error limits of sample 23). Both of these cases of uniform uplift predict  $\sim 3$ -4 km total exhumation occurred in the past 2 Myr.

More complex thermal histories are also permitted by the data, but more helium ages would have to be determined to further constrain the exhumation history of the YR block. We hope to pursue a more rigorous collection and analysis of samples from this block to improve our understanding of its thermal history. Regardless of cooling history, however, the young ages require roughly 3-4 km of exhumation in the past 2 Myr, given the above assumptions. Because there are no older helium ages from the YR block, there is also no constraint on how much exhumation occurred prior to 2 Ma.

If the YR block has risen at least  $\sim 3$ -4 km in the past 2 Myr, the present topography (just over 1-km relief above base level) requires at least 2-3 km of crust to have been removed by erosion. This suggests that the top of the YR block would stand at least 1 km higher than the present crest of the SG block if no erosion had occurred over the past few Myr (Figure 5). Even more exhumation and erosion may have occurred prior to this. In addition, the minimum uplift rate required for post-2-Ma exhumation is  $\sim 1.5$  mm/yr. This rate could be much higher, as shown above, and could rival those observed in other orogenic environments such as the Himalayas [Burbank and Beck, 1991].



**Figure 5.** Schematic block diagram of the San Bernardino Mountains along a north-south transect, showing our interpretation of the relief of major blocks if no erosion had occurred in the last few Myr. The solid line shows the present-day topography along a north-south transect (line of section shown in Figure 1, vertical exaggeration is 2.5 times). The dashed lines represent the relief of the blocks when erosion is restored. Major faults are shown with approximate dips [Allen, 1957; Meisling, 1984; Sadler, 1993]. The Yucaipa Ridge block may have stood at an elevation of  $\sim 4.5$  km, one kilometer higher than the present-day crest of the San Gorgonio block and 2 km higher than the Big Bear block. The San Gorgonio block is shown tilting upward to the south, and the Big Bear block is shown with only minor erosion restored from the top of the plateau and weathered granite surface. Abbreviations are as follows: MB, Morongo block; YRB, Yucaipa Ridge block; SGB, San Gorgonio block; BBB, Big Bear block; and SB-SAF, San Bernardino strand of the San Andreas fault zone.



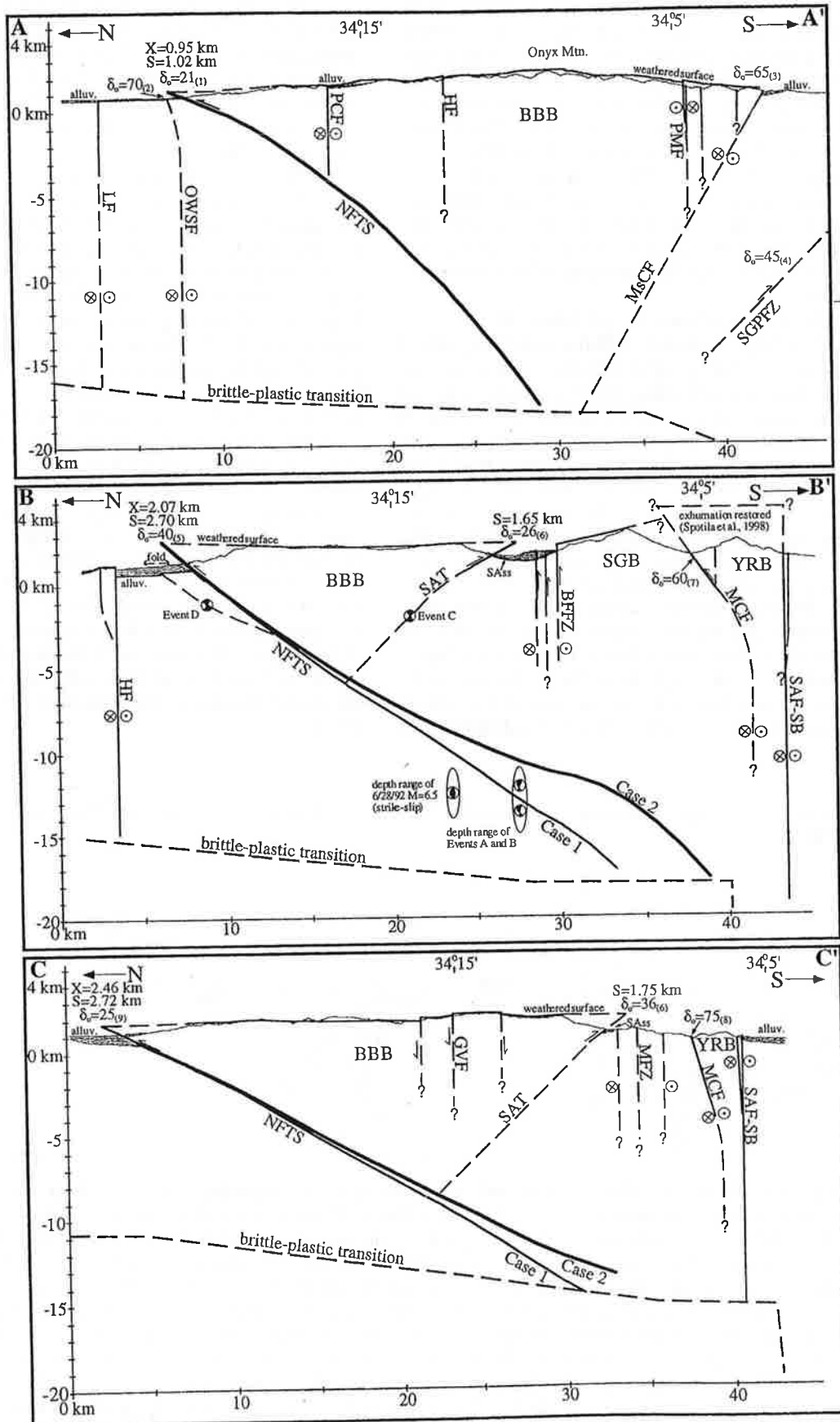
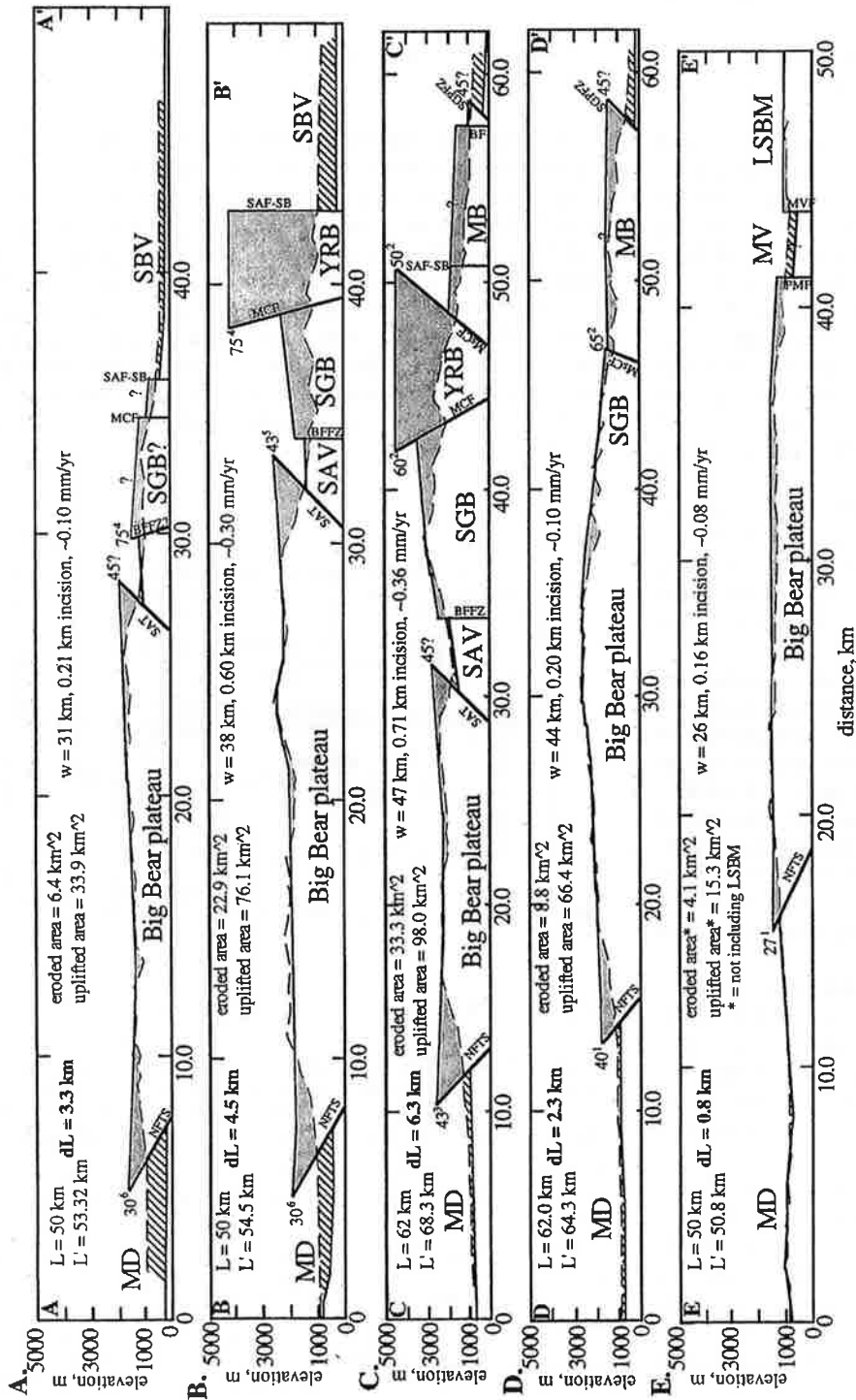


Figure 9.



**Figure 12.** North-south profiles across fault blocks whose magnitude of exhumation are constrained by the weathered surface and thermochronometry, which enable calculation of horizontal shortening across the SBMs (A-E in Figure 7). The thin dashed line represents topography without vertical exaggeration. The thick solid line represents either the weathered surface or topography restored based on thermochronometry [Spotila *et al.*, 1998]. Horizontal shortening (dL) is the difference in horizontal length of each profile (L) and the total length of the heavy solid line (L'). Shortening reaches ~6 km in the center of the range and diminishes to either side, as plotted in Figure 7. Erosion can also be calculated from these profiles. The gray shaded pattern indicates the area removed by erosion, which is summed in each profile. Average incision for each profile is the eroded area divided by profile width w. Incision rates are for the past 2 Myr. The ruled pattern indicates where deposition has buried the weathered surface. The area uplifted in each profile is relative to a base level defined by the elevation of basement north and south of the uplifted region. The total uplifted volume of the range is the sum of the products of uplifted area and the distance between profiles (15.3 km). Fault dips for projections are shown with superscripts that refer to the following: 1, Miller [1987]; 2, Allen [1957]; 3, Rzonca and Clark [1982]; 4, Dibblee [1974]; 5, Jacobs [1982]; 6, Li *et al.* [1992]. Abbreviations are as in Figures 2 and 9; BF, Banning fault; LSBM, Little San Bernardino Mountains; MV, Morongo Valley; MVF, Morongo Valley fault; SBV, San Bernardino Valley.

# Barton Flats Landslide, San Bernardino Mountains, Southern California

GEOLOGY AND MINERAL WEALTH OF THE CALIFORNIA TRANSVERSE RANGES © South Coast Geological Society 1982

Martin L. Stout, Department of Geology, California State University, Los Angeles, California 90032

The Barton Flats landslide covers about 12 square miles and underlies all of the prominent flat rolling surface of Barton Flats (photo 1). The mass is considered a landslide primarily on the basis of (1) derangement of Santa Ana River around the toe; (2) eroded, yet clearly defined scarp at head, which has caused local erratic patterns in South Fork and Barton Creeks (figure 1); (3) a large number of secondary landslides within the larger slide mass, each with the topographic surface of the lower block down-dropped, some with possible rotation; (4) underlain by low shear strength sedimentary materials, with bedding attitudes suggesting the possibility of a rotational failure across an open synclinal structure in the Santa Ana Sandstone (figure 2). The slip surface has not been observed.

With the exception of a few deeply incised valley side slopes, surface exposures show only gravels of multiple lithologies, derived mostly from the South Fork drainage basin. Secondary slides along the Santa Ana River locally have intermixed Santa Ana Sandstone and fanglomerates, and some mixing might have occurred during original movement.

Original movement of the Barton Flats landslide caused derangement of the ancestral Santa Ana River in this area, and the stream gradient was lessened considerably, with resultant alluvial deposition. No lacustrine beds have been found upstream to indicate ponding or formation of a lake. This suggests that the Barton Flats landslide moved slowly, similar to the Portuguese Bend landslide today, rather than as a rapidly moving slide mass. Several of the upstream deposits of fanglomerate have been mapped as Santa Ana Formation (Dibblee, 1964b; McJunkin, 1976), although the age of the fanglomerates is much younger than the more lithified Santa Ana Sandstone.

Massive landsliding also occurred downstream from the Barton Flats landslide, south of Slide Peak, which caused a southerly derangement of the Santa Ana River. Preliminary mapping suggests that this slide caused considerable upstream alluviation, but is not responsible for the upper terraces near the Barton Flats landslide. However, the relation between terraces and early thrusting, if any, has not been established.

The age of movement of the Barton Flats landslide is not known, but taking into account the materials within the slide and the present climate, it appears comparable in age to the Blackhawk landslide on the northeastern flank of the San Bernardino Mountains (Stout, 1975), and to three other landslides in coastal Southern California dated in the time range between 16,000-20,000 years B.P. (Stout, 1976). Conceivably, it might be somewhat younger, about 14,000-15,000 B.P.

No correlation can be made yet between seismic events and movement of large landslide masses in the San Bernardino Mountains. In the Santa Ana drainage, several of the terraces believed related to Barton Flats landslide movement, have in turn been

deformed by thrust faulting (figure 9, p. 16), so large earthquakes have been centered in this area. One recorded event was a M 5.1 earthquake near San Geronio Mountain in 1935.

Jenk's Lake is an artificial lake, (it is drained during the winter), in a pull-away of one of the secondary slides. Other ponds have been similarly constructed elsewhere in Barton Flats for recreational purposes, and springs are numerous. Thus the overall stability of the slide mass would be questionable in a sizeable earthquake, although there was no reported movement here in the 1935 earthquake, and no catastrophic event, such as the Madison slide which occurred during the Hebgen earthquake in 1959, is anticipated.



## REFERENCES CITED

- Dibblee, T. W. Jr. 1982 (this volume) Geology of the San Bernardino Mountains, Southern California in Fife, D. L. and Minch, J. A. (editors) *Geology and Mineral Wealth of the California Transverse Ranges*, South Coast Geological Society, Santa Ana, California.
- Dibblee, T. W. Jr., 1964, *Geologic map of the San Geronio Mountain quadrangle, San Bernardino and Riverside Counties, Calif., U.S.G.S. Map 1-431.*
- McJunkin, R., 1976, *Geology of a portion of the central San Bernardino Mountains, San Bernardino County, Calif., MS thesis, Calif. State Univ., Los Angeles.*
- Stout, M. L., 1976, Barton Flats Landslide in Stout, M. L. (editor) *Geologic Guide to the San Bernardino Mountains, Southern California*, So. Calif. Sect. AEG.
- Stout, M. L., 1975, Age of the Blackhawk landslide, southern California, *Geol. Soc. America, Abstracts with Programs*, v. 7, p. 378-379.
- \_\_\_\_\_, 1976, Radiocarbon dating of landslides in southern California, *California Geology*, in preparation.



Photo 1. Barton Flats landslide as viewed from Skyline Ridge looking eastward.

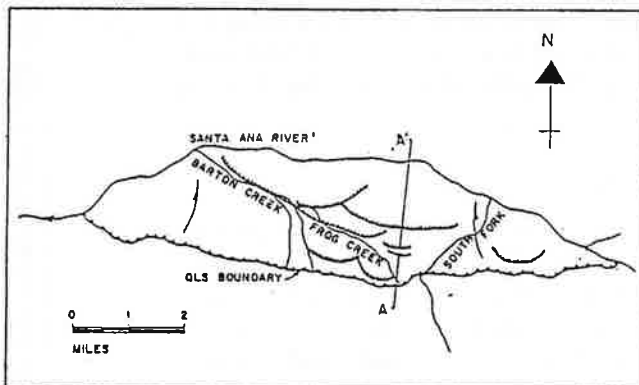


Figure 1. Sketch map of Barton Flats landslide.

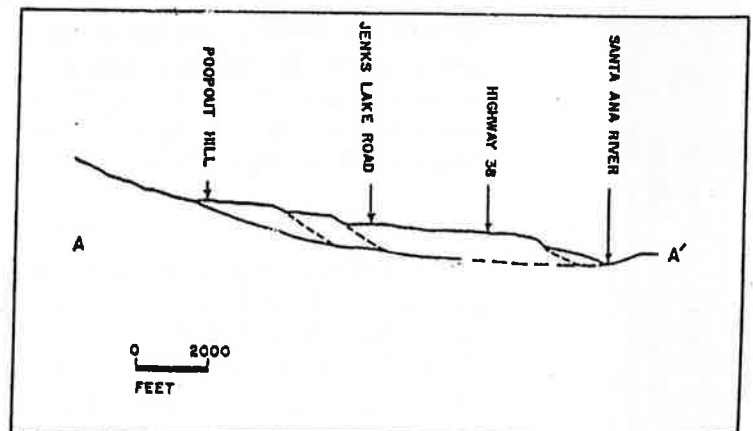


Figure 2. Section through Barton Flats landslide.

[Even though time limitations for our field trip do not allow the opportunity for visiting the Blackhawk landslide, any treatment of the geology of the northern flank of the San Bernardino Mountains would be incomplete without at least some mention of this famous slide. The above is reprinted with permission from the Geology and Mineral Wealth of the California Transverse Ranges, Mason Hill volume, 1982, of the South Coast Geological Society .... editor.]



# American Journal of Science

FEBRUARY 1959

## PLEISTOCENE GLACIERS ON SOUTHERN CALIFORNIA MOUNTAINS\*

ROBERT P. SHARP<sup>1</sup>, CLARENCE R. ALLEN<sup>1</sup>, and MARK F. MEIER<sup>2</sup>

**ABSTRACT.** The deposits of 7 valley glaciers have been mapped in the San Gorgonio area of the San Bernardino Mountains in southern California. These ice bodies headed at elevations between 10,300 and 11,300 feet, the lowest elevation attained was 8700 feet, and lengths were 0.5 to 1.7 miles. Dry Lake glacier was the largest. It covered 0.84 square miles on the north slope of San Gorgonio Mountain.

The principal products of glaciation are cirques and huge terminal embankments of coarse angular debris up to 700 feet high. Sharp-crested end moraines, typical recessional loops, and a number of other relations indicate that these embankments were formed by glaciers rather than as rock glaciers or debris flows. Two separate episodes of glaciation are recognized; both are considered Wisconsin.

Features previously attributed to glaciers in the San Gabriel Mountains were restudied. It is concluded that this range escaped glaciation in the Wisconsin and probably all earlier Pleistocene stages. San Jacinto Peak may have been glaciated, but definite proof has not yet been found.

### INTRODUCTION

Evidence of glaciation on the slopes of San Gorgonio Mountain<sup>3</sup> has previously been reported (Fairbanks and Carey, 1910; Vaughan, 1922, p. 335-336). New maps, air photos, developments in the knowledge of mountain glaciation, and international interest in this occurrence (Klebensberg, 1949, p. 463, 510; Flint, 1957, p. 310) motivated restudy of this and other possible sites of glaciation on southern California mountains. Glaciers in marginal areas are particularly sensitive indicators of environmental change and afford a possible means of establishing links with other Pleistocene events. Field work amounting to 29 man-days was carried on principally during weekends from May of 1954 to December of 1957.

### PHYSICAL SETTING

For this report, southern California is arbitrarily defined as that part of the state south of Latitude 35° N. This eliminates high peaks of the southern Sierra Nevada and Telescope Peak in the Panamint Range. San Gorgonio Mountain (11,502 feet), the highest point in southern California, is in the southeastern part (34° 06' N., 116° 49' W.) of the San Bernardino Mountains (fig. 1). To the southeast across San Gorgonio Pass is San Jacinto Peak (10,831 feet), and to the west is the San Gabriel Range, which attains an elevation of 10,080 feet.

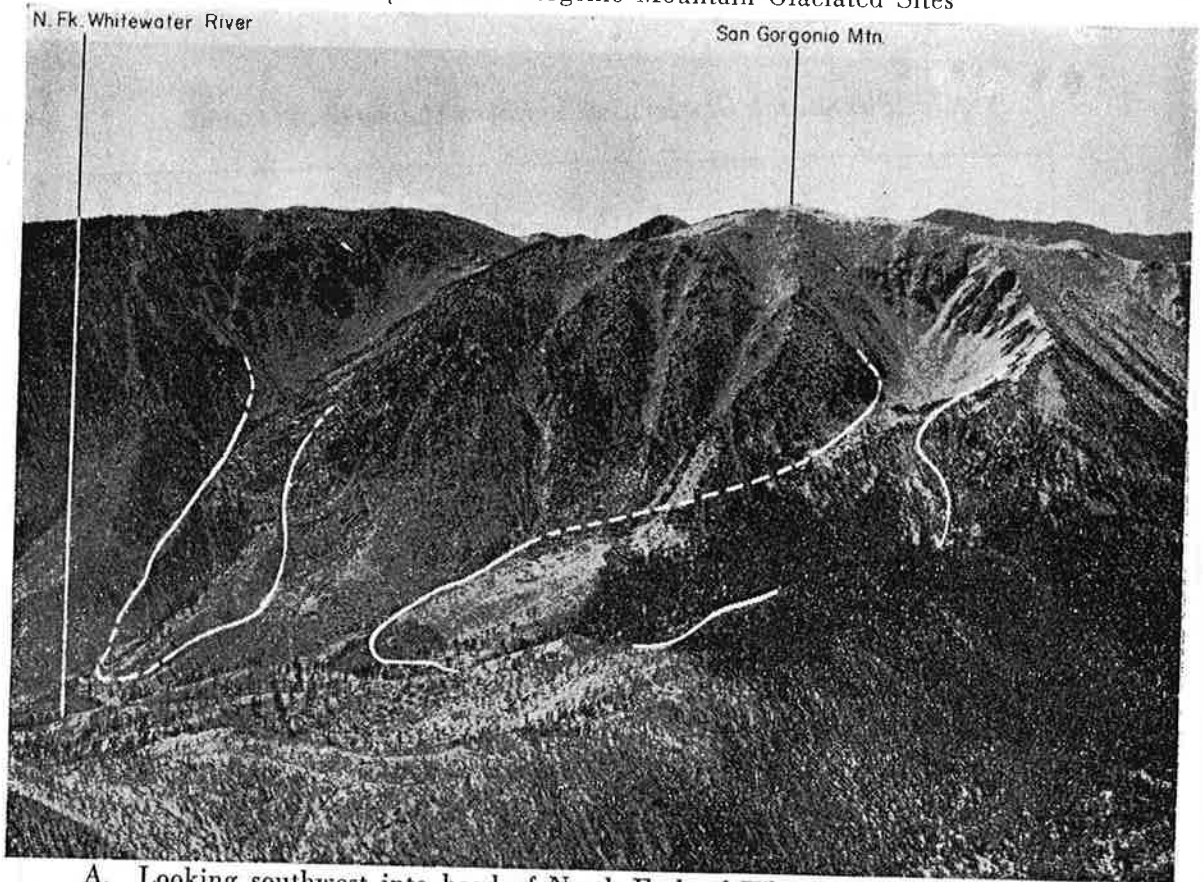
\* Contribution No. 902, Division of Geological Sciences, California Institute of Technology, Pasadena, California.

<sup>1</sup> Division of Geological Sciences, California Institute of Technology, Pasadena, California.

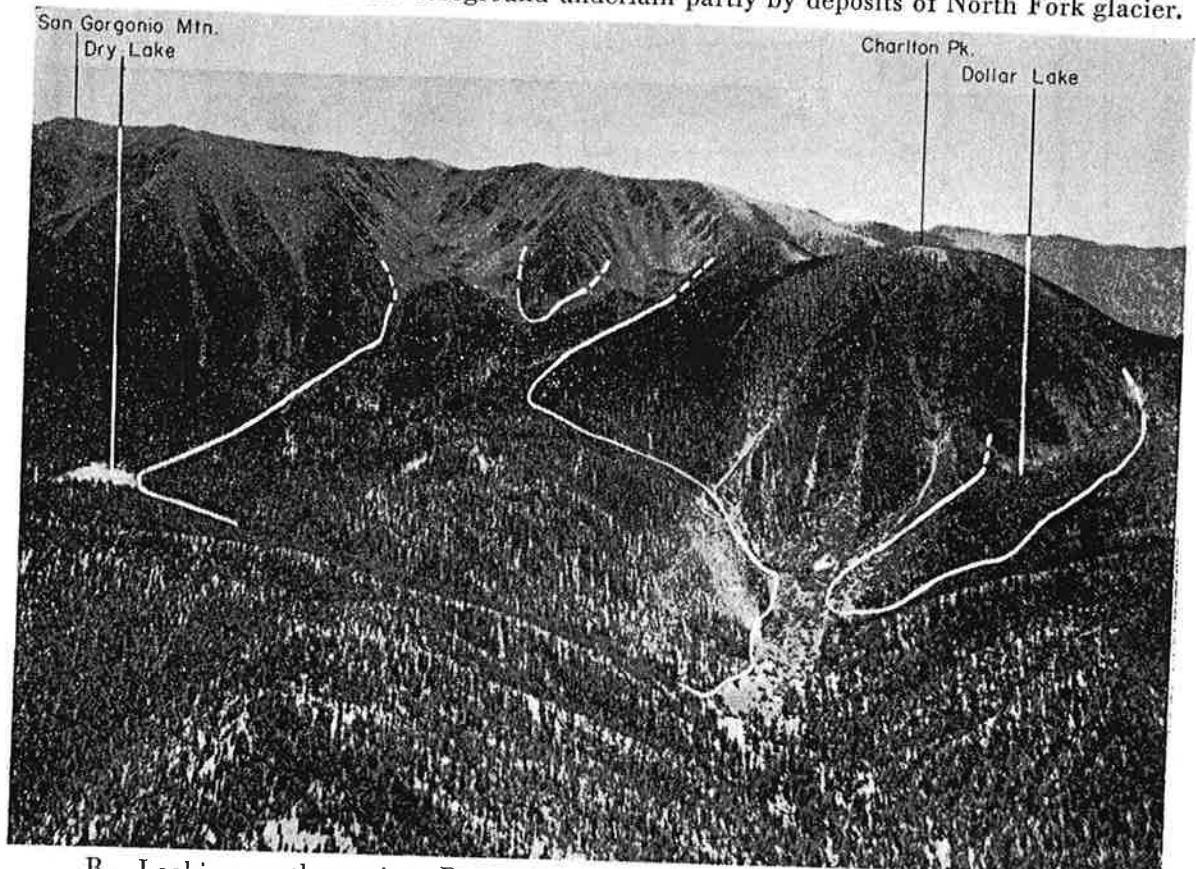
<sup>2</sup> 7409 South 22nd Street, Tacoma, Washington.

<sup>3</sup> Reprint of a paper on this subject by Ingle and Moran (1958) was received after the present article had been set in type.

PLATE 2  
Air Photos of San Gorgonio Mountain Glaciated Sites



A. Looking southwest into head of North Fork of Whitewater River. Cirque at left fed glacier in South Prong and cirque at right fed glacier in North Fork of Whitewater River. Lateral moraines of older stage visible at mouth of South Prong. Irregular topography of burned area in left foreground underlain partly by deposits of North Fork glacier.



B. Looking southwest into Dry and Dollar lakes area. Two central cirques on north face of San Gorgonio Mountain fed Dry Lake glacier. Note complex mass of morainal debris west of Dry Lake. Dollar Lake glacier fed from steep north face of Charlton Peak at right.

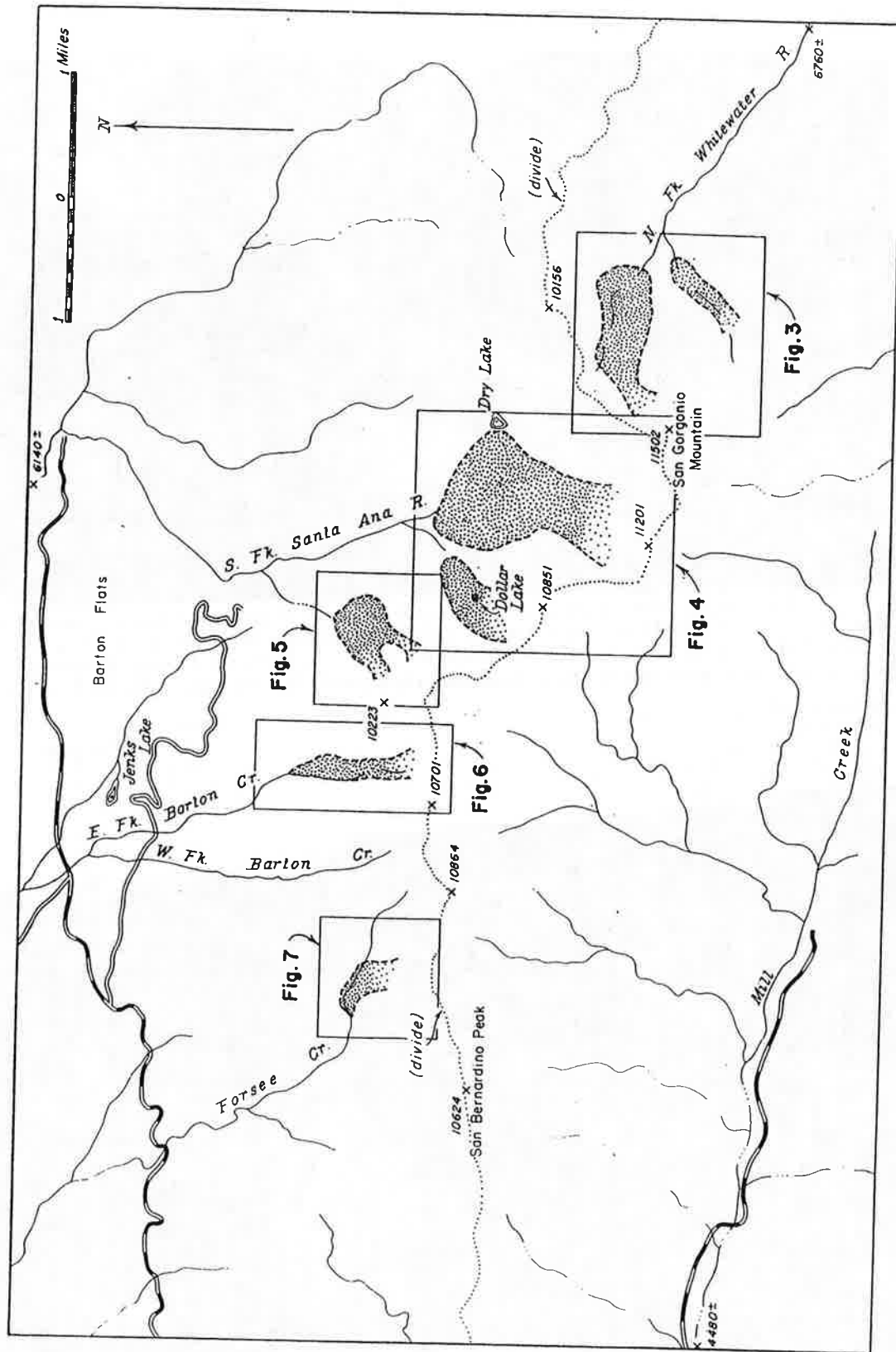


Fig. 2. Glaciated sites in the San Bernardino Mountains.

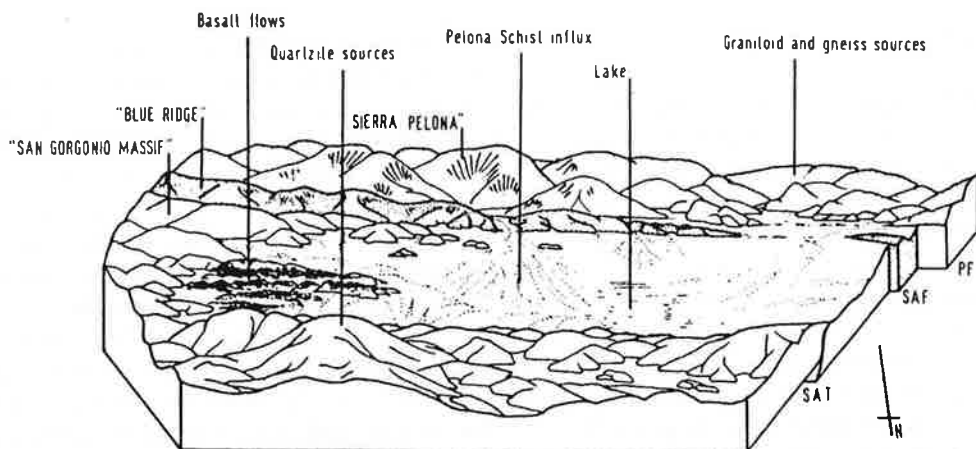


Figure 9. Speculative reconstruction of the Santa Ana basin. PF = Punchbowl fault; SAF = San Andreas fault; SAT = Santa Ana thrust.

Steep zones of crushed basement rock follow the southern limit of the granitoid-dominated facies of the Santa Ana Sandstone. But these beds are tilted northward approaching San Gorgonio Mountain; the north-dipping basal contact with weathered crystalline basement becomes approximately parallel with the steep bedrock slopes to the south. The impression remains that San Gorgonio Mountain is to some extent simply tilted, or warped up.

*Upland Tertiary sediments*

Only the quartzite-bearing facies of the Tertiary Santa Ana basin appears to have any continuation atop the uplifted basement that bounds the younger basin. There are no Tertiary sections on the northern plateau of the San Bernardino Mountains, or on San Gorgonio Mountain, with thicknesses comparable to the Santa Ana basin. But both uplands have remnants of a veneer of quartzite gravels that were derived from residual peaks of rebartholithic rocks, like Sugarloaf Mountain (Sadler and Reeder, 1983). The remnants are sufficiently widespread to preclude the possibility that a major portion of the fill of the Tertiary Santa Ana basin might once have existed beyond the limits of the younger basin.

The age of the veneer is certainly composite and not easy to specify. Some patches of the upland quartzite gravels are still active. Many are probably contemporaneous with the Tertiary Santa Ana basin, and tenuous lines of evidence suggest that others are older than the quartzite-bearing conglomerates of the Santa Ana basin.

Sadler and Reeder (1983) presented permissive evidence that the upland quartzite gravels include a westward transport path that led into Foster's (1980) unit three of the Crowder formation in Cajon Pass. Subsequently published vertebrate faunas and magnetostratigraphy (Reynolds, 1984; Weldon, 1984)

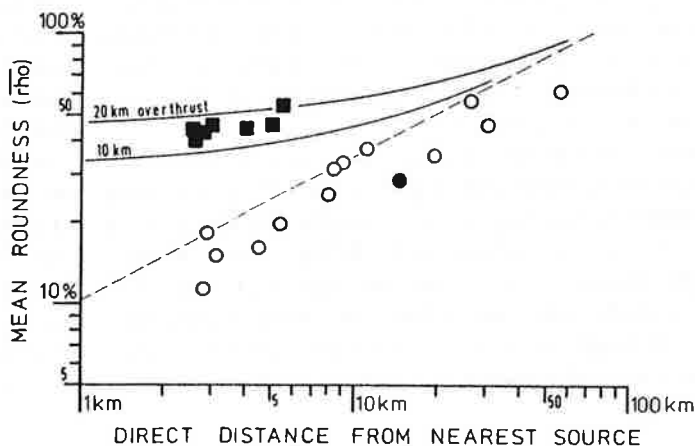


Figure 10. Roundness of quartzite clasts in the upland veneer (circles) and the Santa Ana Sandstone (squares). Solid circle indicates upland veneer remnant south of the Santa Ana basin; dashed regression, modern quartzite clasts in active Santa Ana river basin (Sadler and Reeder, 1983). Roundness determined by the Sames (1966) method, using clasts of 20- to 80-mm intermediate diameter.

show that unit three is at least 11 m.y. old (mid/late Miocene). Gravels of the upland veneer may have been recycled into the Crowder Formation long after their deposition. Indeed, K. E. Meisling and R. J. Weldon (personal communication, 1987) have preferred to explain the changing provenance of the Crowder units solely in terms of the evolution of Mojave Desert sources.

On the eastern ramp of the San Bernardino Mountains, the upland quartzite gravels include an admixture of volcanic and metavolcanic clasts that originated in the Mojave Desert. These portions of the veneer underlie and therefore predate 9 to 6-Ma alkali olivine basalt flows (Sadler, 1982). At Pioneertown, near



**Pelona Schist-bearing facies**

The central portion of the Santa Ana Sandstone includes a higher proportion of sandstone and siltstone. Many of the intercalated conglomerate beds contain distinctive Pelona Schist clast suites, but the proportions of schist types and associated clasts vary appreciably (Fig. 3). Where several conglomerate beds are seen in sequence, each may have its own distinctive provenance. Pelona Schist-bearing conglomerates are found interbedded with others that have no such clasts.

The Pelona Schist clast suite, which accounts for 8 to 51 percent of the clast assemblages in which it occurs, includes varying proportions of muscovite-rich grayschists (25 to 74 percent), greenschists and greenstones with coarse, white albite porphyroblasts (15 to 36 percent), coarse garnet-bearing grayschists (1 to 50 percent), metacherts (0 to 3 percent) and metaserpentinites (0 to 2 percent). The associated clasts include arkosic sandstone that resembles the San Francisquito and the Mill Creek Formations (0 to 5 percent), purple vesicular andesite (0 to 1 percent), porphyritic metavolcanics (0 to 5 percent), quartzite (0 to 14 percent), the "polka-dot granite" (0 to 2 percent) of Pelka (1971) and Ehler and Ehlig (1977), and a variety of monzonites and diorites (35 to 81 percent).

I have examined this clast assemblage at several localities and on separate occasions with help from Perry Ehlig (California State University, Los Angeles) and Douglas Morton, both of whom are well acquainted with Pelona Schist terranes (e.g., Ehlig, 1981). At one locality we uncovered three small clasts of a chalky white plagioclase with coarse polysynthetic twinning. Although such clasts might be derived from an anorthosite, we were unable to find large clasts of anorthosite. Further-

more, clasts of the distinctive syenites and Mount Lowe Granodiorite, which accompany anorthosite outcrops in the San Gabriel Mountains, were not found in the Santa Ana Sandstone despite a deliberately focused effort.

The largest Pelona Schist clasts are nearly of half-meter diameter (garnet schist, 48 cm; albite-porphyroblast greenschist, 45 cm; grayschist, 45 cm) and are from the southernmost outcrops of the Santa Ana Sandstone, close to the faulted north side of the San Gorgonio massif. The largest arkosic sandstone (28 cm) and "polka-dot granite" (29 cm) clasts occur at the same locality. The areal distribution of the maximum sizes of Pelona Schist clasts (Fig. 6) indicates a northward-transport direction.

The quartzite and metavolcanic clasts are the most durable ones, yet are typically better rounded and often significantly smaller than the softer clasts. No metavolcanic clasts coarser than 6 cm were seen; most are 2 to 3 cm in diameter. The quartzite clasts have a bimodal size distribution; most are as small as the metavolcanic clasts, but, at two locations near the western limit of the facies, white and pale pink quartzite clasts of 15 to 25 cm were present. These larger clasts are indistinguishable from quartzite clasts in the eastern third of the Santa Ana Sandstone, and in a Miocene gravel veneer on the northern plateau of the San Bernardino Mountains (Sadler and Reeder, 1983). By contrast, the smaller quartzite clasts are brown and have surface pits and shatter marks more typical of clasts from better indurated conglomerates. The unexpectedly high roundness of these durable clasts can be explained if they are recycled from older sediments. One such source, with a maximum grain size of less than 10 cm probably supplied all the metavolcanic clasts and the clasts of smaller, pitted quartzites.

The "polka-dot granite," vesicular andesite, and arkose

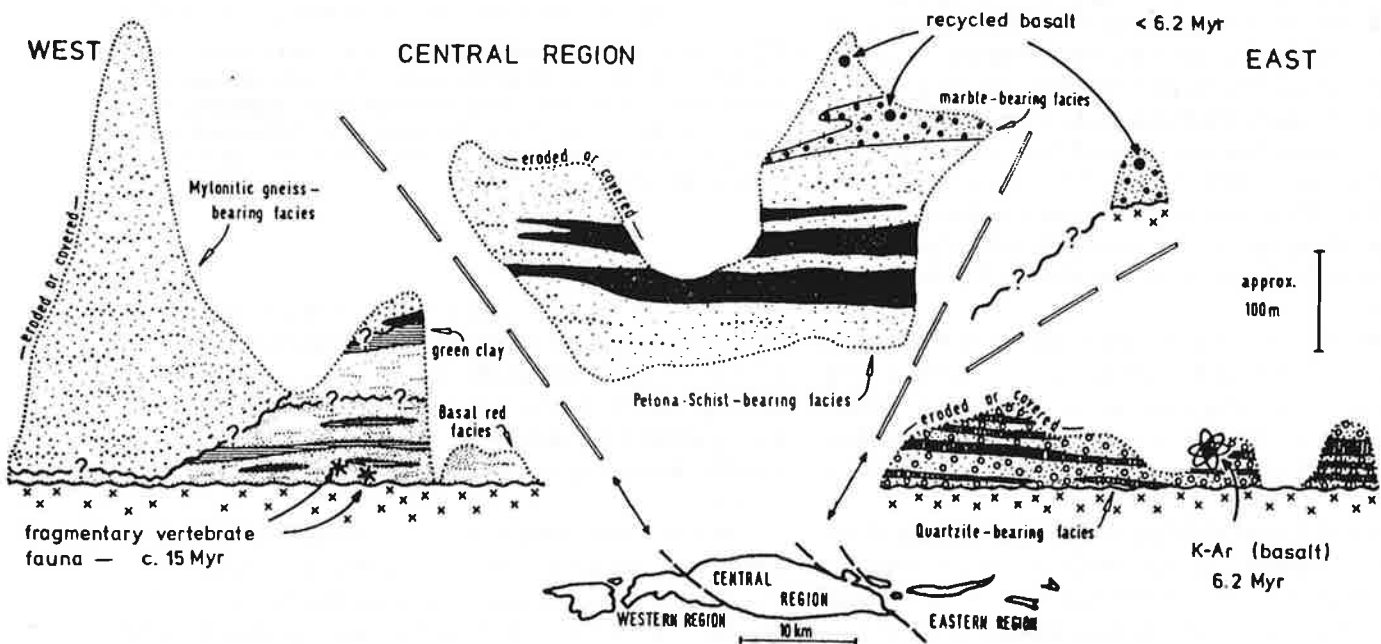


Figure 5. Tentative reconstruction of stratigraphy of the Santa Ana basin, showing evidence of age. Facies symbols as in Figure 4.

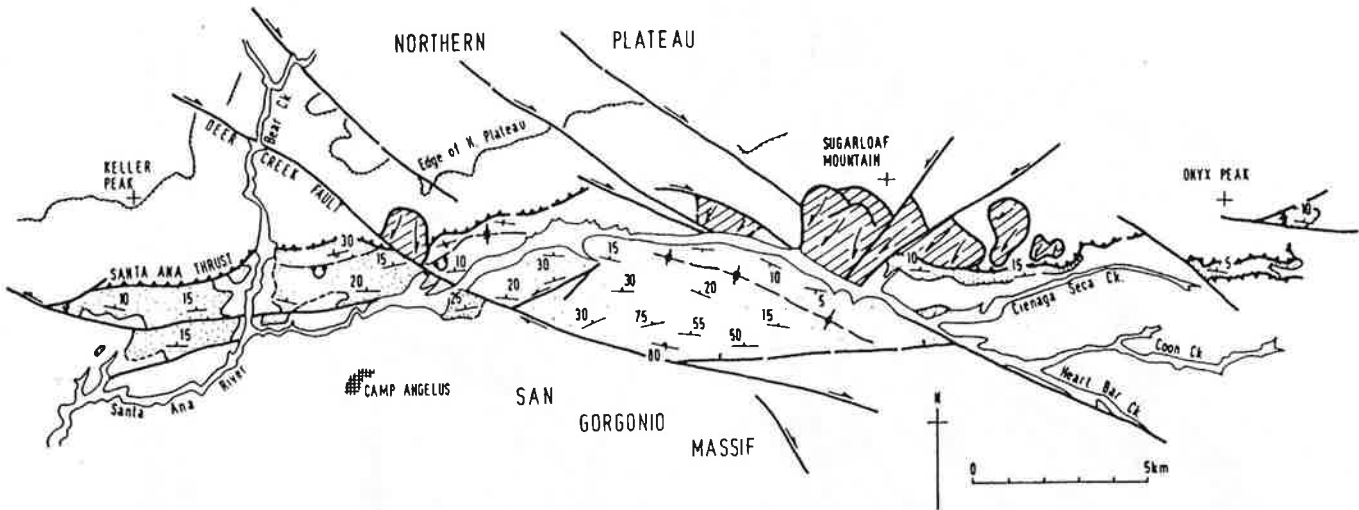


Figure 2. Structure map of the Santa Ana Sandstone, with the cover of surficial deposits removed. Dense stipple indicates fault blocks where base of formation is exposed; light stipple, base not seen. Diagonal ruling indicates large bedrock landslides.

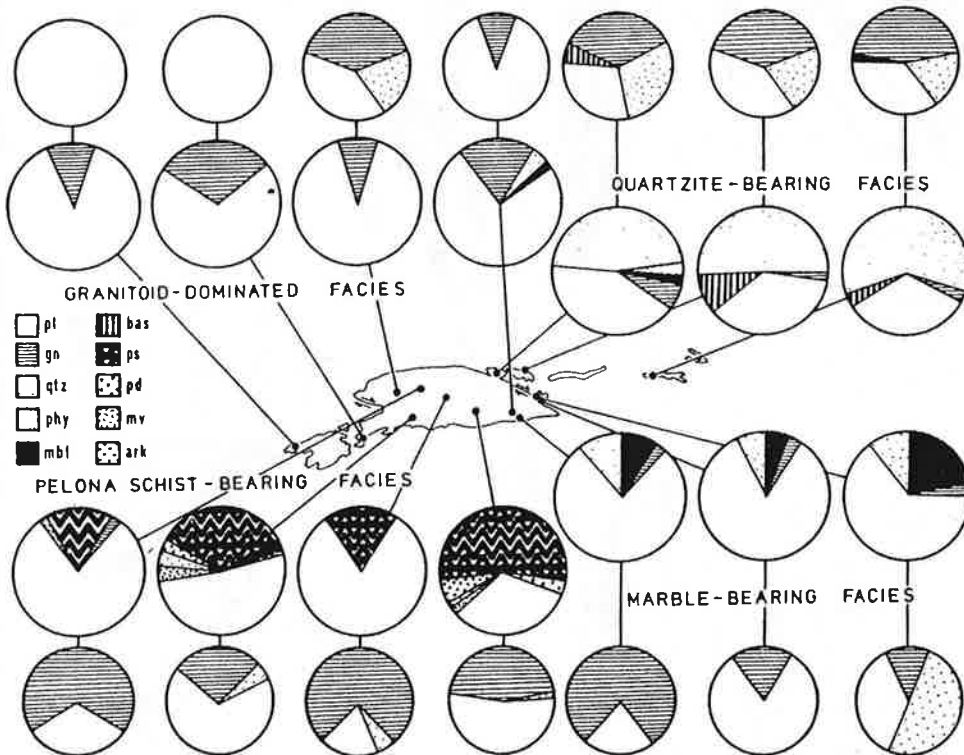


Figure 3. Clast compositions in the Santa Ana Sandstone (indicated by large divided circles) compared with overlying surficial deposits (small circles). The location of samples is shown on an outline version of Figure 4, with restoration of strike slip. Key: pl = plutonic rocks; gn = gneiss; qtz = quartzite; phy = phyllite; mbl = marble; bas = basalt; ps = Pelona Schist; pd = "Polka-dot Granite"; mv = volcanic and metavolcanic rock; ark = arkose.

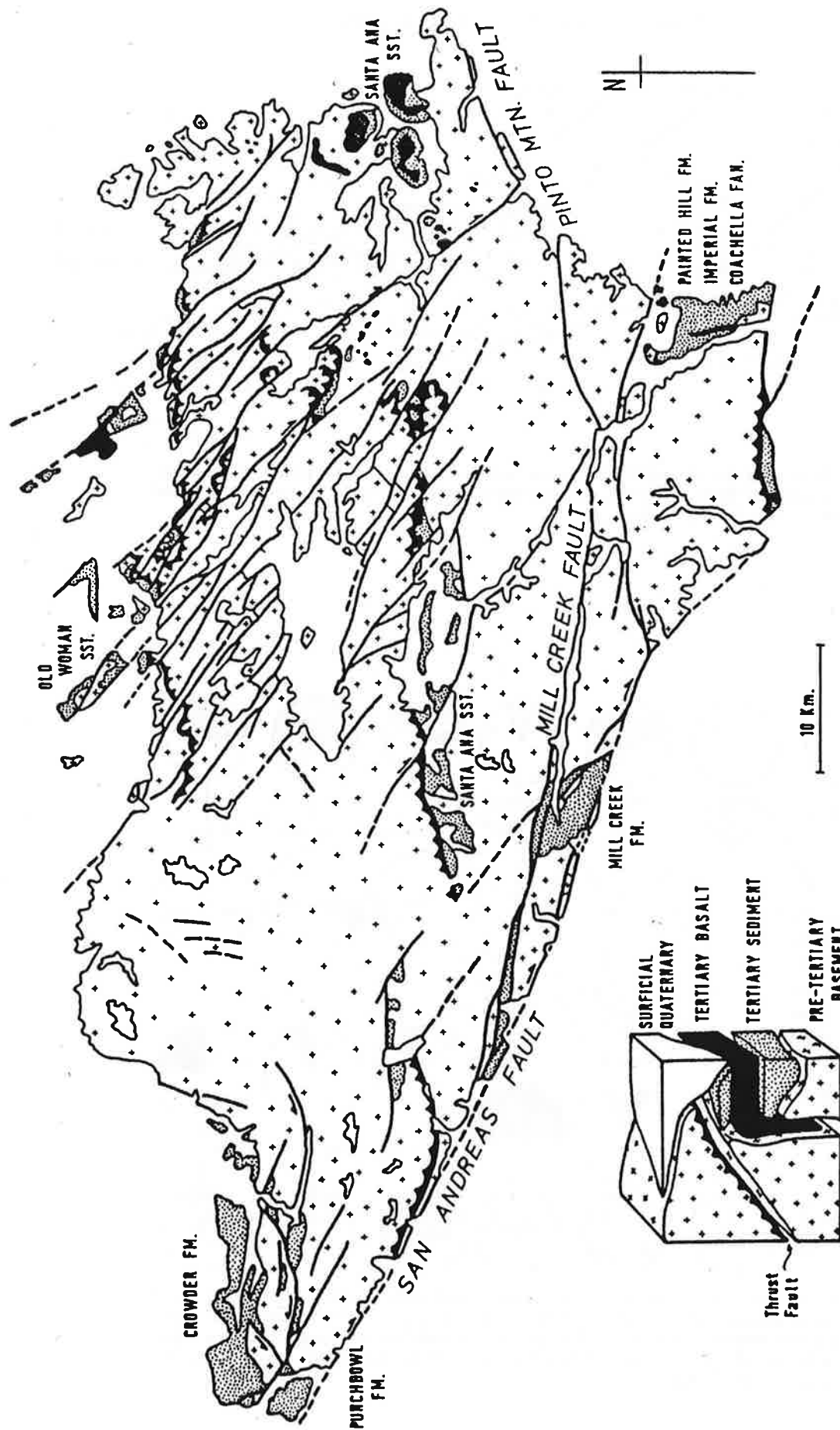


Figure 4. Tertiary sediments and volcanic rocks of the San Bernardino Mountains. After: Allen, 1957; Rogers, 1967; Gibson, 1971; Woodburne and Goltz, 1972; Morton and Miller, 1975; Foster, 1980; Weldon and others, 1981; Strathouse, 1982; Sadler, 1982.

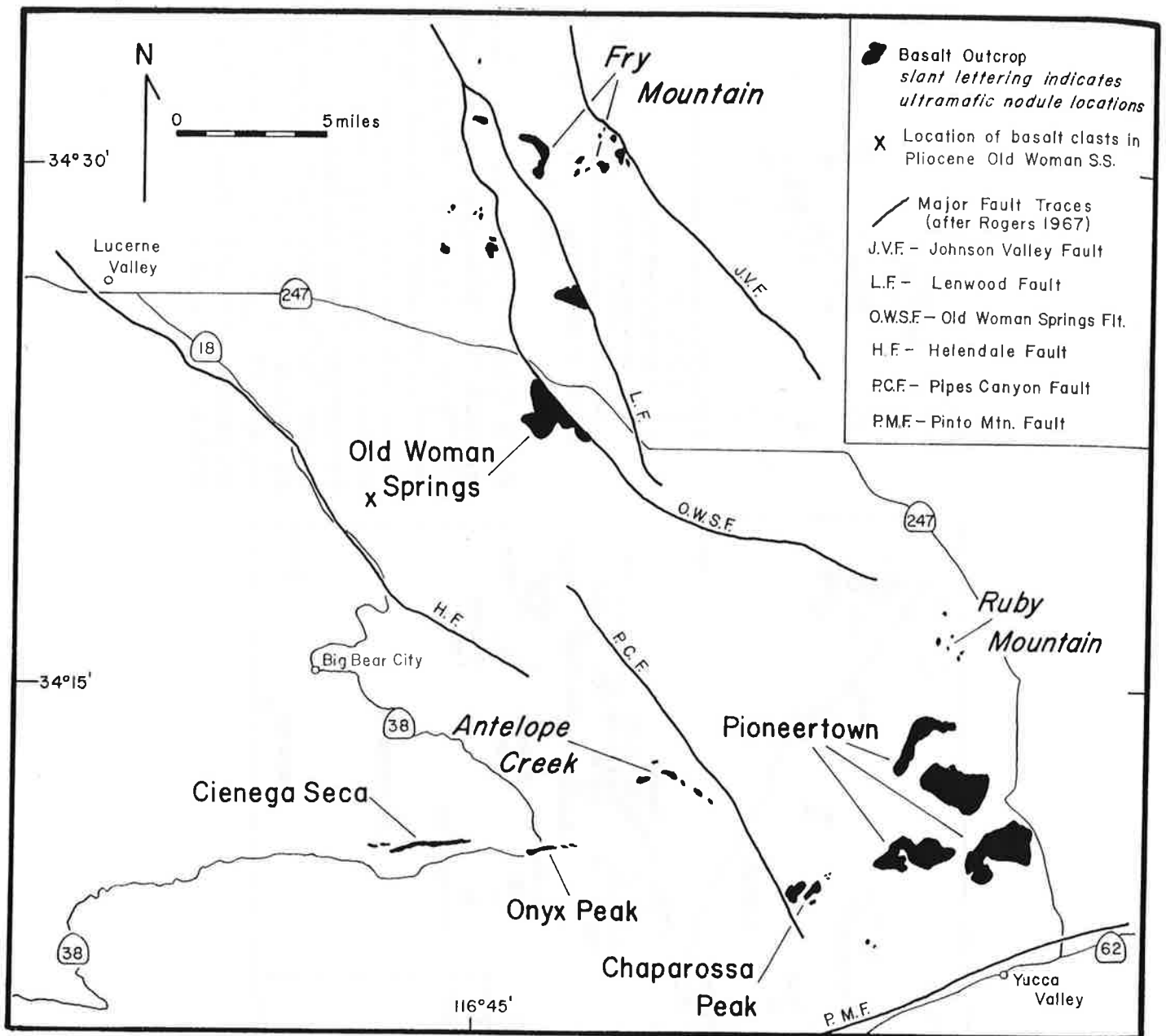


Figure 1. Distribution of basalt outcrops in the eastern San Bernardino Mountains and adjacent areas.

about 1% by volume. The vesicles may be lined partially or completely by yellowish chalcedony, calcite, or colorless zeolites.

Three textural types of basalt are recognized in outcrop: 1) abundant platy; 2) reddish-brown blocky; and 3) reddish to purplish cindery. A feature common to the platy and blocky lavas is a mottling pattern of white to pinkish dots, averaging 5 mm in diameter, which pervade the surface and interior of the rock. This is produced by alteration of the olivine phenocrysts to a mixture of iddingsite and hematite which form circular zones around the crystals.

The major structural features in the Old Woman Springs area are two high angle faults. The N45W-trending Old Woman Springs fault and a N10W-trending offshoot have an opposed sense of dip-slip motion such that a large basalt-capped mass is uplifted between

them. Dip slip of at least 50 m was observed along the Old Woman Springs fault as indicated by downward displacement and juxtaposition of Tertiary sediments and basalt. At least 25 m of Tertiary sediments have been downfaulted against quartz monzonite basement and capping basalt along the N10W fault.

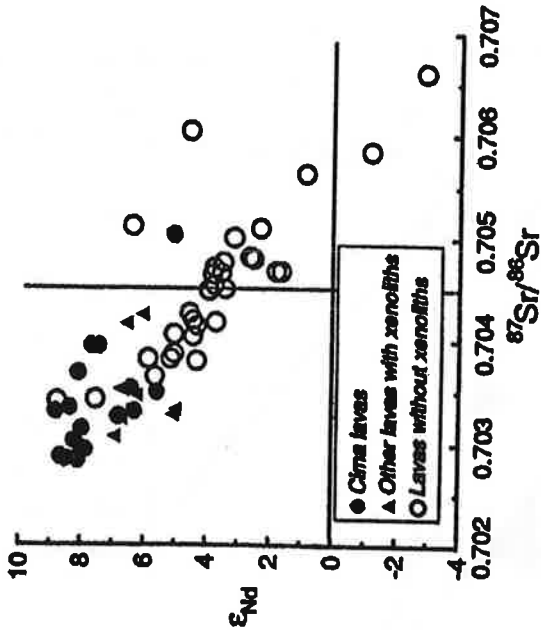
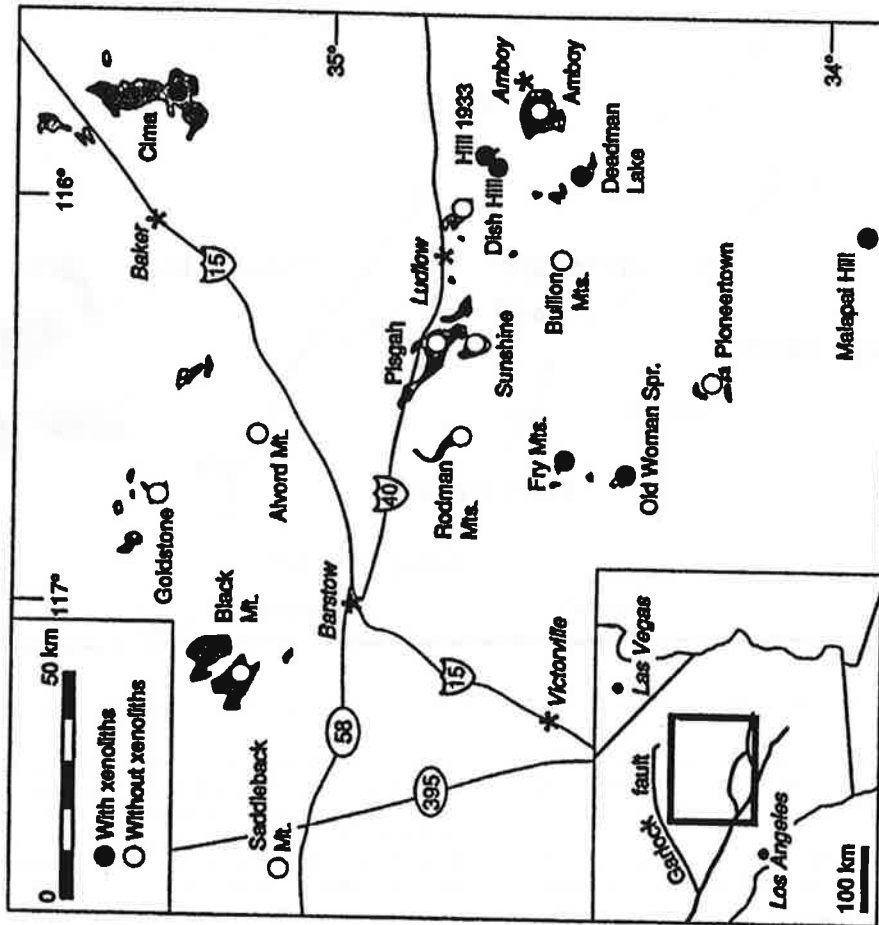
The cindery basalt is found on the tops or flanks of small hills in association with small volcanic bombs. Fourteen of these small cinder and bomb piles could be located, suggesting that the basalts were extruded through a series of small vents rather than one large cinder cone.

#### SUMMARY

Within this geographic province two distinctive types of alkaline basalt are found: basalts which contain untramafic xenoliths and associated high



**Fig. 1.** Locations of flat-lying Neogene basalts in the Mojave Desert region of California. Only undeformed or weakly deformed, generally mid-Miocene to Pleistocene basalts are shown (shaded areas). Samples from Saddleback Mt., Black Mt., Alford Mt., Pisgah, Ludlow, Redman Mts., Fry Mts., Old Woman Spr., Bullion Mts., Dish Hill, Amboy, Amboy, Deadman Lake, Plonsetown, and Malepai Hill. Symbols of general locations of samples in Table 1; where several samples were taken from a given locality, only one symbol is plotted.



**Fig. 2.** Nd-Sr isotope relations. Only lavas without mantle xenoliths have low  $\epsilon_{Nd}$  values and high  $^{87}Sr/^{86}Sr$  ratios, characteristics that are generally ascribed to derivation from ancient lithospheric mantle. Lavas that carry mantle xenoliths (and presumably traversed the crust rapidly, avoiding contamination) consistently have high  $\epsilon_{Nd}$  values and low  $^{87}Sr/^{86}Sr$  ratios. Slight alteration probably accounts for high  $^{87}Sr/^{86}Sr$  (0.705) of Cima sample Ci-53. Data shown include 20 analyses of xenolith-free Pisgah and Amboy basalts from (9) which are not listed in Table 1.

al' / (Moore, 1976). Braided-  
presence of shallow channels  
s that suggest transverse and  
fine-grained deposits, and by  
e-grained sandstone and con-  
genous detrital sequence are  
persistent along sedimentary  
ction, and they change facies  
k , generally in an east-west  
the units is truly remarkable.  
e (Lower Cambrian) is rec-  
e t Basin region of Nevada  
n Bernardino Mountains re-  
e Laborca region of Sonora,  
dora Quartzite (Stewart and  
st ke, units commonly be-  
to the west. This relation is  
in at Basin where units such  
ie. from quartzite in the east  
re and finally to almost en-  
in the west. Shallow-marine  
lostone of eastern California  
t e west and lens out east-

e anges in thickness from a  
an 6,000 m locally in west-

is detrital sequence contains  
mbrian biotas consisting of  
si all shelly fossils, sponges,  
algal-like microorganisms,  
) 1966; Stewart and others,

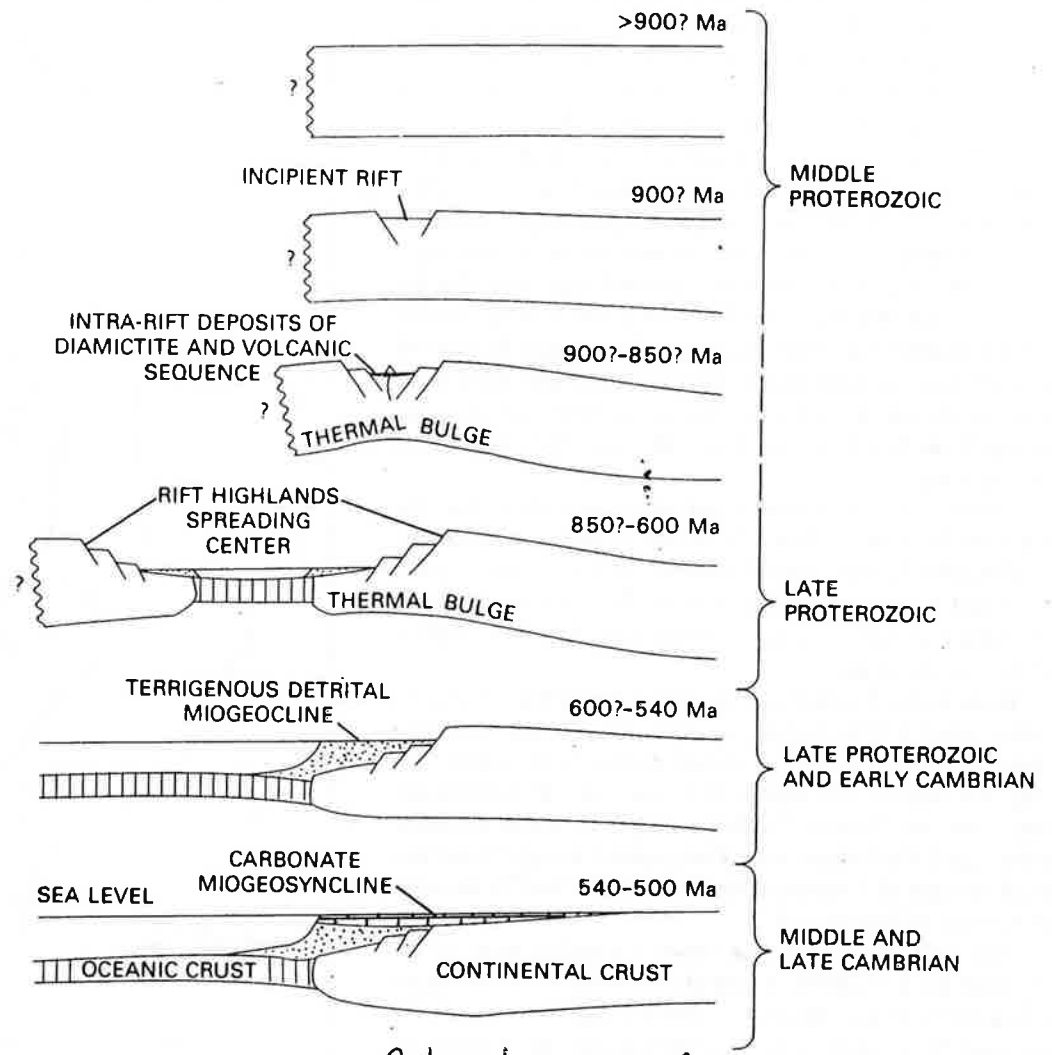


Figure 5. Tectonic model of late Proterozoic and Cambrian development of the western U.S. Modified from Stewart and Suczek (1977).

of presumably rift-related volcanic rocks (tholeiitic? basalt) in the sequence, and by the indication of significant faulting during deposition of the sequence. In British Columbia, the term "East Kootenay orogeny" has been used to describe tectonic events prior to deposition of the diamictite and volcanic sequence (Windermere Supergroup) in Canada. Recent work, however, indicates that the term "East Kootenay orogeny" is better restricted to a 1350-611 300 Ma event that apparently terminated

rocks record protracted rifting of the western margin of North America and the establishment of a passive continental margin by Early Cambrian time (Gabrielse, 1972; Stewart, 1972, 1976; Stewart and Poole, 1974; Dickinson, 1974; Burchfiel and Davis, 1975; Young, 1982; Armin and Mayer, 1983; Bond and others, 1983, 1985; Devlin and Bond, 1988; Christie-Blick and Levy, 1989a; Levy and Christie-Blick, 1991b). Cordilleran Late Proterozoic strata, discussed in this paper, generally consist of glaciogenic diamictite and mafic volcanic rocks overlain by a thick section of quartzose sandstone and mudstone. Although few would question that the lower Paleozoic portion of the Cordilleran miogeocline was deposited on a passive margin, the tectonic setting of the underlying Late Proterozoic strata, the timing of the rifting events, and the identity of the continental fragments that separated from North America have only begun to be understood in recent years.

These rocks are present in different outcrop belts than the early Late Proterozoic Uinta Mountain Group, Chuar Group, and Sixtymile Formation (Link, this chapter; Elston, this chapter) and record a different tectonic regime. They are *sensu stricto* "late-Late Proterozoic" (Fig. 5), but this term is awkward and is not used in this paper.

Because the Precambrian time scale is geochronologic, not geochronometric (Harrison *in* Chapter 1, this volume) we refer to "Late Proterozoic rocks" deposited during "Late Proterozoic time," but because the Phanerozoic time scale is chronostratigraphic we use "Lower Cambrian rocks" for those deposited during "Early Cambrian time." Furthermore, though "Late" is a formal division of Proterozoic time and rocks, "late" is an informal division of Paleozoic time.

The Late Proterozoic and Lower Cambrian strata of the Cordillera are dominantly unfossiliferous, except for the uppermost sandstones and mudstones that contain Early Cambrian trace and body fossils. Fossil occurrences are summarized by Horodyski (this chapter). Stratigraphic definition of these rocks exists for nine more-or-less distinct areas in the western United States, as shown in Figure 34. Representative stratigraphic columns for Washington, Idaho, Utah, eastern Nevada, and California are shown in Figure 35.

Late Proterozoic strata of the United States Cordillera have been divided into a lower *diamictite and volcanic succession* (shown with heavy line to left of stratigraphic column on Fig. 35, and designated on correlation chart, Fig. 39, below) and an upper *terrigenous detrital succession* (shown with open column symbol to left of column on Fig. 35). In describing these strata, we use the nongenetic term "succession" instead of "sequence," which was used initially by Stewart (1972) and Stewart and Suczek (1977). We here follow the definition of Mitchum and others (1977) that a "sequence" is a relatively conformable stratigraphic section bounded by unconformities or their correlative conformities. Specific parts of the successions described here can be called sequences following this definition. To apply the name "sequence" to the entire succession, however, would apply the term in a different way and would be confusing.

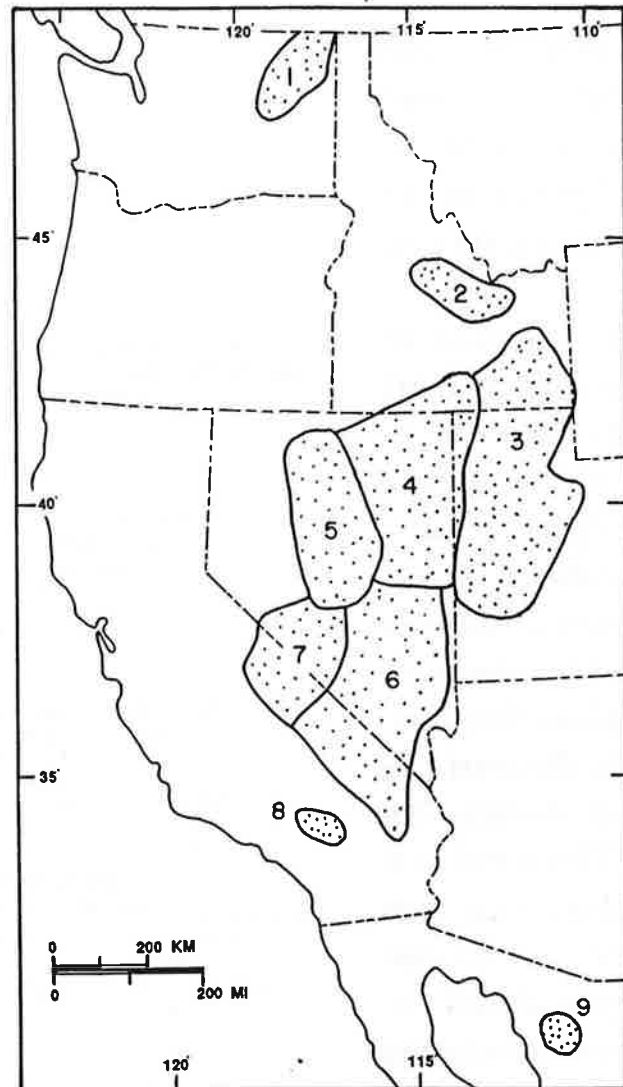


Figure 34. Map showing general distribution of Late Proterozoic sedimentary rocks of the western United States and northwestern Mexico (stippled). Rocks crop out in discontinuous uplifts within the stippled areas, see Plate 1. The nine geographic divisions used in this article are: 1, northeast Washington; 2, east-central Idaho; 3, southeastern Idaho and northern Utah; 4, northeastern Nevada and adjacent parts of northwestern Utah and southern Idaho; 5, central Nevada; 6, southern Nevada and eastern California; 7, White-Inyo Mountains and adjacent regions, eastern California and western Nevada; 8, western Mojave desert and San Bernardino Mountains region, southern California; 9, Caborca, Mexico.

In this paper we follow U.S. Geological Survey terminology except in the use of the term "Windermere Supergroup," which is a Canadian term equivalent to the "Windermere Group" of northeastern Washington (Miller and others, 1973). The supergroup designation has been used in recent discussions of these rocks (Eisbacher, 1981a, 1985; Devlin and others, 1985, 1988; Devlin and Bond, 1988; Ross and others, 1989), which are best exposed north of the Canadian border.

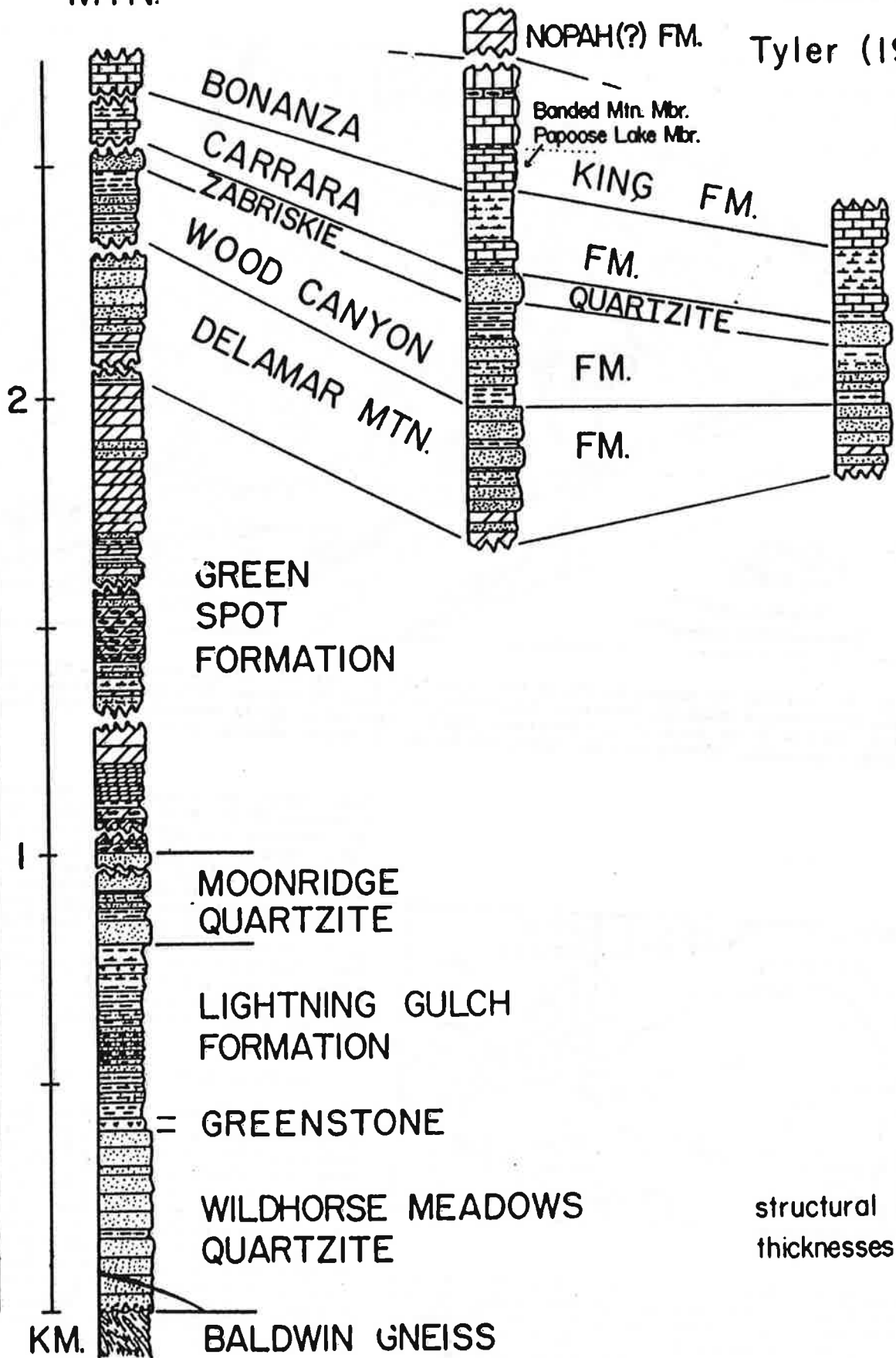
SUGARLOAF MTN.

DELAMAR MTN.

CHICOPEE CANYON

Tyler (1975)

BIG BEAR GROUP



CAMBRIAN

PRECAMBRIAN

KM.

BALDWIN GNEISS

WILDHORSE MEADOWS QUARTZITE

GREENSTONE

LIGHTNING GULCH FORMATION

MOONRIDGE QUARTZITE

GREEN SPOT FORMATION

DELAMAR MTN.

WOOD CANYON

ZABRISKIE

CARRARA

BONANZA

NOPAH(?) FM.

Banded Mtn. Mbr.  
Papoose Lake Mbr.

KING FM.

FM.  
QUARTZITE

FM.

FM.

structural thicknesses



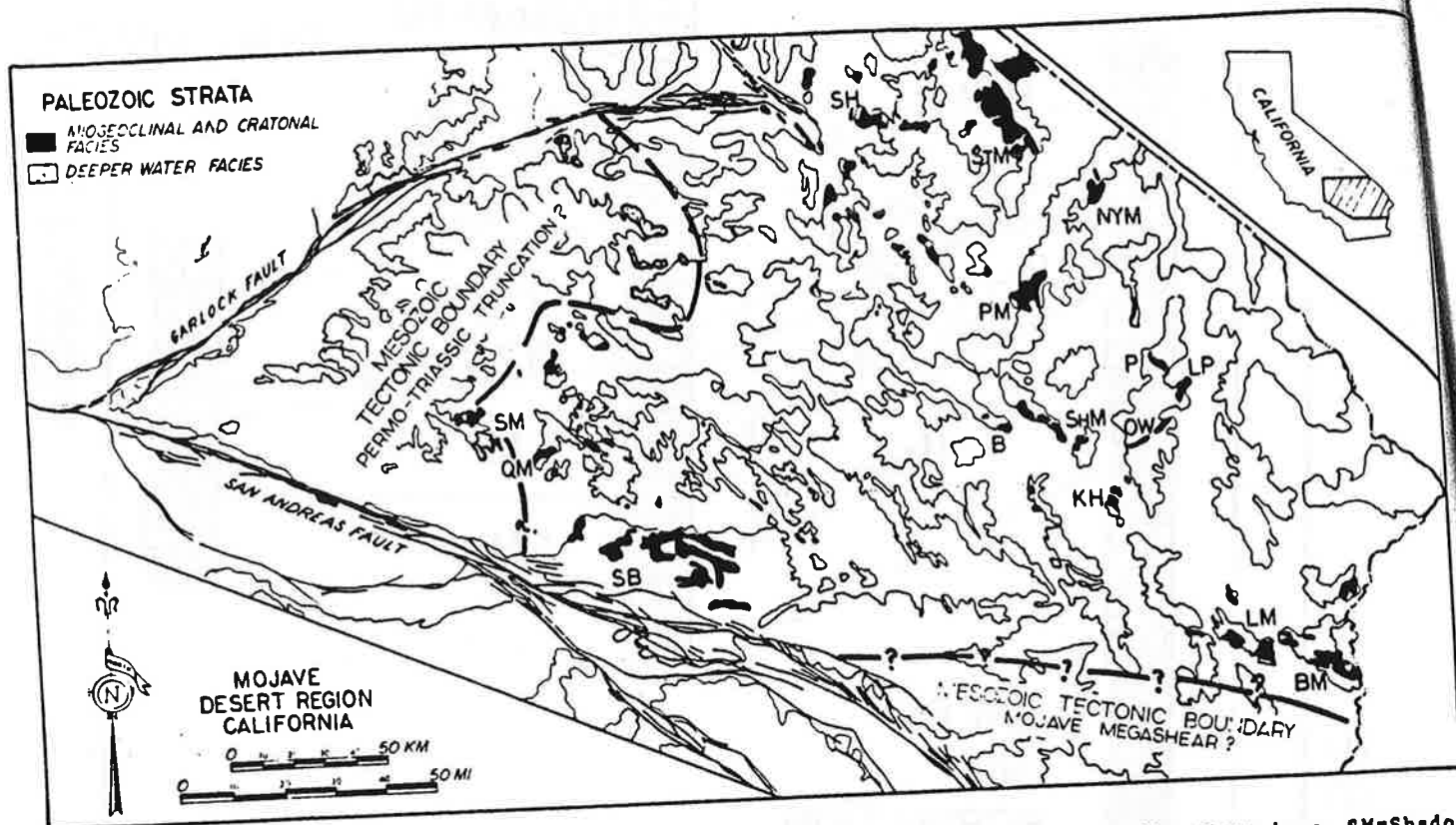


Figure 1. Map showing Paleozoic strata in the Mojave Desert region. SB=San Bernardino Mountains, SM=Shadow Mountains, QM=Quartzite Mountain, B=Bristol Mountains, SHM=Ship Mountains, P=Piute Mountains, LP=Little Piute Mountains, OW=Old Woman Mountains, KH=Kilbeck Hills, LM=Little Maria Mountains, BM=Big Maria Mountains, PM=Providence Mountains, NYM=New York Mountains, STM=Striped Mountain, SH=Silurian Hills.

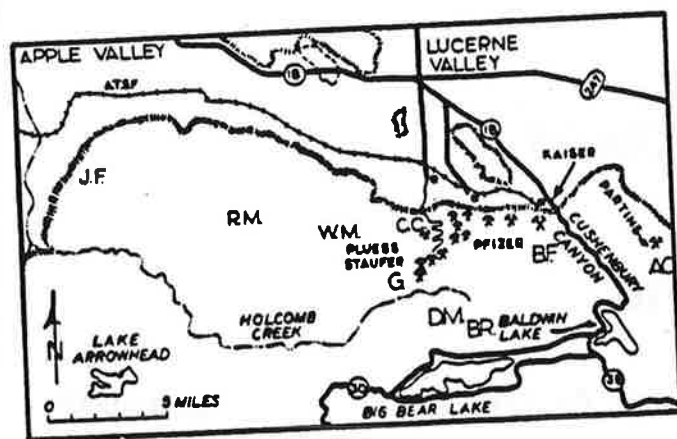


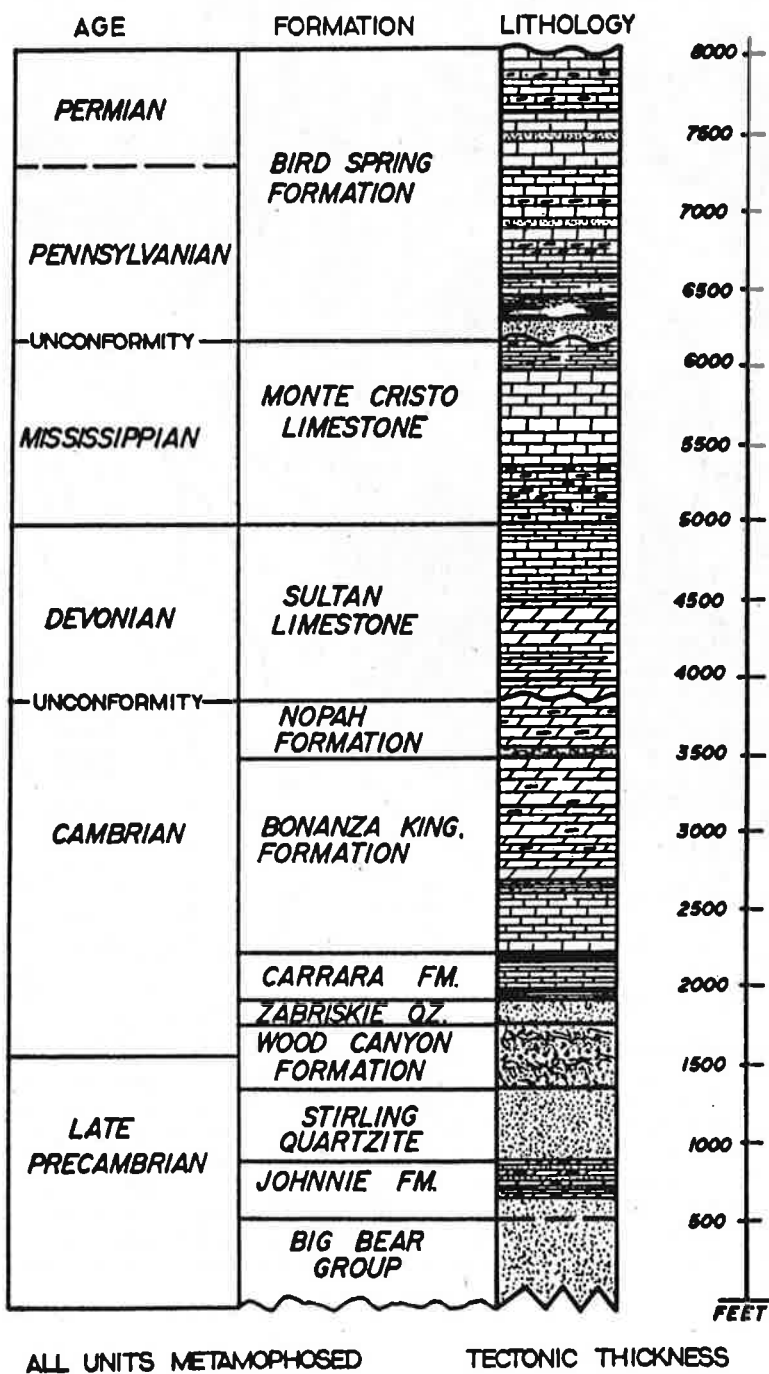
Figure 2. Map of the Lucerne Valley area and northwestern San Bernardino Mountains showing locations of areas mentioned in the text. JF=Juniper Flats, RM=Rattlesnake Mountains, WM=White Mountain, CC=Crystal Creek, G=Greenlead Mine area, BF=Burnt Flat area, DM=Delamar Mountain, BR=Bertha Ridge, AC=Arrastre Creek.

Bear Group, and assigned a late Precambrian age (Cameron, 1982). Buff dolomite, calc-silicate rock and quartzite correlative with the upper Precambrian Johnie Formation and Stirling Quartzite overlie the Big Bear Group (Fig. 4). Younger upper Precambrian and Lower Cambrian metasedimentary rocks include; cross-bedded and pebbly quartzite, phyllite, and dark schist correlative with the Wood Canyon Formation, white vitreous quartzite correlative with the Zabriskie Quartzite, and a heterogeneous sequence of red-brown and green calc-silicate rock, schist, hornfels, and dark grey siliceous marble correlative with the Lower and Middle Cambrian Carrara Formation (Fig. 4).

#### Middle to Upper Cambrian and Devonian Strata

Middle to Upper Cambrian and Devonian strata are widely exposed in the area, and form a distinctive dolomite dominated sequence (Fig. 4). Visually and chemically distinctive (Brown, 1984c), thin-banded to mottled, light to dark grey, slightly dolomitic marble of the Lower Member of the Bonanza King Formation is overlain by a thick sequence of buff, tan, light to dark grey, and white dolomite (Brown, 1982b, 1984c). Recognition of distinctive, regionally persistent hornfels and calc-silicate marker beds (Table 1) allows the thick dolomite dominated sequence to be subdivided into several formations and members including the Cambrian Bonanza King Formation (three members), Cambrian Nopah Formation (Dunderberg Shale Member and Upper Member), and the unconformably

# COMPOSITE STRATIGRAPHIC COLUMN PALEOZOIC ROCKS WESTERN SAN BERNARDINO MOUNTAINS



ALL UNITS METAMORPHOSED

TECTONIC THICKNESS

H. J. BROWN 84

Figure 4. Composite stratigraphic column of Paleozoic rocks in the northwestern San Bernardino Mountains.

Age belts (brought together by collisional process) occurred before Pangea.

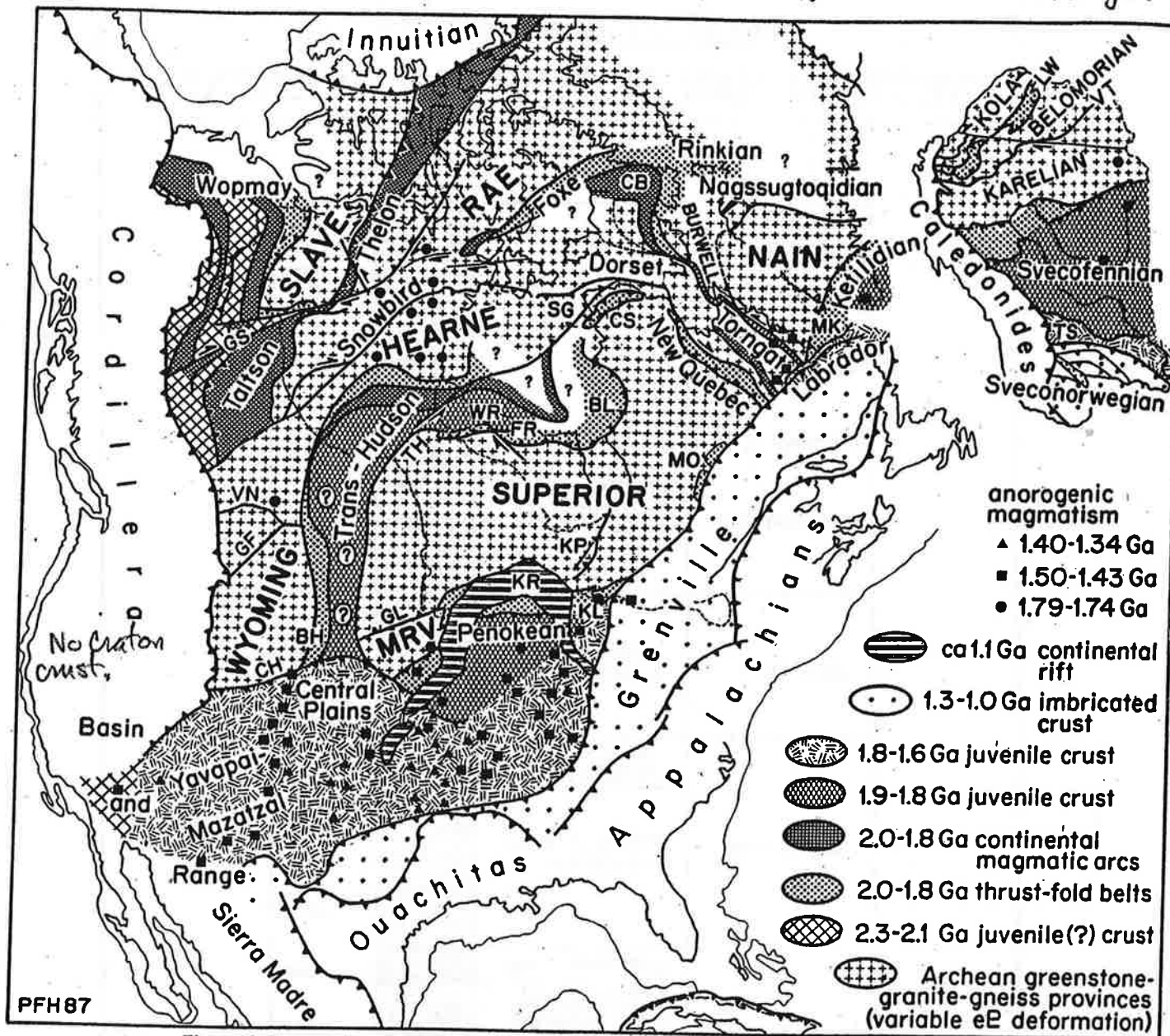
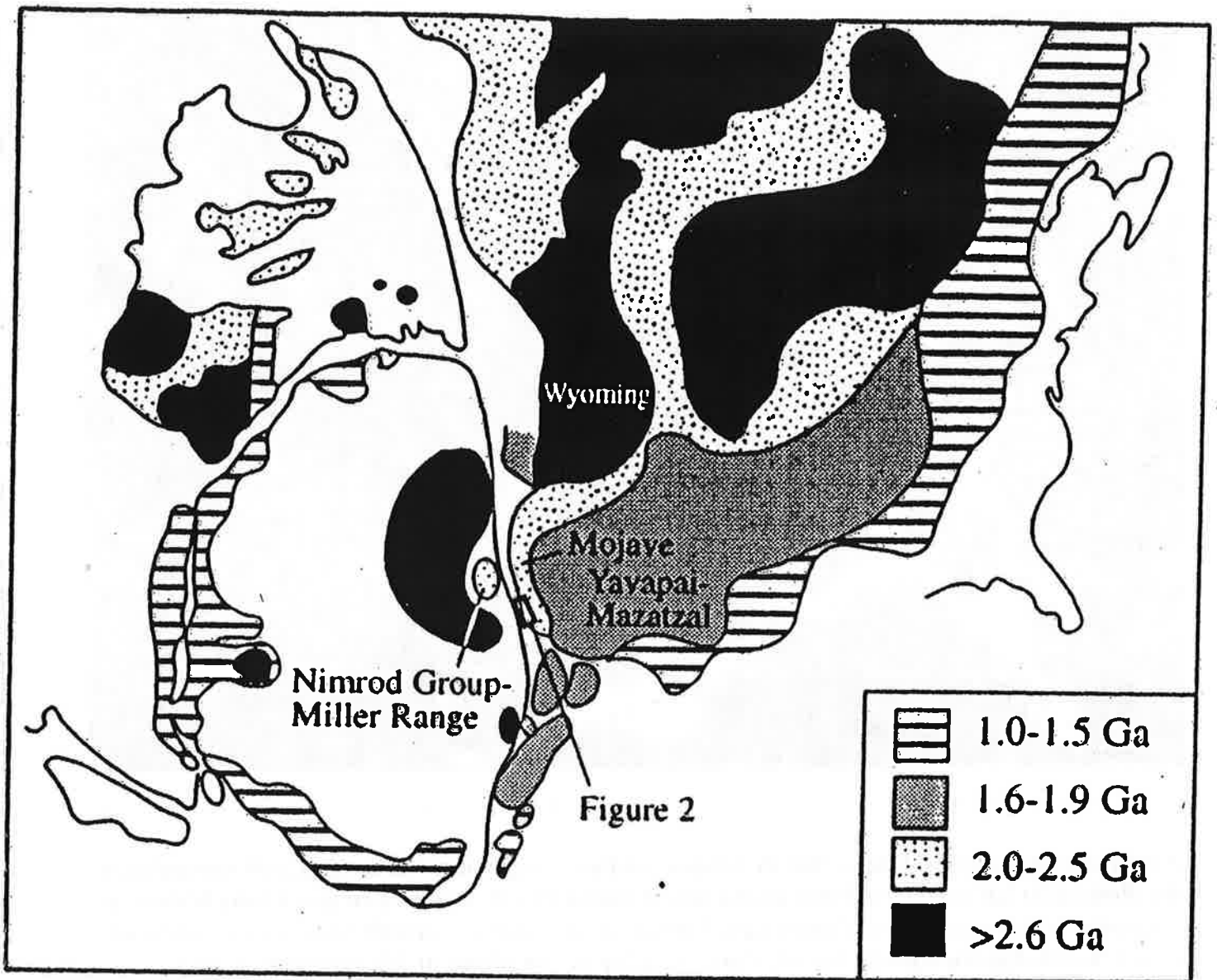
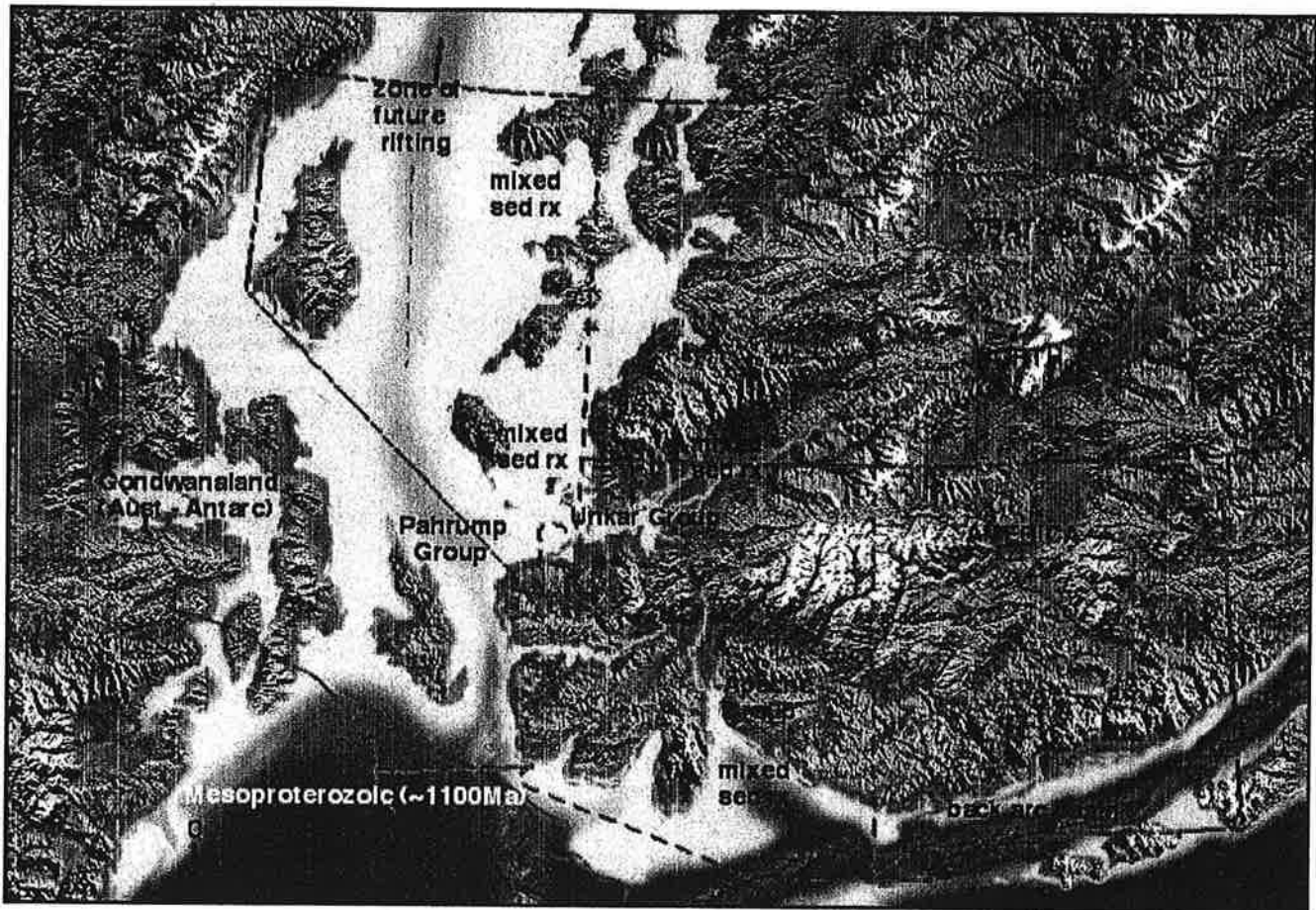


Figure 13. Precambrian tectonic elements of the North American craton (platform cover removed) and Baltic shield. Upper case names are Archean provinces; lower case names are Proterozoic and Phanerozoic orogens. BH, Black Hills inlier; BL, Belcher fold belt; CB, Cumberland batholith; CH, Cheyenne belt; CS, Cape Smith belt; FR, Fox River belt; GF, Great Falls tectonic zone; GL, Great Lakes tectonic zone; GS, Great Slave Lake shear zone; KL, Killarney magmatic zone; KP, Kapuskasing uplift; KR, Keweenaw rift; LW, Lapland-White Sea tectonic zone; MK, Makkovik orogen; MO, Mistassini and Otish basins; MRV, Minnesota foreland; SG, Sugluk terrane; TH, Thompson belt; TS, Trans-Scandinavian magmatic zone; VN, Vulcan tectonic zone; VT, Vetrenny tectonic zone; WR, Winisk River fault.



**Figure 1.** Crust formation age provinces of the North American craton and possible adjacent cratons prior to Late Proterozoic rifting of Rodinia and formation of the Cordilleran miogeocline (adapted from *Borg and DePaolo [1994]*). Rectangle shows the study area in the Transverse ranges, in the westernmost Mojave Province of Laurentia on the shoulder of the Cordilleran rifted margin.





**Neoproterozoic (~ 650 Ma) -- North America rifted away from Antarctica and Australia as the Precambrian supercontinent broke up. Western North America began a long history as a passive margin as the continent moved away from a mid-ocean rift zone. Some blocks of rifted North America likely lay off shore, similar to the island of Madagascar off east Africa today**

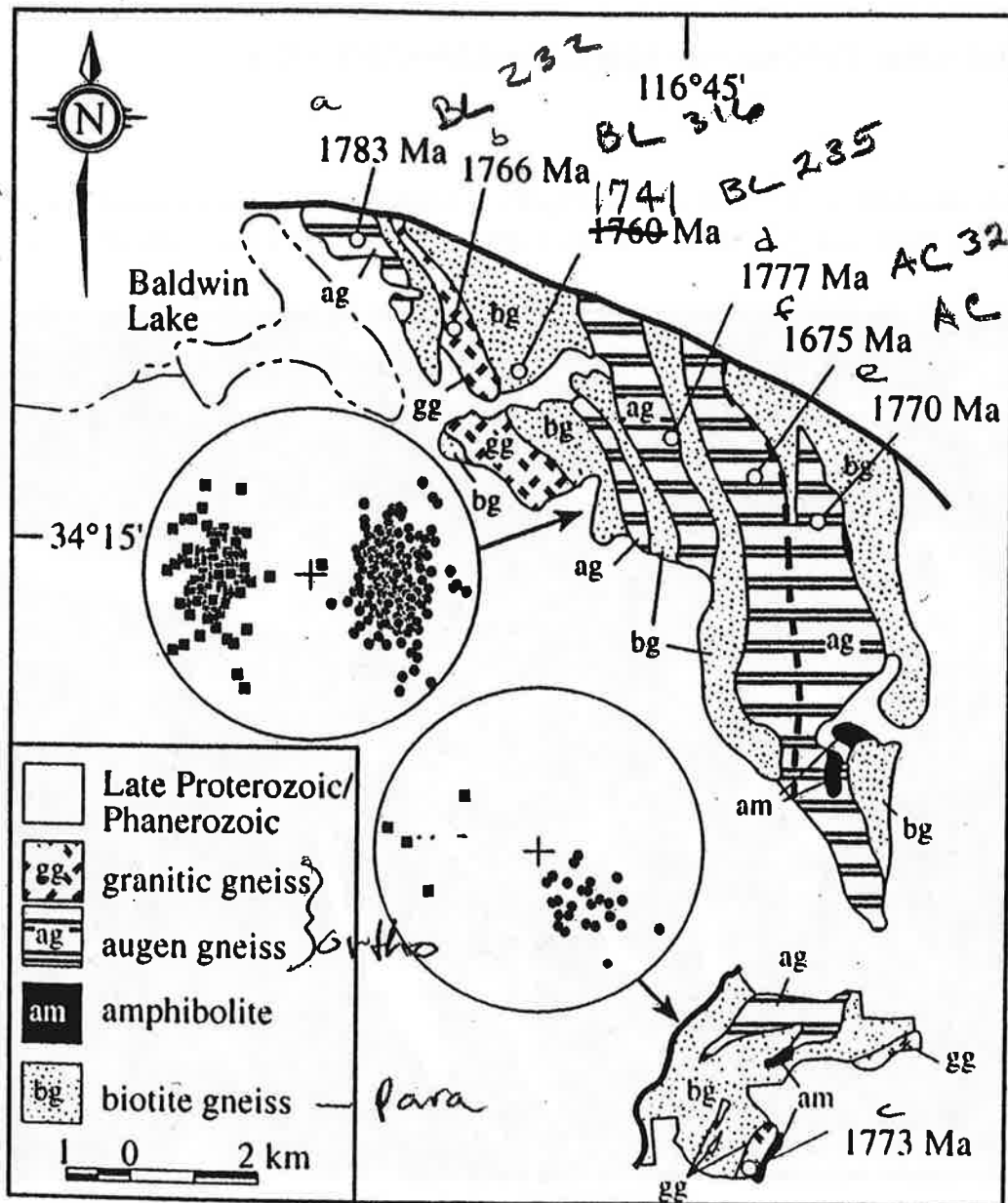
## Precambrian Paleogeography, Southwestern US

---

**Middle Proterozoic (~ 1.7 Ga) -- This highly speculative reconstruction is based on recent work by geologists at Northern Arizona University and the University of New Mexico**



**Mesoproterozoic (~1.1 Ga) -- North America was part of the supercontinent Rodinia and was possibly adjacent to Antarctica and Australia**



**Figure 3.** Geologic map of Proterozoic rocks in the Baldwin Lake area, central San Bernardino Mountains, southern California. U-Pb zircon sample localities are shown with protolith crystallization or depositional age indicated. Inset stereonet plots show penetrative  $D_2$  deformation fabrics  $s_2$  (circles) and  $l_2$  (squares) by subarea.

# THE CORDILLERAN MIOGEOSYNCLINE AND SEVIER(?) OROGENY IN SOUTHERN CALIFORNIA<sup>1</sup>

DAVID L. TYLER<sup>2</sup>

## ABSTRACT

The San Bernardino Mountains, California, on the southern edge of the Mojave Desert, contain Precambrian crystalline rocks and Upper Precambrian and Paleozoic metasedimentary rocks which are exposed in roof pendants in the Mesozoic plutonic rocks which comprise the bulk of the range. Upper Precambrian–Lower Cambrian clastic metasedimentary rocks exposed there, correlative with similar rocks in the Clark Mountains, California, constitute part of the initial deposits along the eastern margin of the Cordilleran miogeosyncline.

Compressional deformation and contemporaneous greenschist facies metamorphism affected the San Bernardino Mountains during early Mesozoic (Sevier?) orogeny. Structures produced by this event were intruded by post-tectonic granitic plutons in Triassic(?) and Cretaceous time. These igneous rocks are part of the Sierran Andean-type magmatic arc and it is the area's location within the arc that controlled its tectonic style.

## INTRODUCTION

Thick sequences of clastic metasedimentary rocks have long been recognized in roof pendants in Mesozoic intrusive rocks of the Sierran arc in the San Bernardino Mountains (Fig. 1) (Vaughan, 1922; Guillou, 1953; Richmond, 1960; Dibblee, 1964a, 1964b, 1967a, 1967b). Vaughan (1922) considered these rocks to be early Paleozoic in age, whereas subsequent workers thought them to be Carboniferous in age. Recently, Stewart and Poole (1975) correlated these rocks with known uppermost Precambrian and lower Paleozoic rocks of the southern Great Basin. Detailed mapping of these rocks in the eastern San Bernardino Mountains (Fig. 1) has provided additional data for correlation and also some insight into the structural history of this geologically complex area.

## ROCK UNITS AND CORRELATION

Stewart and Poole (1975) recognized for the first time in the San Bernardino Mountains four formations of Late Precambrian to Middle Cambrian age that are typical of the basal part of the miogeosynclinal sequence of the southern Great Basin. The four formations are, in ascending order, the Stirling Quartzite, Wood Canyon Formation, Zabriskie Quartzite, and Carrara Formation. In the area of this study the three younger formations were mapped, with only slight differences in the horizons selected as contacts from those used by Stewart and Poole (1975). There is, however, an important difference between the stratigraphy of the basal part of the section, the Stirling Quartzite, pre-

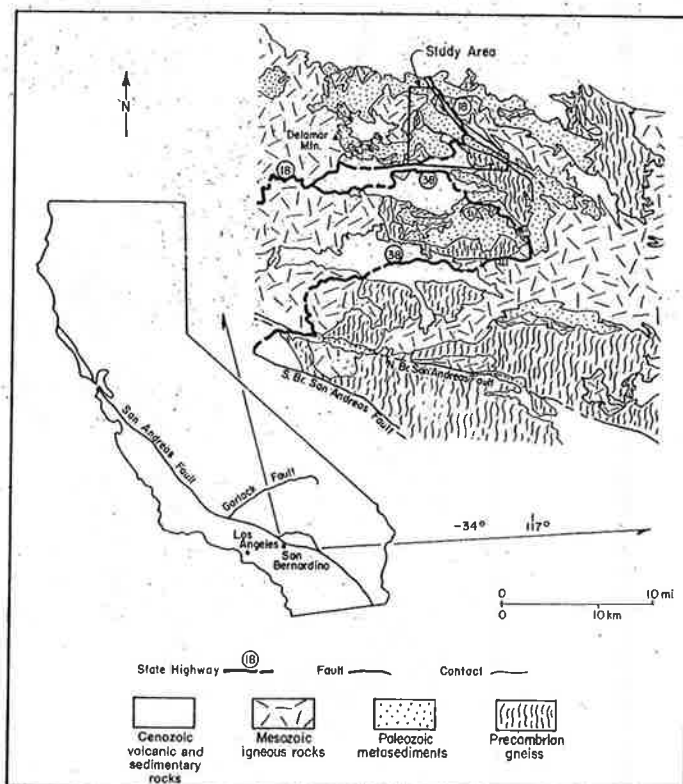


Figure 1.—Index Map of the San Bernardino Mountains and the Baldwin Lake study area.

<sup>1</sup>Editor's Note: Although the San Bernadino Mountains are not in the Basin and Range, this paper is included in this volume because it provides significant control on the position of the Paleozoic Hinge-line and the Mesozoic thrust belt in the southern Basin and Range Province.

<sup>2</sup>Chorney Oil Co., Denver, Co.



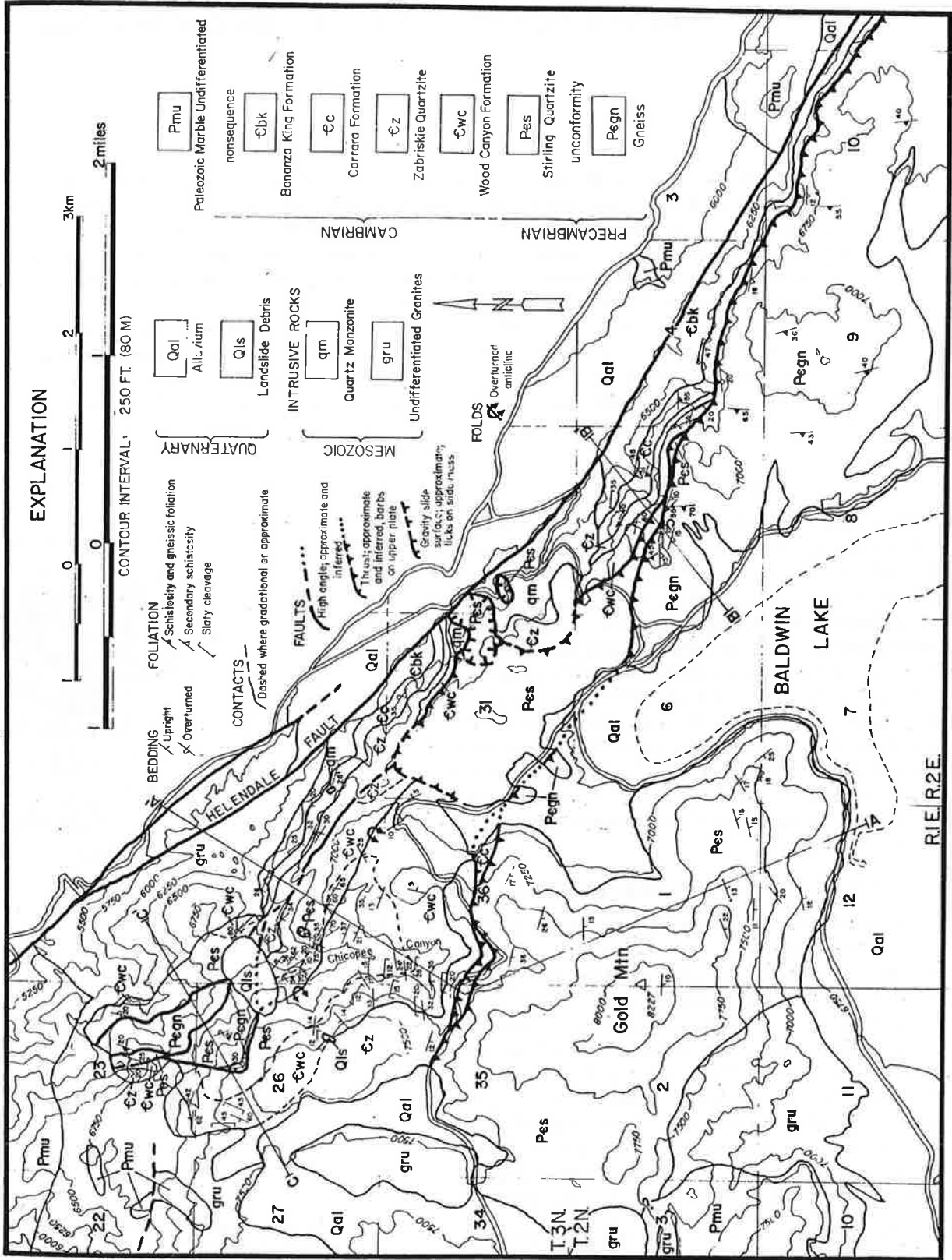


Figure 3.—Geological map of the Baldwin Lake area, San Bernardino Mountains, California.

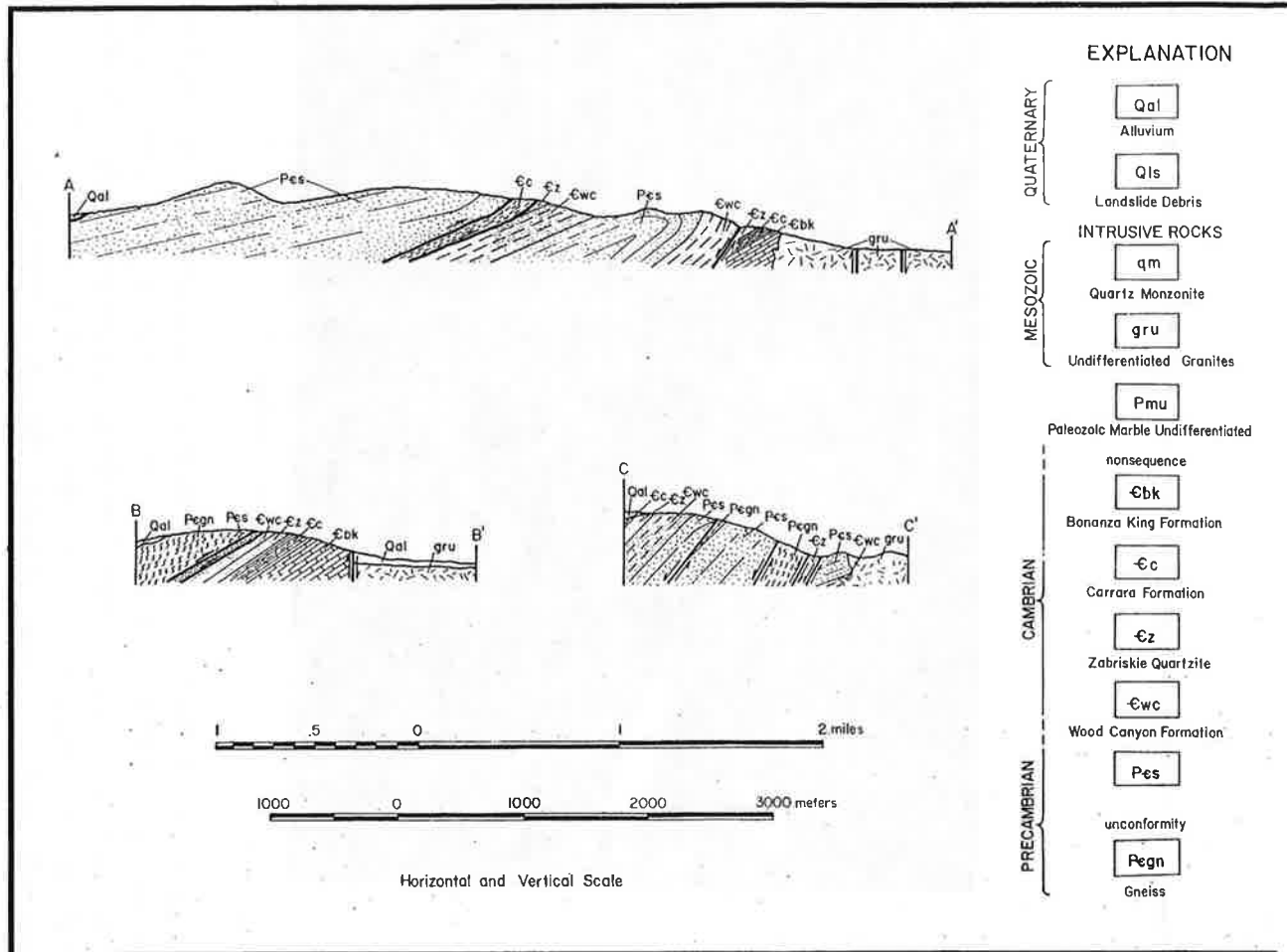


Figure 4.—Geological cross-sections of the Baldwin Lake area.

chlorite, actinolite, and epidote. Foliation is developed as slaty cleavage in the Lower Cambrian Carrara Formation, and as secondary foliation in the Precambrian crystalline rocks.

The foliation is parallel to the axial plane of a large, northwest-trending, northeast-vergent anticline exposed in Chicopee Canyon. Foliation in the Carrara schist is locally folded into secondary recumbent isoclinal folds with axes parallel to the large fold. Overriding the large fold with northeast vergence is a thrust sheet of lower Stirling Quartzite and Precambrian basement. The thrust cuts obliquely across the fold in the lower plate and formation contacts in the upper plate (Fig. 3). The geometry of faults in the northwest axial portion of the large fold is shown on cross-section C-C (Fig. 4), but the evolution of these faults is unclear.

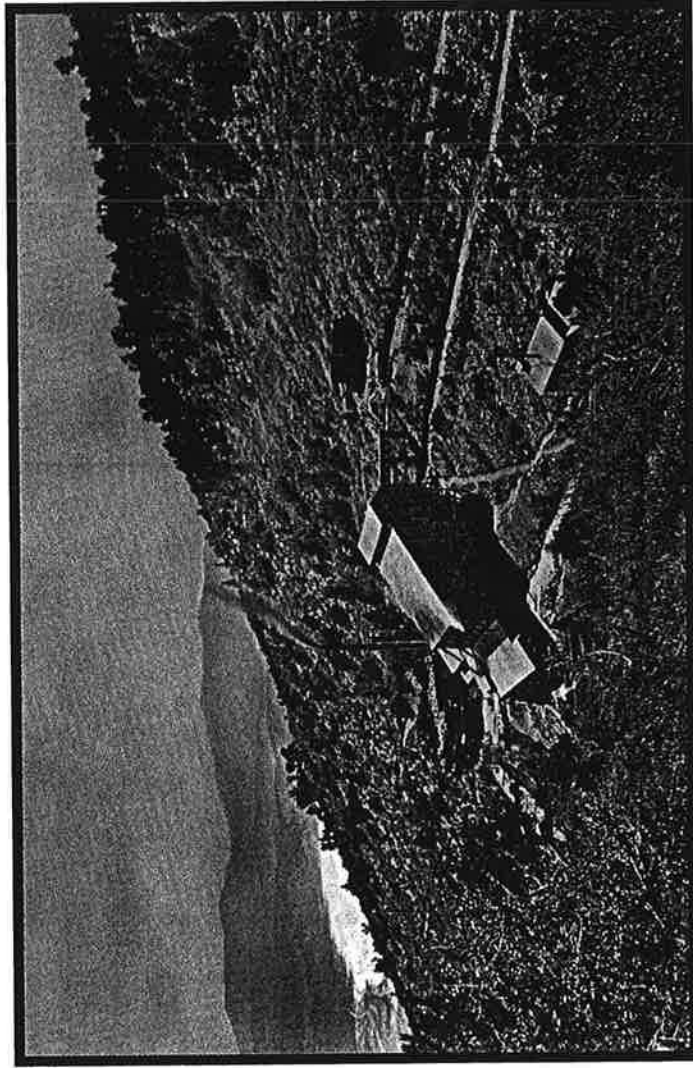
Burchfiel and Davis (1971a) have reported a similar

oblique relationship between stratigraphy and thrust Clark Mountains. In the Winter's Pass thrust plate Clark Mountains, as at Baldwin Lake, the thrust shows no stratigraphic control and involves Precambrian basement, a geometry unlike thrusts farther north in the Sevier belt. Burchfiel and Davis (1971a) have suggested that this change in deformational style, associated with greenschist facies metamorphism, is related to the cutting relationship between Paleozoic geosynclinal and Mesozoic magmatic trends (Fig. 6). Although east of the Cretaceous Sevier thrust belt, the Winter's Pass metamorphism has been dated as early Mesozoic (Burchfiel and Davis, 1971b). By analogy, the Baldwin Lake structure also can be considered early Mesozoic in age.

Post-tectonic plutons of intermediate to acid position intrude the metamorphic rocks. Hornblende and biotite K-Ar ages reported by Armstrong and Supp

---

# Mining the Mountains



*Lucky Baldwin Mine - Circa 1900*

It was mining that first brought people in large numbers to Bear Valley. Bill Holcomb's discovery of gold in Holcomb valley started a Gold Boom. However, the Gold Boom never really lived up to expectations. Over the years many different men and companies were to try their luck wrestling gold and other precious metals from the surrounding mountains. The 40 stamp mill built by "Lucky Baldwin" averaged about 120 tons of ore per day. The ore was of such low grade that mining never turned much of a profit for the operators. The stamp mill is now gone. You can wander through its foundations, and the loading chute still over looks the valley where Bairdstown used to sit. Among the attempts to extract gold from the Big Bear area was a railroad steam shovel operated by the Valley Gold Company Ltd. This steam shovel managed to dig a trench 8 feet deep, 16 feet wide and over a half mile long across Holcomb Valley in 1895. It proved to be both an expensive and futile effort.

Furnace marble was thrust over biotite quartz monzonite. Debris, eroded from marbles brought into higher relief by movement on thrust faults, formed terrace deposits of Pleistocene(?) age along the north front of the range and talus breccias on the rising upland surface.

Later the range front was further elevated along northwest-trending high-angle reverse faults. Some of the faults cut terrace deposits. South of Holcomb Valley a fault block was elevated. Depression of the south part of the block along normal faults left the westward-trending ridge that now separates Holcomb and Bear Valleys.

Along the north front of the range, the south side of Holcomb Valley, and the north side of Bear Valley, older alluvium in some places conceals high-angle faults and in other places is cut by them. Rejuvenated northward-flowing streams have deeply dissected the terrace deposits at the front of the range.

## MINERAL RESOURCES

### Introduction

In May 1860, William F. Holcomb discovered placer gold in the valley that was later named for him. The diggings were generally shallow and easily worked. The richest deposits were found in Upper Holcomb Valley where the boom camp of Belleville recorded a voting population of nearly 100 in November 1860. In the State election of September 4, 1861, more than 300 votes were cast in Belleville precinct as compared to 959 votes for all of San Bernardino County (Holcomb, 1900). The *Mining and Scientific Press* (vol. 2, no. 43, January 4, 1861) reported "we are informed that there was great excitement in San Bernardino, last week, because of the recent discovery of rich diggings in Holcomb Valley . . . we are credibly informed of some parties making 50 dollars a day with a rocker". The *Los Angeles Star*, quoted in the *Mining and Scientific Press* (vol. 4, no. 22, February 15, 1862) reported "a large number of placer claims are being worked . . . there were about 100 men in the mines . . . the average amount of gold obtained from the placer diggings ranges from 5 to 15 dollars a day to the man". Later the *Mining and Scientific Press* (vol. 9, no. 2, July 9, 1864) reported "late intelligence from there states that a large amount of work is now in progress; a number of lodes are being opened".

The richer known placers, however, were soon exhausted and, handicapped by the scarcity of water, Holcomb Valley was again nearly deserted by 1880. Later the Holcomb Valley Company, Ltd., an English concern, unsuccessfully developed the placers from the late 1880s to 1894. The area has been intermittently worked since and was last seriously mined during 1933-41 by the Holcomb Valley Placer Company. A few abandoned cabins stand on the old placer sites (fig. 70) and one placer (Lee Placers) is intermittently in operation, but the current economic activity of Holcomb Valley is limited to the summer grazing of cattle.

Scores of idle adits, shafts, and pits in the highlands and north slopes of the San Bernardino Mountains attest to the search for primary metallic deposits. The known occurrences of metallic minerals including gold, silver, lead, zinc, iron, manganese, and tungsten and the non-metallic deposits of the area are described in the accompanying tabulated list. Some of the claims for metallic

minerals have been operated extensively in the past; but all of them have been non-productive for at least 15 years, some for more than 50 years, and their past production was not determined by the writer. Intermittent development work and exploration, however, on a small scale continues at some properties. The nonmetallic minerals of the area, especially limestone and dolomite, were being actively explored during 1958.

### Metals

#### Lode Gold

Primary gold deposits in the mapped area have been extensively explored since their discovery nearly 100 years ago, but recent activity has been mostly small scale prospecting. During 1958 the most active exploration was at the Independence mine No. 1 (no. 16, fig. 61) but there was no production. Gold claims have been located in nearly equal numbers in three geologic types of primary deposits in the Holcomb area.

1. Mineralized shear or fracture zones in quartz monzonite:

Typical examples of fissure fillings in thin shear zones occur at the Wright mine (no. 33, fig. 61); Harvey K mine (no. 13, fig. 61); Ozier mine (no. 25, fig. 61); and Osborne mine (no. 24, fig. 61). Rarely, free gold is recovered from small pockets in thin shear zones (Alvin Linder, owner-operator of Wright mine, personal communication, 1953). More commonly gold is associated with hematite or pyrite although chalcopyrite, galena, and sphalerite occur in small quantities. Thin sulfide and hematite lenses are reported by local residents to have been encountered in the Harvey K and Ozier mines.

2. Mineralized fault contacts:

Numerous shafts and adits are distributed along thrust fault contacts between carbonate and plutonic rocks in lower Furnace Canyon (sec. 18, T. 3 N., R. 1 E.) and west of Crystal Creek Canyon (sec. 11, T. 3 N., R. 1 W.). More extensive workings, as judged by tailing piles such as that at the Gold Button mine in lower Silver Canyon (no. 10, fig. 61), followed faults in granite cataclasis.

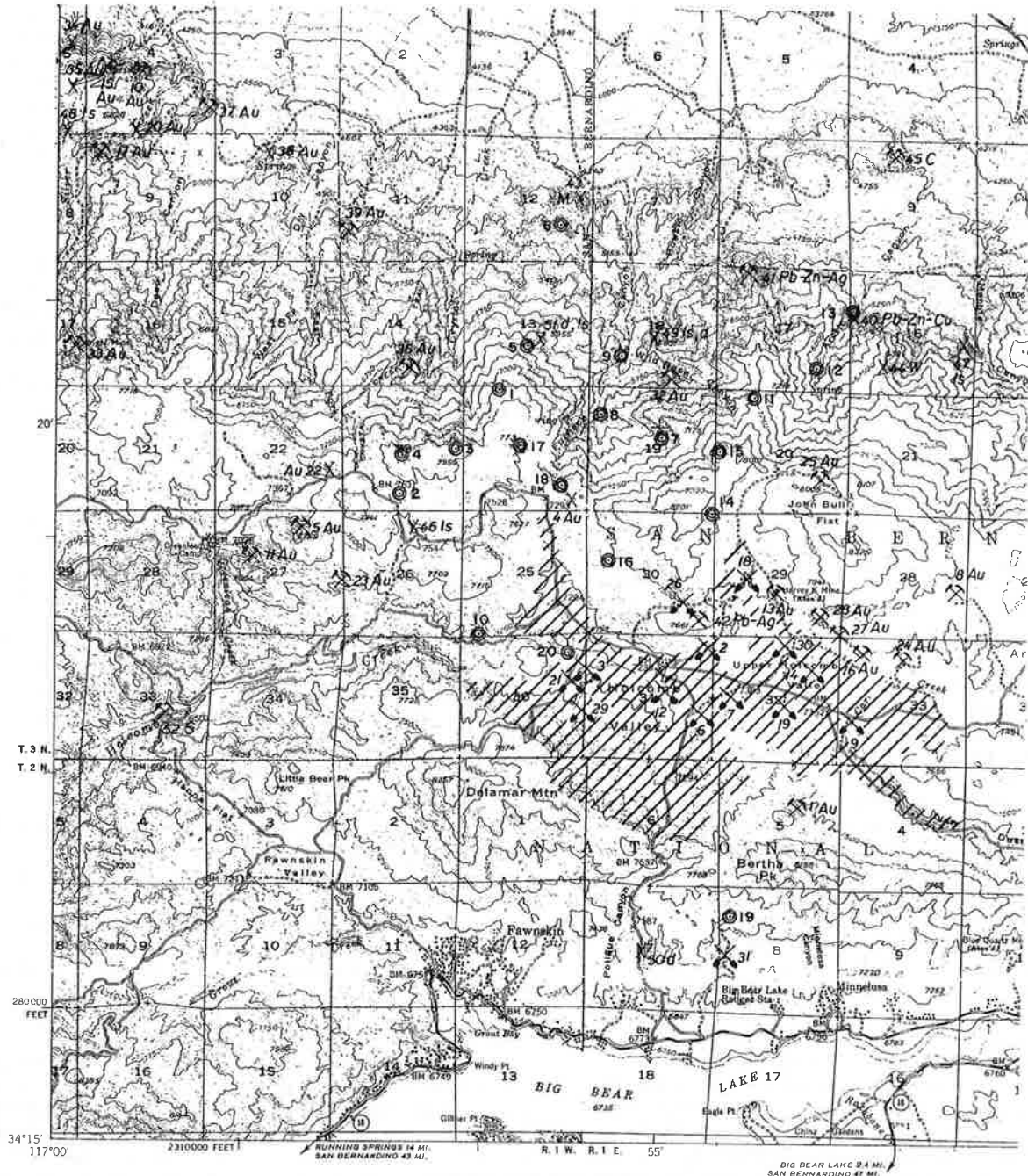
3. Mineralized contacts between carbonate rocks and plutonic intrusive rocks:

The Greenlead mine (no. 11, fig. 61) is perhaps the oldest (patented 1876) and largest of operations at intrusive contacts into the Furnace formation. Although the adit was re-opened and cleaned to a length of 370 feet in 1953, no ore body was discovered and the mine has not been in production since about 1900. In the earlier operations, gold and some silver are reported to have been recovered from a drift that followed a quartz vein along a contact between biotite quartz monzonite and crystalline limestone. Elsewhere in the area north of Big Bear Lake, as on the slope at elevation 7450 east of the head of Furnace Canyon (SE $\frac{1}{4}$  sec. 24, T. 3 N., R. 1 W.), gold is associated with hematite in a quartz breccia where biotite quartz monzonite or granite porphyry intrude marble of the Furnace formation. Only a few of the gold claims are located directly at taconite or skarn deposits.

#### Placer Gold

The Holcomb Valley placer gold deposits were extensively worked for a few years following their dis-





EXPLANATION

Numbers refer to tabulated list entries

- 28 Mine or quarry
- 43 Metal prospect or nonmetallic deposit which has not been operated
- 30 Placer gold
- 49 Mineral processing plant
- 13 Carbonate rock sample locality, chemical analyses listed in table I.

ABBREVIATIONS:

Metals: Au=gold; Pb-Zn-Ag=lead,zinc,silver; M=manganese; W=tungsten; Pb-Ag=lead,silver; Pb-Zn-Cu=lead,zinc,copper.  
 Nonmetallics: C=clay; ls=limestone; d=dolomite; S=sand and gravel.



Holcomb Valley gold placer area, covered with Recent and older alluvium and gravels. Gold bearing in places.



SCALE  
 Contour interval 50 feet

Figure 61. Economic map of San Bernardino Mountains north of Big Bear Lake.

covery in 1860 and this probably was the first large mining operation in San Bernardino County. The area is said to have been first worked by Mexicans who screened the soil for small lumps of gold-bearing hematite. The last reported productive placer mining was during the period 1933-41 when Mr. George Knudsen and Mr. William G. Lacy (Holcomb Valley Placer Company) operated the Holcomb and Garvey Placers in Upper Holcomb Valley (figs. 63, 64). Initial operations were by small scale hand methods, but in 1935 a four-bowl washing plant (fig. 69) was installed and mining was done with a small power shovel and two dump trucks. Beginning about 1938 the mining was done by Caterpillar tractor and carryall until operations ceased in 1941. Mr. Knudsen reports (personal communication May 1958) that the placer deposit was shallow, as thin as one foot deep in places. He estimates that 200,000 cubic yards of placer material were handled, yielding an average gold value of about 38 cents per yard.

The gold-bearing material mined in the central part of Holcomb Valley (fig. 63) is Recent alluvium and gravel and the material along the margins of Holcomb Valley and occupying most of Upper Holcomb Valley is older alluvium and gravels. Locally the gold-bearing gravels are termed "bench gravels" (figs. 65, 66, 67). These are included in the older alluvium and gravels shown on the accompanying geologic map (pl. 1). The older alluvium consists principally of deeply weathered massive quartzite and granitic rocks and small quantities of marble in a matrix of sand and gravel. The largest fragments rarely exceed 8 inches in diameter. Little is known of the depth of the older alluvium, but a water well completed in 1952 in the SE $\frac{1}{4}$  sec. 31, T. 3 N., R. 1 E. is said to have penetrated 100 feet of gravel and an additional 200 feet of interlayered clay and gravel without striking bedrock. The Recent alluvium and gravels is largely derived from the older alluvium, but lacks the reddish yellow color that characterizes the older alluvium.

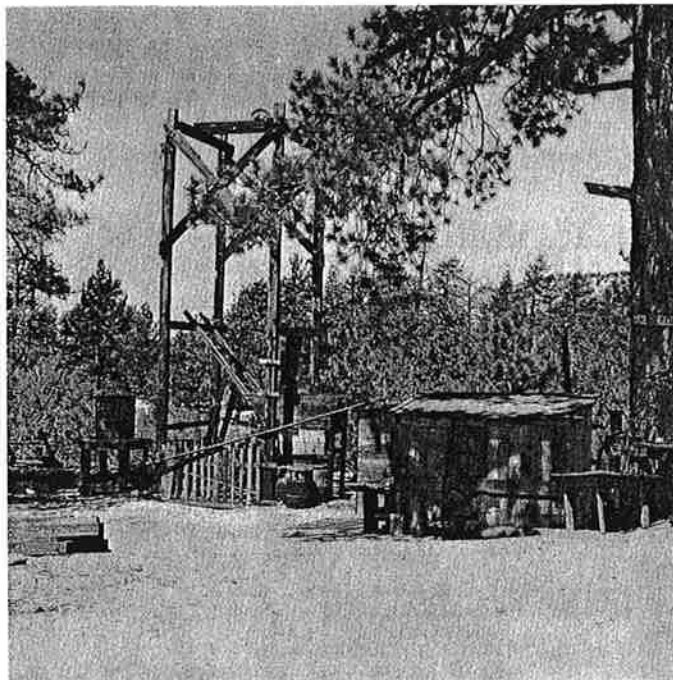


Figure 62. Idle Harvey K mine, east side of Upper Holcomb Valley, 1956. This shaft, inclined about 45°, explores a mineralized fracture zone in biotite quartz monzonite.



Figure 63. Panorama of Upper Holcomb Valley gold placer area, east part of the Slap Jack claim. Camera facing south; February 1940. Tailing pile, left middleground, at Plant No. 1 of Holcomb Valley Placer Company. Ditch, in foreground, for water development, is in Recent alluvium and gravels locally termed "meadow ground". The gold-bearing gravels that were mined, included in the older alluvium and gravels shown on plate 1 and locally termed "bench gravels", occupy the gently rolling topography in the background, commencing at about the tree line. Photo courtesy Lacy Oil Tool Company, Los Angeles, California.

## HIGH BRIGHTNESS, HIGH PURITY LIMESTONE IN THE SAN BERNARDINO MOUNTAINS OF SOUTHERN CALIFORNIA, GEOLOGY, GENESIS AND MINING

Howard Brown, Pluess-Staufer (California), Inc., P.O. Box 825 Lucerne Valley, CA 92356.

### INTRODUCTION

The San Bernardino Mountains and nearby Mojave Desert area of southern California contain the largest high brightness, high purity limestone and some of the largest cement grade limestone mining operations in western North America (Fig. 1). Combined annual production of high brightness limestone products from several open pit mines is approximately 1.5 million tons, with an estimated gross value of \$75 million dollars per year. An additional 5.0 million tons of cement grade limestone is mined by several large cement producers in the San Bernardino Mountains and nearby Mojave Desert area.

### GEOLOGIC SETTING

Late Precambrian and Paleozoic metasedimentary rocks unconformably overlie earlier Precambrian basement. Paleozoic sequences in the San Bernardino Mountains contain elements of both cratonal and miogeoclinal affinity (Fig. 2). A major unconformity is present between Upper Cambrian and Devonian strata throughout the region. Upper Precambrian and Lower Cambrian rocks are of miogeoclinal aspect, middle Cambrian strata are of cratonal aspect, and upper Paleozoic rocks are similar to inner miogeoclinal facies of the central and eastern Mojave region (Brown 1984).

High brightness, high purity crystalline limestone deposits and cement grade limestone deposits occur in upper Paleozoic miogeoclinal limestone formations in the San Bernardino Mountains.

Several major tectonic events have been recognized in the San Bernardino Mountains, including Mesozoic age multiphase folding and thrust faulting, contact and regional metamorphism, and intrusive events. Cenozoic activity includes high and low-angle faults, mild folding, and the area continues to be seismically active as evidenced by the large number of significant earthquakes in the area during 1992.

The complex geologic history of the San Bernardino Mountains has allowed the formation of several large high brightness, high purity limestone deposits and cement grade limestone deposits which are currently being mined or will be mined in the future.

### GENESIS OF WHITE HIGH CALCIUM LIMESTONE DEPOSITS IN THE SAN BERNARDINO MOUNTAINS

Carbonate rocks are found extensively on all continents, but high purity, high brightness (white) limestone deposits are relatively uncommon in nature because their formation is dependant on the superposition of several independent geologic processes, acting over a long period of time.

Among the processes are:

- 1) Deposition of originally pure limestone in high energy agitated, shallow marine environment.

- 2) Post depositional changes including metamorphism and/or magmatic processes to bleach and recrystallize the rock, and disperse any impurities which may have been present.
- 3) Structural controls including folding, faulting and orogenic processes to place the rocks in desirable structural settings.
- 4) Uplift and erosion.
- 5) Preservation thru geologic time.

Because all the geologic processes are required, deposits of high calcium white crystalline limestone are relatively uncommon in nature, and are vastly different from common limestone.

Within the southwestern United States, currently productive, and potentially productive deposits of white, high purity limestone are present in the San Bernardino Mountains. and the area is by far the largest producing district in western North America.

#### USES AND SPECIFICATIONS OF HIGH BRIGHTNESS, HIGH PURITY LIMESTONE

High purity white crystalline limestones have a large number of uses as white fillers and extenders with value added characteristics. The products are finely ground, high brightness, high purity limestone, and are the whitest, purest, and most valuable per ton of all limestone products.

Desirable characteristics are high brightness (white color), low tint, uniform fine particle size, freedom from grit, and chemical purity. Color and purity are of utmost importance in virtually all applications. Limestone suitable for white fillers and extenders is limited to a minimum of 98%  $\text{CaCO}_3$ , and a maximum of 2% combined  $\text{MgCO}_3$ ,  $\text{SiO}_2$ , and all other impurities combined. Brightness requirements range from low 90's to greater than 95. Tint values are generally below 2.0.

The greatest uses of fillers and extenders are paint, rubber products, putty, pottery, paper, a variety of plastics, food, flooring, PVC pipe, white ink, tooth paste, wire coating, glue, caulking compounds, resins, and polyesters. Uses in the housing industry include ceiling and wall textures, dry wall mud, joint compounds, stucco, and fiberglass roofing shingles.

For most uses, white fillers and extenders requires not only the most pure limestone, but also the whitest color of all limestones. The restricted nature of the deposits and the fact that products are shipped as far as 2000 miles from the source, indicates a large demand by our society for these valuable products.

#### EXISTING HIGH BRIGHTNESS LIMESTONE MINING OPERATIONS SAN BERNARDINO MOUNTAINS

Several large, open pit, white, crystalline limestone/calcite marble quarries and undeveloped deposits are present in the San Bernardino Mountains. Combined annual production is approximately 1.5 million tons with an estimated gross value of \$75 million dollars per year. Pfizer Inc., Pluess-Staufer (California), Inc., and Partins Limestone (Riverside Cement) are the major producers of white crystalline limestone products (Figure 1).

An estimated 5.0 million tons of cement grade limestone is also mined by several large cement producers from the San Bernardino Mountains and nearby Mojave Desert area.



## SPECIALTY MINERALS INC. (PFIZER INC.) MINING OPERATIONS

Specialty Minerals Inc. (formerly Pfizer Inc.) Lucerne Valley operation is the largest producer of high brightness limestone products in the San Bernardino Mountains, and has been in continuous operation for 30 years. During the 1960's and 1970's ore came from quarries in Furnace Canyon, which were developed in complexly folded and faulted, and overturned Devonian Sultan Limestone Crystal Pass Member, which has been metamorphosed to a medium grained white calcite marble.

Since 1980, all ore has come from the Marble Canyon quarry. This large quarry has been continuously mined by various operators since 1972. The orebody is composed of medium grained, white calcite marble of the Mississippian Monte Cristo limestone Bullion Member, which has been multiply folded and is steeply dipping but overturned in the quarry area.

The Marble Canyon deposit is a multi-bench side hill quarry. Two to three working levels are operated at any one time to supply the rock needed to meet production requirements.

The projected Marble Canyon deposit life is 20 years, depending on customer demand. Pfizer mined the Marble Canyon deposit continuously since 1980. Completion of mining activities will result in approximately twenty-three million (23,000,000) tons of ore and about nine million (9,000,000) tons of low grade material and overburden having been removed from the quarry.

## PLUESS-STAUFER (CALIFORNIA), INC. MINING OPERATIONS

Pluess-Staufer (California), Inc. mines and processes high quality white limestone from extensive deposits in the San Bernardino Mountains, and is the second largest producer of high quality limestone fillers and extenders in the western United States (Fig. 1).

Pluess-Staufer (California), Inc. took over operations during the late 1970's, and has discovered new deposits, and proven sizable reserves at existing mines. Existing proven minable and permitted reserves are currently adequate for over 25 years.

Currently three active mines are producing limestone from the Bullion Member of the Monte Cristo limestone of Mississippian Age. The stratigraphic section at the Claudia and Sentinel quarries is upright, while the White Knob Quarry is developed in an overturned section. At Sentinel quarry the full thickness of Bullion Member is present, and the deposit is up to 400 feet thick. The White Knob Quarry deposit occurs in the core of a tight overturned isoclinal fold, and the thickness of the Bullion Member has been increased. At White Knob, rocks have been multiply metamorphosed to granulite facies, forming exceedingly coarse grained, very white translucent calcite marble. Individual calcite rhombs are commonly over 1 inch across.

Mining from the multibench open pit quarries is accomplished by conventional methods. Ore is drilled and blasted and loaded by 13 cubic yard front end loaders, into 50 and 85 ton rear dump haul trucks and trucked to primary crushers located at the Sentinel and White Knob quarry sites. At the crushers, ore is crushed, screened and stockpiled by various quality grades.

Crushed ore is hauled on 85 ton haul trucks, to the plant in Lucerne Valley at the base of the mountains. At the plant computer controlled grinding systems allow very precise blending and grinding of the material to very narrow product specifications, or any specific specification a customer desires. Pluess-Staufer produces a full range of coarse, fine, and ultra fine grind, high brightness, high purity calcium carbonate products. Plant facilities offer both bulk and bagged materials in rail or truck quantities.

## PARTINS LIMESTONE (RIVERSIDE CEMENT) MINING OPERATION

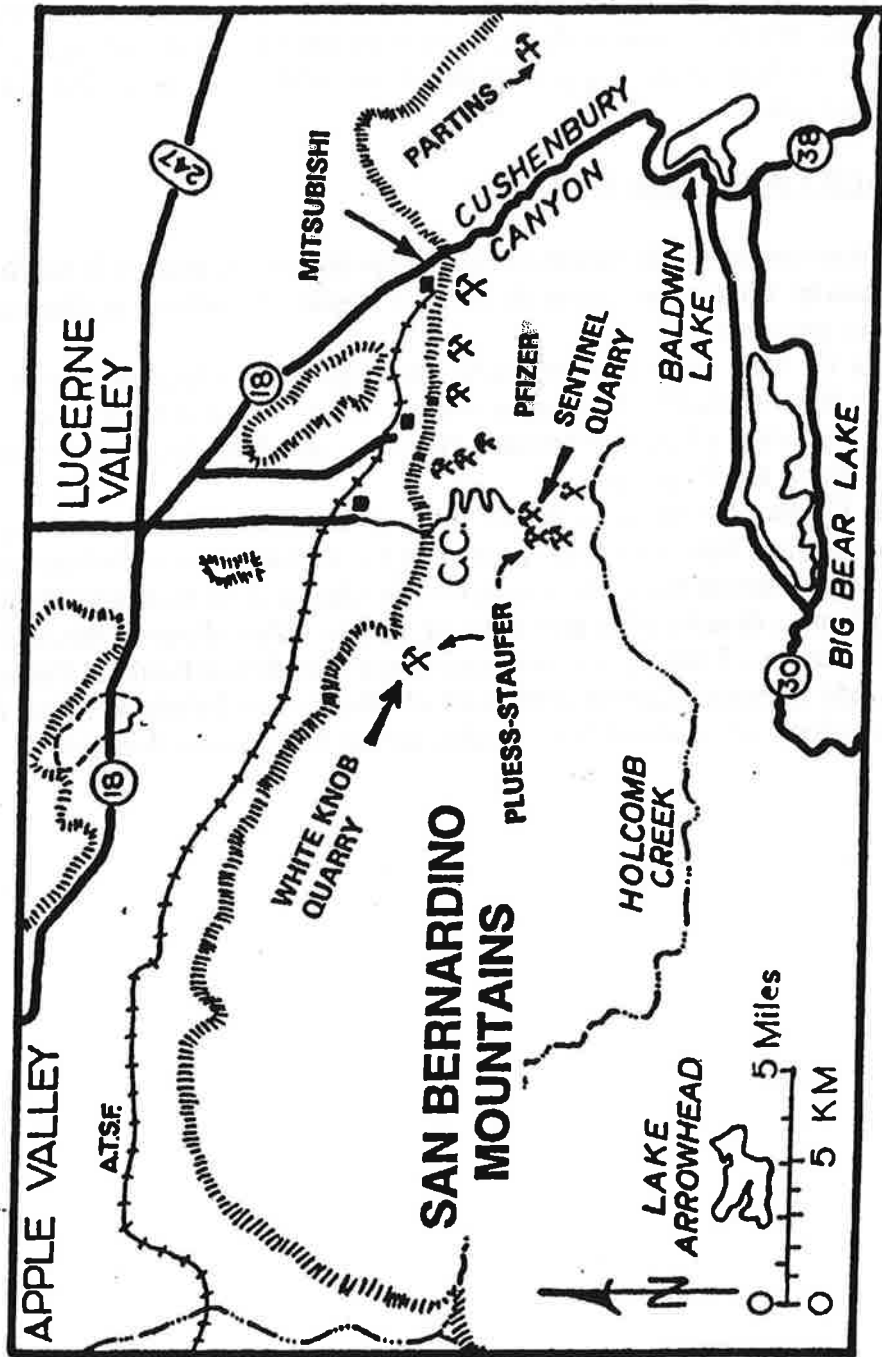
Partins Limestone (Riverside Cement) mines White calcite marble from a quarry east of Cushenbury Canyon along the range front (Figure 1). White marble has been mined for many years at this location. The moderate to steeply dipping, folded and metamorphosed, white marble deposit occurs in the Bird Spring Formation of Pennsylvanian age (Brown 1986), and is about 40 to 50 feet thick. The rock is generally pure, medium grained, white calcite marble. The main product produced is white swimming pool sand. Some of the rock is hauled to Crestmore and utilized for white cement.

## CEMENT GRADE LIMESTONE QUARRIES

Several large cement grade limestone quarry operations are present in the San Bernardino Mountains and nearby Victorville area of the Mojave Desert. Combined production is estimated at 5.0 million tons per year.

Mitsubishi Cement mines cement grade limestone from a large quarry along the north range front of the San Bernardino Mountains (Figure 1). The Cushenbury Quarry is developed in dominantly grey marble, which is overturned Pennsylvanian Bird Spring Formation. Reserves are said to be adequate for 75 years.

Riverside Cement Company and Southwest Portland Cement Company mine large quantities of cement grade limestone from quarries in the Victorville area. Riverside Cement Co. obtains most of its production from the Sparkhule Hill Quarry near Quartzite Mountain, a large multilevel open pit mine developed in grey colored, metamorphosed upper Paleozoic marbles of the Bird Spring Formation of Pennsylvanian-Permian age. Southwest Portland Cement Co. mines a large cement grade limestone deposit composed of Triassic age Fairview Valley Formation, a grey limestone conglomerate derived from erosion of the Bird Spring Formation.



## DESCRIPTION OF THE FAULT SYSTEM

The frontal fault system on the north side of the San Bernardino Mountains appears to be made up of numerous reverse fault segments which in subsurface may or may not form a single throughgoing fault. At places, especially on the east and west ends, the zone appears to be relatively simple, consisting of only one or two breaks that can be traced several kilometers. However, exposures are poor at the west end of the range, and the system may consist of a complex zone of multiple breaks there. At many places faults may exist farther back in the range, but they are difficult to recognize in the more heterogeneous crystalline units. Small discontinuous shear zones are common in these crystalline rocks more than a mile back from the range front. The aggregate movement distributed across these shears zones could make

up a significant proportion of the total offset across the zone.

Along the central two-thirds of the range front, the fault system consists of a complex zone that ranges from about 1 km to as much as 6 km in width. Most of the individual faults in this part of the zone are short and discontinuous, averaging no more than 2 to 4 km in length. A few of the scarps, interpreted on the strip map (pl. 5.1) as fault scarps, may or may not be of tectonic origin. Some short scarp segments are easily confused with the sharply defined distal scarps of debris flows which are present at several places along the range front (fig. 5.2).

At the relatively few localities where the dip of individual faults in the zone can be measured, it is in all cases toward the south, ranging from about  $10^\circ$  to as much as  $70^\circ$ ; the average dip is about  $45^\circ$ . The dip of individual breaks in one part of the system is not constant for very

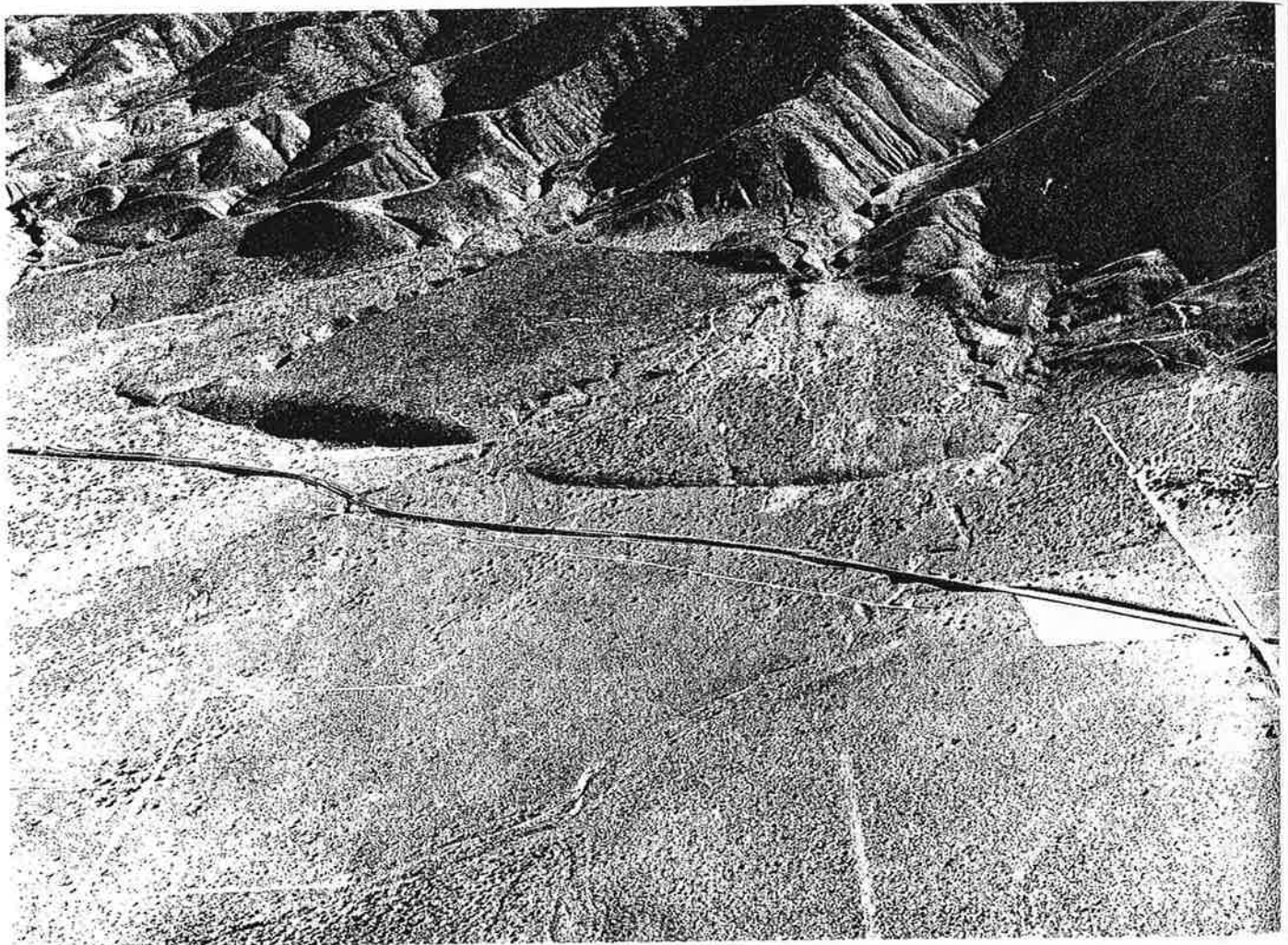
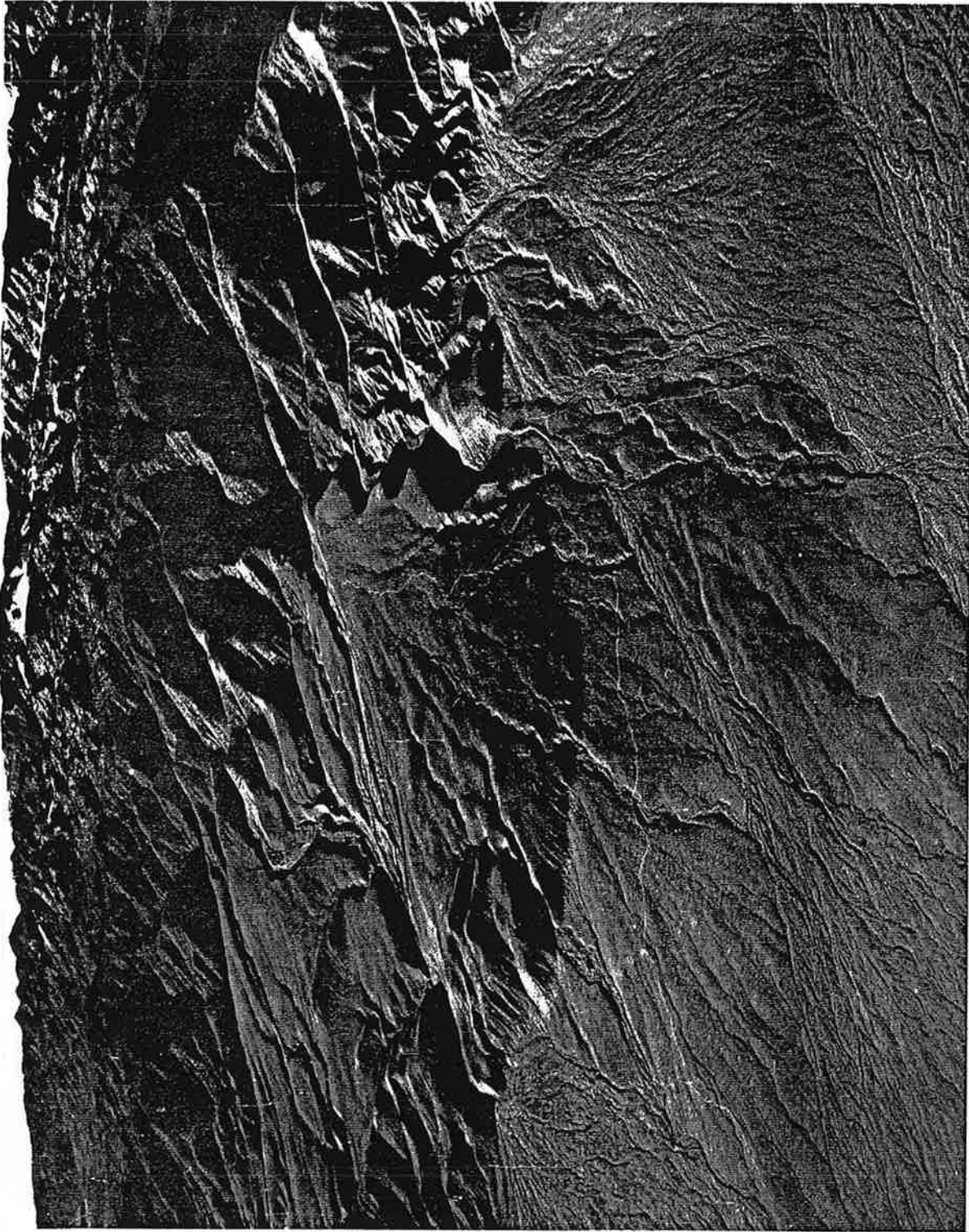
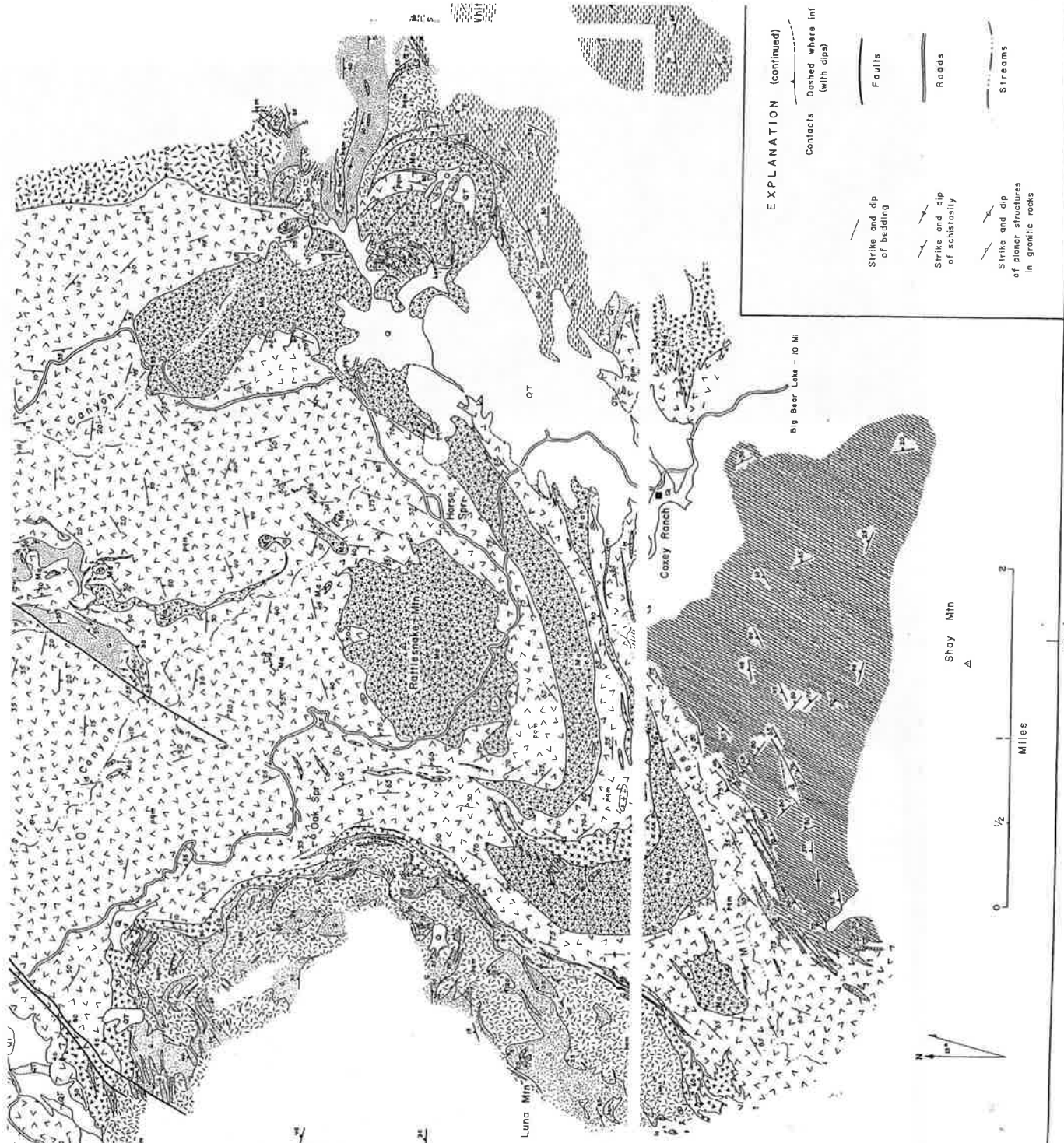


FIGURE 5.2.—Scarp developed near distal end of alluvial fan about 3 km east of Grapevine Canyon; view is toward the south. Scarp is flanked on both sides by debris flows and may or may not be of tectonic origin. Degree of erosion appears to be about the same as that of scarps at west end of range (fig. 5.5). The aligned series of scarps near the head of the fans is developed along the high-angle fault shown in figure 5.4.





**Figure 4.** Oblique aerial view of thrust fault scarps in alluvium about 3.5 miles southeast of the Blackhawk slide. Photograph by John Shelton # 3095

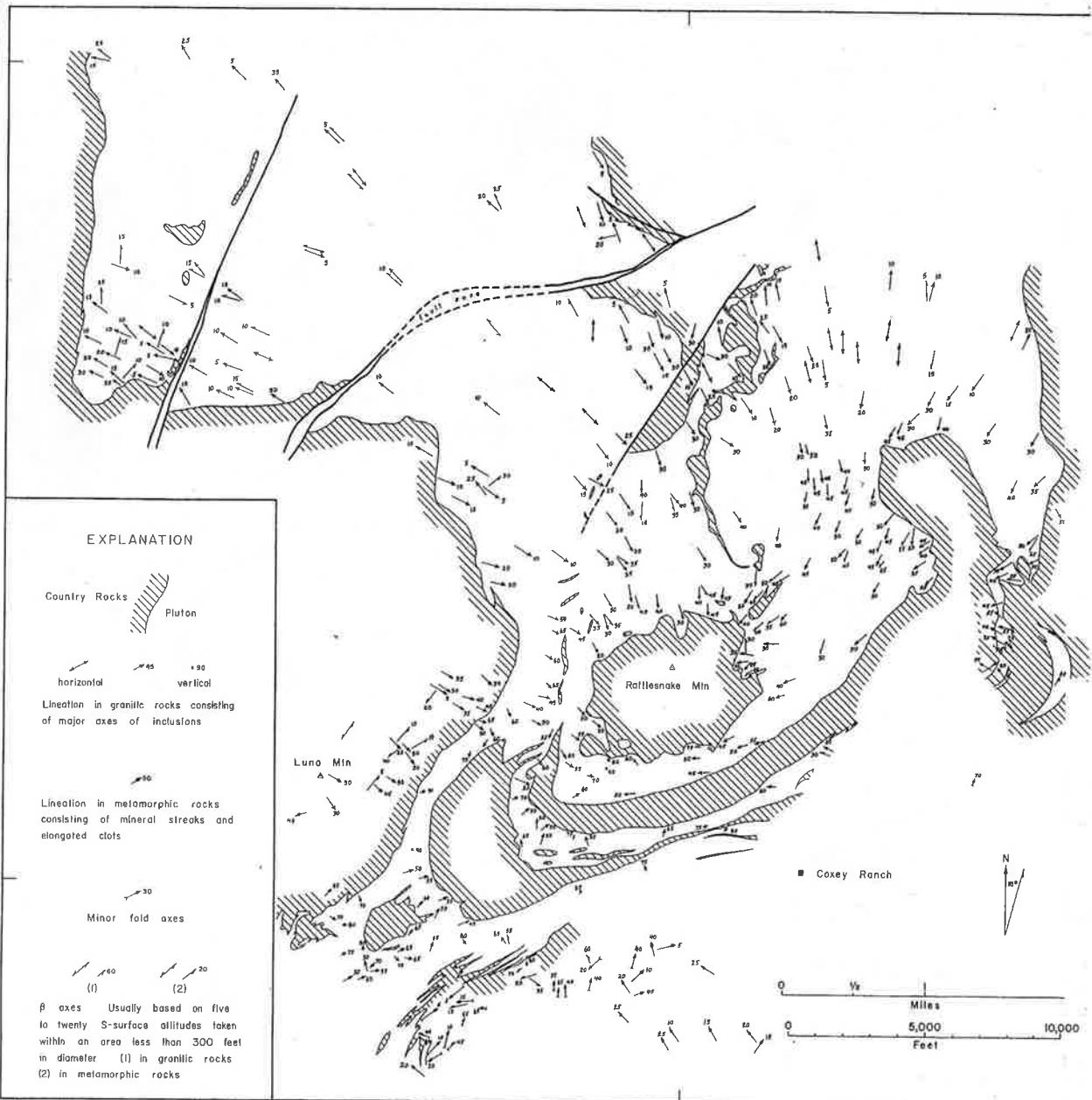


**EXPLANATION**


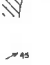
- Quaternary alluvium and terrace deposits
- Lower Pleistocene ? conglomerates, sandstones, and siltstones
- Rattlesnake pluton (porphyritic biotite-quartz monzonite)
- Diorite
- Biotite-quartz monzonite (includes granodiorite and quartz diorite)
- Hornblende monzonite and quartz monzonite
- G - Undifferentiated granulite and diorite  
a - Alaskite
- Marble rocks
- White Mountain complex  
M - marble  
S - schist  
Ct - calc-silicate
- Shay Mountain complex




- EXPLANATION (continued)**
- Contacts (dashed where inf. with dip)
  - Strike and dip of bedding
  - Strike and dip of schistosity
  - Strike and dip of planar structures in granitic rocks
  - Faults
  - Roads
  - Streams

STRI  
the m  
etween  
normal




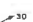
EXPLANATION



Country Rocks  Pluton 

horizontal  45  50 vertical 

Lineation in granitic rocks consisting of major axes of inclusions

Lineation in metamorphic rocks consisting of mineral streaks and elongated cots 

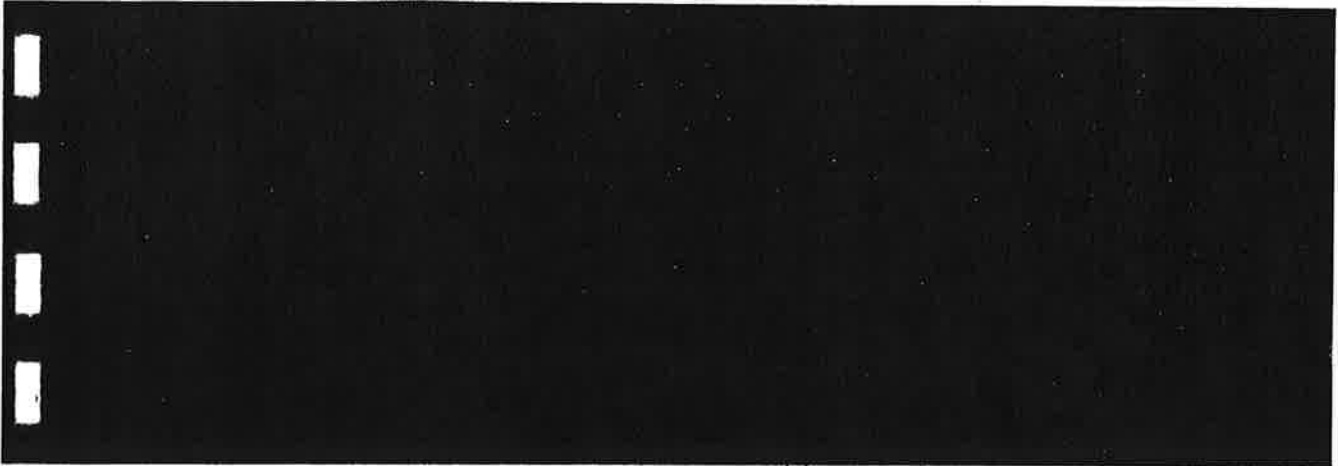
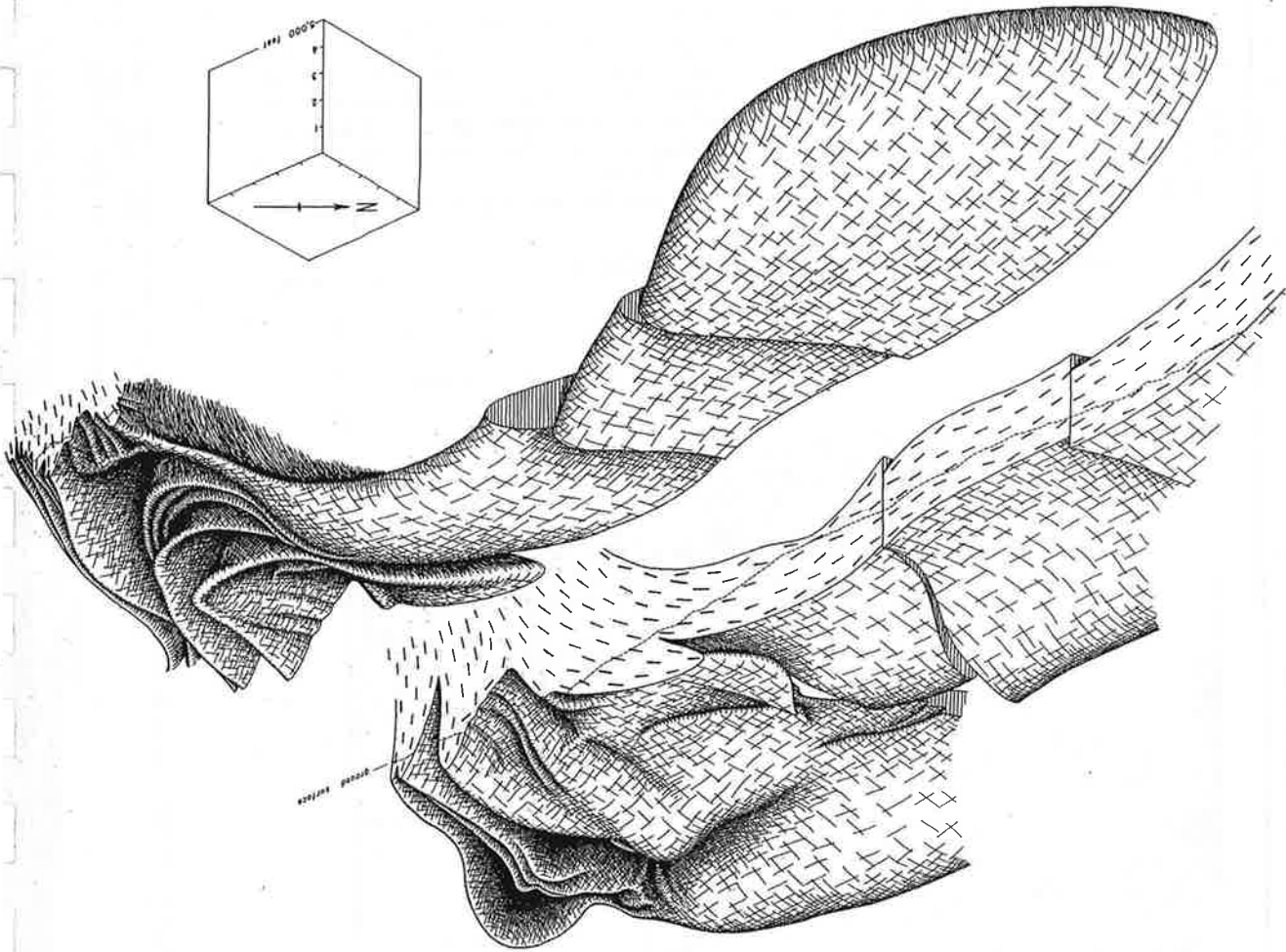
Minor fold axes 

$\beta$  axes (1)  40 (2)  20

$\beta$  axes Usually based on five to twenty S-surface altitudes taken within an area less than 300 feet in diameter (1) in granitic rocks (2) in metamorphic rocks

MAP OF LINEAR STRUCTURES IN AND AROUND THE RATTLESNAKE MOUNTAIN PLUTON, SOUTHERN CALIFORNIA

ORTHOGRAPHIC PROJECTION OF THE RATTLESNAKE MOUNTAIN PLUTON,  
SOUTHERN CALIFORNIA





onal structures within  
surrounding the Rattle-  
pluton . . . . . 816

granulite northeast of Luna  
 . . . . . 818

ctures within and beneath  
lobe in granulites of Luna  
 . . . . . 820

Facing

be Rattlesnake Mountain  
n California . . . . . 805

Following

n in porphyritic, biotite-  
ite containing mafic in-  
 . . . . . 814

orphyritic, biotite-quartz  
aced by shear zones  
g schlieren and inclusions  
 . . . . . 814

Facing

tures in and around the  
ountain pluton, southern  
 . . . . . 816

if the Rattlesnake Moun-  
thern California . . . . . 818

tion of the Rattlesnake  
i, southern California . . . . . 822

nitic rocks . . . . . 808

- (2) The structures within the pluton form systematic geometric patterns related to the over-all shape of the body.
- (3) These structures are easily observed because of the presence of numerous elongated and flattened inclusions; thus linear as well as planar structures may be measured.
- (4) The pluton is well exposed; the climate

is semiarid and supports only a sparse vegetative cover, and the granitic rocks are exposed in blocky outcrops that in places protrude as much as 50-100 feet above the ground. The exposure surfaces lie at all angles and are ideal for determining the orientations of the inclusions in three dimensions.

The combination of good outcrops and nu-

ning the axis of the funnel  
of the elliptical outcrop  
E. and dips 75° SE. The  
orthwest perpendicular to  
his plane. The smaller lobe  
the northeast end of the  
d is rooted in a layer that  
and above the larger lobe.  
e funnel, 1½ miles west of  
of the sheets are bowed  
small rudimentary pro-  
the larger lobes, remain  
of the funnel.

e pluton covers about 21  
g the screens and central  
unnel portion of the body  
ng and 2 miles wide. The  
rop area occurs mainly  
west lobe. The exposed  
is a maximum width of 4  
les from the center of the  
ent of the lobe is not  
d is overlain by country  
he smaller lobe is about  
it is exposed along its  
ile.

E the pluton has been  
because:  
small, well-defined unit  
and structural bounda-

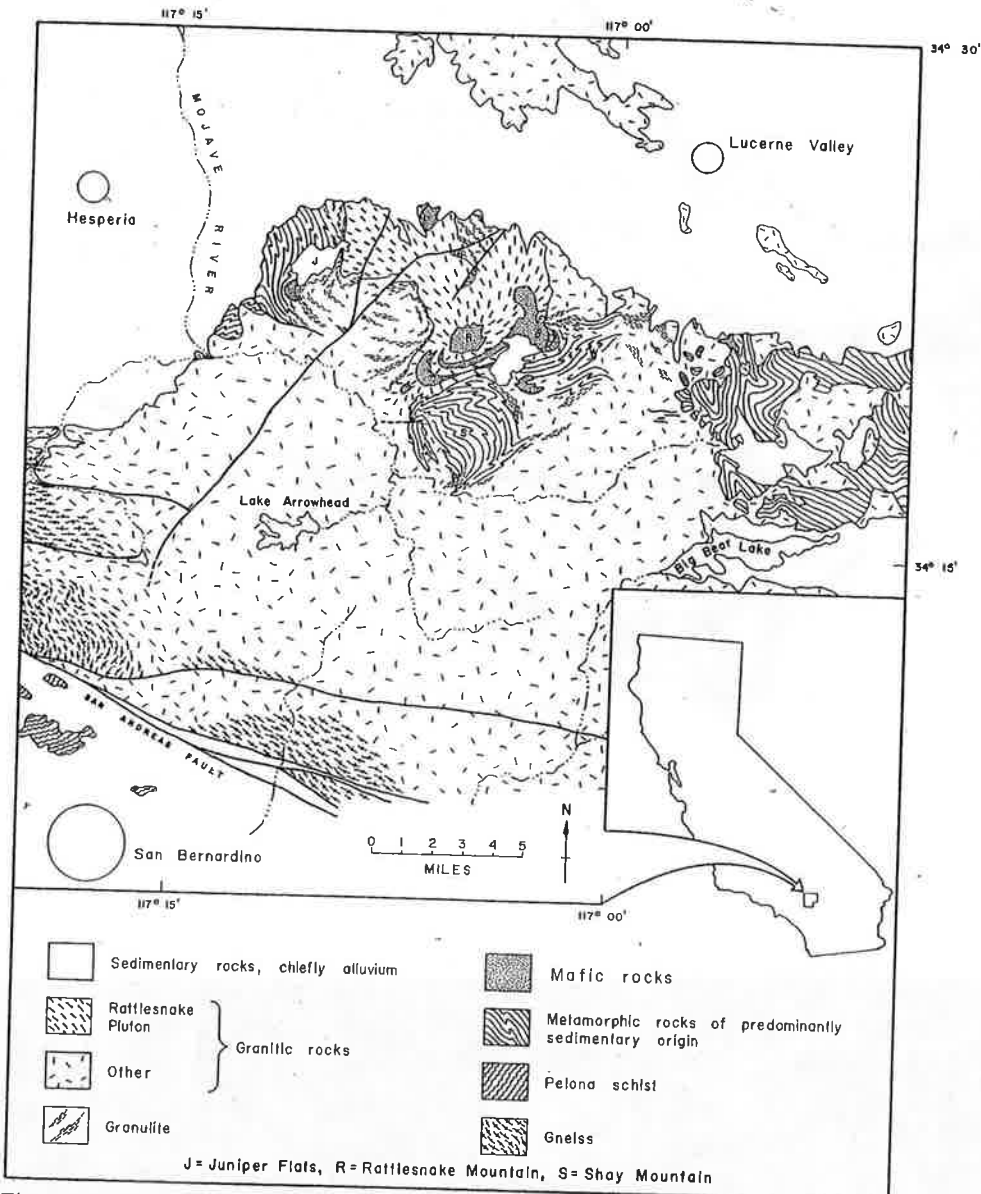


Figure 1. Index map of the western part of the San Bernardino Mountains, California. Geology north of San Bernardino condensed from unpublished maps of Dibblee (personal communication). Geology northeast of Big Bear Lake condensed from Richmond (1960)

R. S. MacCOLL<sup>1</sup>

# Geochemical and Structural Studies in Batholithic Rocks of Southern California: Part 1, Structural Geology of Rattlesnake Mountain Pluton

**Abstract:** The Rattlesnake Mountain pluton, a funnel-shaped body of coarse-grained porphyritic quartz monzonite, is an offshoot from a batholithic mass of biotite-quartz monzonite forming the central part of the San Bernardino Mountains in Southern California. The pluton intrudes a structurally complex region of metamorphic and igneous rocks that borders the batholith on the north side of the mountains. The metamorphic rocks consist of marbles, calc-silicate hornfels, schists, quartzites, amphibolites, gneisses, granulites, and migmatites. The degree of metamorphism is in the higher grades of the almandine-amphibolite facies and of the granulite facies. Igneous rocks of the pluton range from quartz monzonite through granodiorite to quartz diorite and were emplaced at the same time as the main part of the batholith. The intrusion of the pluton was postkinematic and disrupted the regional structure.

The most distinctive features of the Rattlesnake

Mountain pluton are its shape and internal structure. The upper part of the funnel flares outward and is divided into several lobes and sheets separated by screens of mafic rocks. The sheets follow the funnel pattern, lying concentrically within one another and dipping inward toward a central point. The lobes are tongue-shaped and extend from the upper edge of two of the sheets. One of the lobes extends outward for more than 5 miles from the funnel. An unusual abundance of inclusions, schlieren, and dikes are present. These structures are in many cases oblique to one another; schlieren commonly cut across or are truncated by other schlieren, and inclusions lie in various orientations. Structural data were plotted on equal-area projections; in any one area, normals to the flattened surfaces of inclusions and schlieren form a pattern that commonly consists of an incomplete great circle containing a central maximum.

## CONTENTS

Introduction . . . . .	806	Biotite-quartz monzonite of the pluton . . . . .	808
General statement . . . . .	806	Country rocks . . . . .	809
Petrologic nomenclature . . . . .	808	Metamorphic rocks of sedimentary origin . . . . .	809
Geologic setting . . . . .	808	Mafic rock . . . . .	810
Acknowledgments . . . . .	808	Granulite and alaskite . . . . .	810
Rocks of the pluton and country terrain . . . . .	808	Granitic rocks . . . . .	810

<sup>1</sup>This paper presents the results of a thorough structural investigation of an apparently unique plutonic body in the San Bernardino Mountains. R. S. MacColl died in an accident while working with the U. S. Geological Survey in Alaska during the summer field season of 1961. The degree Master of Arts was awarded posthumously to MacColl by the Claremont Graduate School.

The structural study of Rattlesnake Mountain pluton has formed a necessary basis for an extensive program of geochemical sampling. Had MacColl lived, he would have been an active participant in this work. Geochemical studies now completed by A. K. Baird, D. B. McIntyre, and E. E. Welday are aimed at determining the distributions of major and minor elements in rocks of the pluton and relating these distributions to the petrology

and structure. These results will appear as Part II of this report. A chemical and petrological comparison between Rattlesnake Mountain pluton and another unit of the Southern California batholith, centered at Cactus Flat, San Bernardino Mountains, has also been completed and will appear as Part III. Studies in progress are concerned with extending the sampling of granitic rocks to include all portions of the San Bernardino Mountains. This research is supported by the National Science Foundation (grant number GP-1336), whose continuing aid is gratefully acknowledged.

The paper was submitted to the Society by A. K. Baird and D. B. McIntyre (Pomona College, Claremont, California).

# Age and Engineering Geologic Observations of the Blackhawk Landslide, Southern California

GEOLOGY AND MINERAL WEALTH OF THE CALIFORNIA TRANSVERSE RANGES © South Coast Geological Society 1982

Martin L. Stout, California State University, Los Angeles, CA. 90032

The Blackhawk landslide, extending outward from the mountain front for 4.5 miles and covering about 5.5 square miles on a gently sloping (2.5°) alluvial surface of the Mojave Desert, is one of the better known landslides in southern California, largely because of the Ph.D. dissertation and later G. S. A. Special Paper of Shreve (1968). The only other landslide in southern California, known to the writer, which has been the sole subject of a Ph. D. dissertation is the Portuguese Bend landslide (Vonder Linden, 1972). Both slides are certainly well deserving of this special emphasis.



The Blackhawk Canyon area and landslide were first studied in detail by Woodford and Harriss (1928), who recognized large scale landsliding in the region. Shreve (1968) concluded that the landslide debris, largely limestone breccia from the Paleozoic Furnace Formation on Blackhawk Mountain, was the result of a huge rock fall which generated enough momentum to be launched into the air, and then rode a low friction, air-layer to its final resting place (Fig. 1). Hsü (1975) has taken exception to the airrafting concept contending that lobate features, similar to and including the Blackhawk landslide, can be produced by flowage, without an air cushion.

Although the mechanism of failure is not of prime concern here, the evidence now available indicates that the Blackhawk slide moved during a time of known heavy precipitation, and highly saturated ground conditions may have been the triggering mechanism. The influence of montmorillonitic clays found within the slide debris remains to be evaluated, but certainly could have lowered the overall shear strength of the calcareous materials before failure occurred. Interestingly, Hsü (1975) used bentonite suspensions for some of his model studies. Other large landslides in the San Bernardino Mountains, such as the Barton Flats landslide (Stout, 1976a) probably also moved during this time of heavy precipitation during the Tioga glaciation. This is also undoubtedly the case for many other large landslides throughout the now generally arid Great Basin and southwestern United States.

The writer was interested for some time in dating the Blackhawk in conjunction with carbon-14 age determinations of landslides in various geographic areas of southern California (Stout 1976b). After many unsuccessful drilling attempts to get

through the hard, calichified limestone slide debris to obtain carbonaceous material on or below the depositional surface (to determine the maximum age of movement), this approach was abandoned and methods were considered which would establish a minimum age.

Extensive alluviation occurred over the Blackhawk landslide debris following slide movement, resulting in the almost complete burial of the upper portion of the Blackhawk landslide (Fig. 1). Local depressions farther down on the landslide allowed ponds to form, one at least 7 acres in size, and at least 20 feet deep, which was subject to rapid deposition of fine grained sediments. Thus, any organic material deposited with these sediments might provide a minimum age of slide movement.

Radiocarbon dating of fresh water gastropod and pelecypod shells from one of these lake bed deposits indicates a late-Wisconsin age of  $17,400 \pm 550$  years BP (Stout, 1975). The shells were taken from calcareous mudstone resting directly on Blackhawk landslide debris (Fig. 2). Most of the carbonate in this 3-foot thick bed is believed to be material pulverized during landslide movement, so the age is probably very close to the time of movement. The fossiliferous bed is overlain by about 17 feet of non-fossiliferous micaceous siltstone, derived principally from crystalline gneisses and plutonic rocks exposed about 3 miles upstream in Blackhawk Canyon.

This sedimentary sequence is interpreted as consisting largely of pulverized carbonate and montmorillonite materials generated largely by landslide movement and washed into the local depression and deposited directly on an irregular surface underlain by slide debris. The pond existed for a short time without the normal clastic, micaceous sediments reaching it and the organisms flourished. Eventually, the rapidly growing alluvial apron derived primarily from the extensive erosion of Blackhawk Canyon, which was eroded in post-slide time, reached the basin and probably filled it with fine grained sediments in a very short time. The absence of evaporite minerals in the sedimentary section suggests the presence of a perennial lake. The stream draining the basin finally breached the landslide debris exposing the entire lake bed section, and cutting an arroyo about 70-100 feet across and 25 feet deep, the channel of which provides easy 4-wheel drive access to the lake beds today (Fig. 3). Unfortunately, the lake beds cannot be seen from Old Woman Springs Road.

Between the Blackhawk landslide and Kaiser's Permanente Cement Plant to the northwest, the northern side of Blackhawk Mountain is covered with other large massive failures, most of which are more conventional rotational failures, which have provided loose materials for a number of mappable debris flows. Most of these debris flows have in turn been subjected to Holocene anticlinal folding—breaching of the folds by stream erosion provides the exposures necessary to map the debris flows. Regional compression is also expressed by numerous thrust fault scarps in alluvium along the entire northern side of the San Bernardino Mountains. In the vicinity of the Blackhawk landslide, none of the spectacular fault scarps in alluvium are present—the thrusts apparently are higher on the hillside, and well exposed in Blackhawk Canyon. The fault scarps in alluvium southeast of the



**Figure 5.** Oblique aerial view of Blackhawk landslide shows alluviated upper area and well formed transverse ridges in lower half. The arroyo crossing from mid-left to mid-right provides 4-wheel drive access to fossil locality shown in Figure 2. Baldwin Lake just visible in upper center.. Photograph by John Shelton # 3097



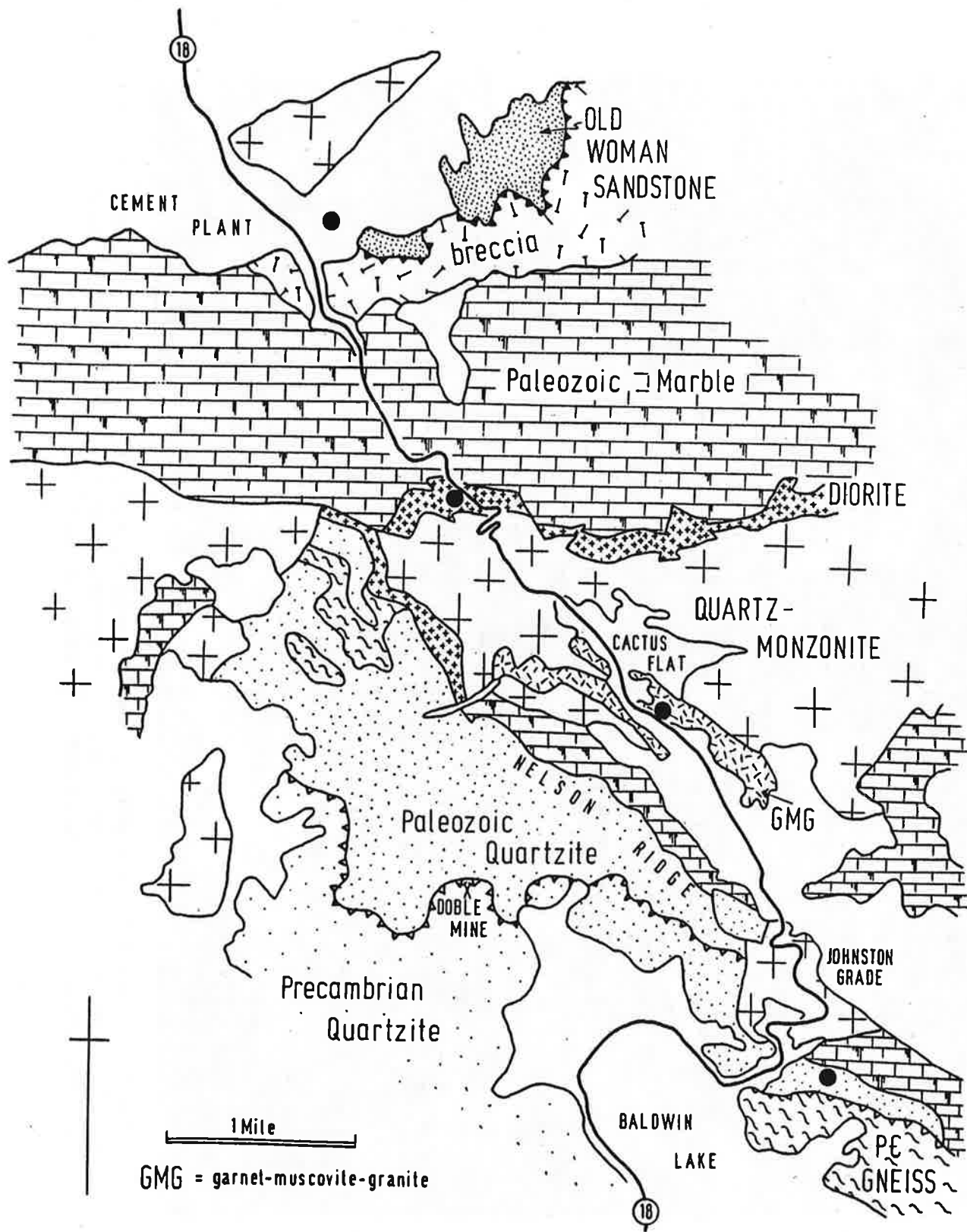


Figure 7. Generalized geologic map of the Johnson Grade area.

into a near horizontal thrust. Steep, NW-striking faults displace the thrust surface.

Pioneertown

The largest remnants of the late Miocene basalt flows cap mesas at the east end of the mountains, where they merge with the Mojave Desert. The flows

-  Active Surficial Deposits
-  Relict Gravel
-  Lake Beds
-  BLACKHAWK LANDSLIDE showing ridges

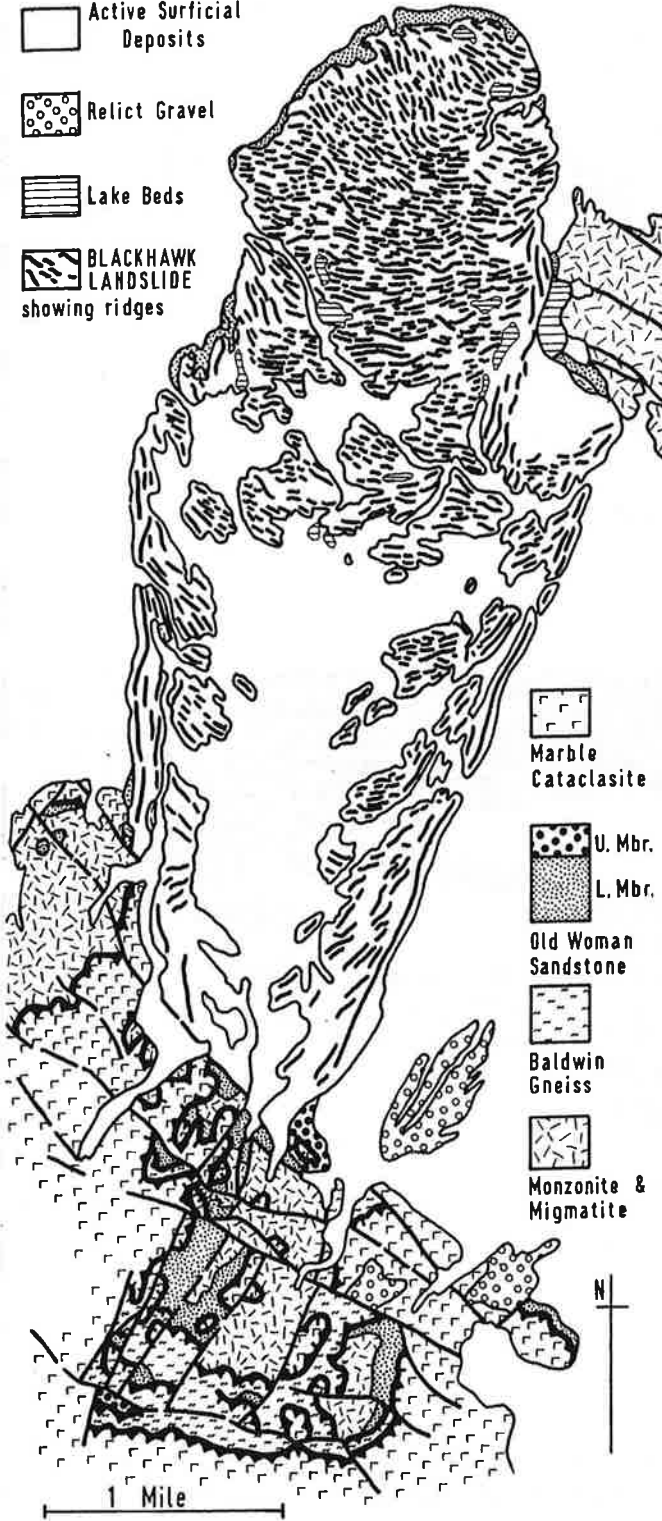


Figure 4. Map of the Blackhawk Landslide.

around Pioneertown cover an eastward thinning wedge of arkosic sands and pebbly sands. On one mesa, Black Hill, a second tongue of sandstone is preserved between flows (Fig. 2f). Their relationship with the basalts permits these sands to be grouped with the Santa Ana Sandstone.

West of Pioneertown on Chaparrosa Peak (Fig. 2e) basalts cover a cobble conglomerate with ferruginous cement. The cobbles are the well rounded quartzites and porphyries encountered sporadically along the range front. This occurrence shows that they had reached the eastern portion of the range by late Miocene times.

The Pioneertown basalts and Santa Ana Sandstone are still sub-horizontal, are uncovered by surficial deposits, and are nowhere overridden by thrusts. The area probably resembles the autochthonous terrains of the north range front and Cienaga Seca prior to thrusting.

Onyx Mine

The Miocene (?) quartzite- and porphyry-bearing conglomerate of Chaparrosa Peak crops out again near Onyx Mine. There is no basalt cap here, and the cobbles are uncemented. The conglomerate is succeeded by interlayered marble-conglomerates and travertine (Fig. 2g) of unknown age. The sequence is capped by monzonite which is interpreted to be an overthrust klippe. Thus, the structure resembles the nearby Cienaga Seca occurrence but the sedimentary facies are quite different.

Antelope Creek

Scraps of late Cenozoic stratigraphy on either side of the upper Antelope Creek can be tied together because they include the quartzite- and porphyry-bearing conglomerate. A composite section (Fig. 2h) shows the conglomerate to be overstepped by basalt and locally underlain by buff arkosic sands.

Rattlesnake Creek

Several disjunct late Cenozoic sequences occur in the upper Rattlesnake Creek valley. A strip of arkosic sands and gravels with some marble clasts extends along the north side of the uppermost gorge below Round Valley. It is difficult to interpret fully because of landsliding and patches of surficial deposits plastered onto the canyon wall. What can be shown is that the southern end of the strip is over-thrust by monzonitic basement. At the north end the arkoses are seen to be succeeded by a coarse marble conglomerate reminiscent of the central facies of the Old Woman Sandstone. Part of the outcrop of this conglomerate is a persistent line of float halfway up a slope in monzonites. The site was not excavated, but is interpreted to be a slice of conglomerate trapped by over thrusting (Fig. 2i).

On the north side of Mineral Mountain, as on Granite Peaks, there is a relict outcrop of quartzite- and porphyry-bearing gravel. It cannot be shown to be late Miocene here, and may have been deposited during later recycling. Certainly other remnants of this gravel on the south side of Mineral Mountain have fed colluvial deposits covering the thrust discussed above.

Where Rattlesnake Creek skirts the flats between Mound Spring and Viscera Spring, the anomalous, rounded cobbles of quartzite and porphyry reappear.

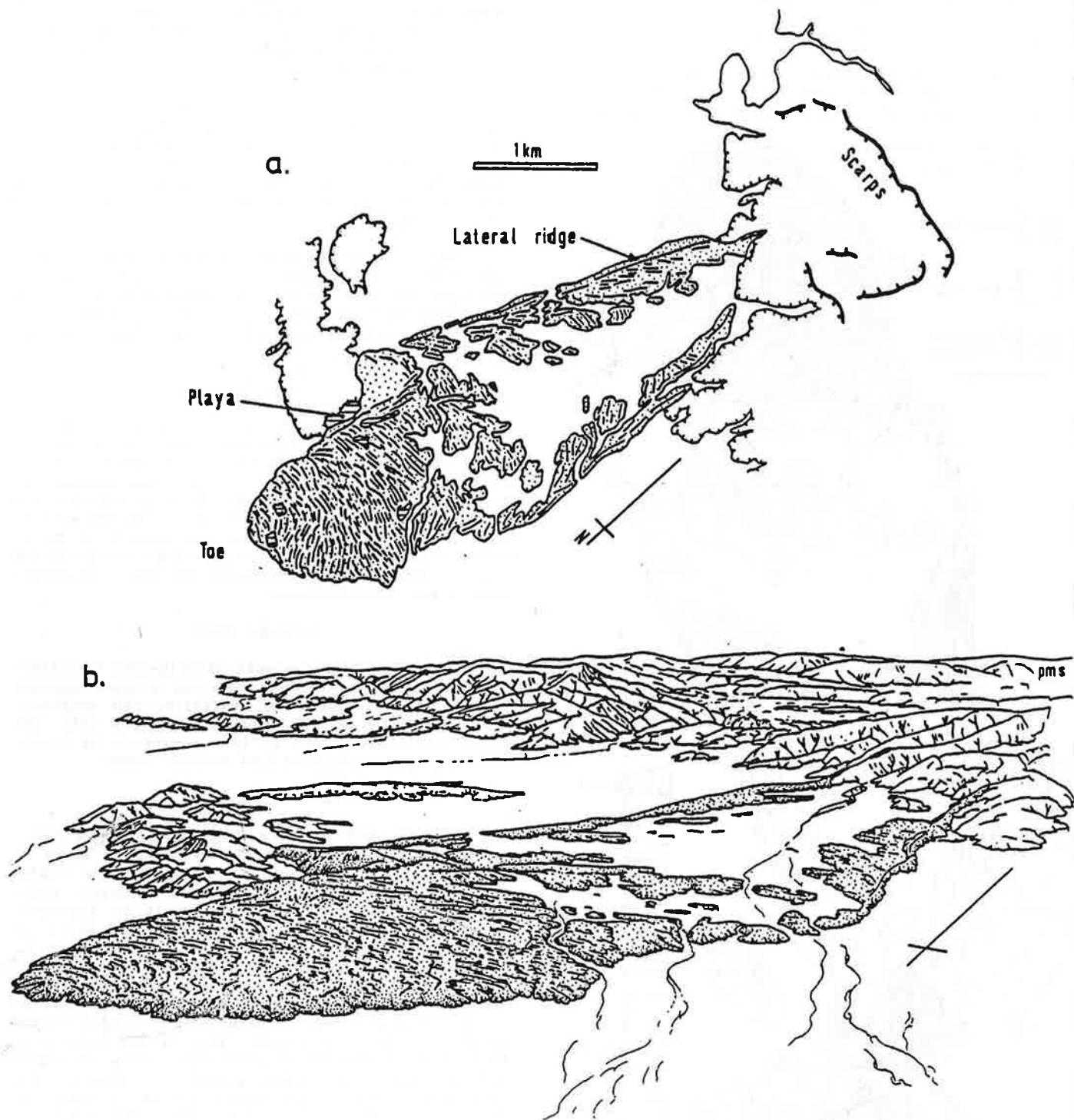


Figure 21. The Blackhawk landslide (stippled). Schematic map (a) showing surface ridges and oriented for comparison with oblique aerial view (b).